Convective Transport of Macromolecules in Gels

by

Scott Travis Johnston

M.S. Chemical Engineering Practice
Massachusetts Institute of Technology, 1995

B.S. Chemical Engineering
Carnegie Mellon University, 1993

Submitted to the Department of Chemical Engineering
in partial fulfillment of the requirements for the degree of

Doctor of Philosophy
at the
MASSACHUSETTS INSTITUTE OF TECHNOLOGY

September, 1999

Signature of Author _____
Department of Chemical Engineering
July 27, 1999

Certified by _____
William M. Deen
Carbon P. Dubbs Professor of Chemical Engineering
Thesis Supervisor

Accepted by _____
Robert E. Cohen
St. Laurent Professor of Chemical Engineering
Chairman, Committee for Graduate Students

Convective Transport of Macromolecules in Gels

by

Scott Travis Johnston

Submitted to the Department of Chemical Engineering
on July 27, 1999 in partial fulfillment of the
requirements for the degree of
Doctor of Philosophy

ABSTRACT

In porous or fibrous materials where the pore diameter or interfiber spacing is comparable to the dimensions of a protein or other macromolecule, the rates of diffusion or convection of the macromolecule tend to be lower than in bulk solution. This phenomenon, termed "hindered transport," is explained in large part by a combination of steric and hydrodynamic interactions between the permeating molecule and the medium. The primary goal of this thesis was to examine the hindered convection of macromolecules in fibrous gels. This was done by measuring the sieving coefficient (Θ, the ratio of filtrate to retentate concentration) of globular proteins and Ficoll, a crosslinked copolymer of sucrose and epichlorohydrin (Stokes-Einstein radius, r_s = 2.5 - 7.0 nm), in agarose membranes as a function of protein size and gel concentration. The proteins used were lactalbumin (r_s = 2.1 nm), ovalbumin (r_s = 3.0 nm), bovine serum albumin (BSA) (r_s = 3.6 nm), and bovine immunoglobulin G (IgG) (r_s = 5.2 nm). The volume fraction of agarose (ϕ) was varied from 0.04 to 0.08. Agarose membranes were prepared on polyester mesh supports and studied in a stirred ultrafiltration cell, and the Darcy permeabilities of the gels were determined in addition to Θ. The values of Θ decreased with increasing r_s or ϕ, as expected. From the measurements of Θ and estimates of the protein diffusivity and equilibrium partition coefficient, the convective hindrance factor (K_c) was calculated for each protein-gel combination. This is the ratio of the average solute velocity (in the absence of diffusion) to the superficial fluid velocity. For the smallest value of ϕ (0.04), it was found that K_c exceeded unity for all macromolecules studied. At this gel concentration, K_c increased with increasing solute size up to approximately 1.5 for the largest Ficoll. For larger values of ϕ, it was found that K_c decreased with increasing solute size. In these gels, K_c exceeded unity for smaller solutes, whereas $K_c < 1$ at larger values of r_s. At an intermediate ϕ (0.06), K_c for the largest Ficoll remained close to unity (0.94). For the most concentrated gels (ϕ = 0.08), K_c for this Ficoll decreased to approximately 0.5. The observed experimental behavior for K_c was qualitatively, but not quantitatively, consistent with predictions from existing hindered transport theories for media consisting of parallel fibers or straight pores. Given evidence from previous partitioning and diffusion data that an agarose gel is better represented as a randomly oriented array of fibers, the quantitative discrepancies between the data and models are not entirely surprising. Thus, the present results suggest that there is a need to extend theories of hindered convection to random arrays of fibers.

In order to correctly interpret the experimental results, the measured sieving coefficients were corrected for the effect of concentration polarization. A model was developed using laminar boundary layer theory to quantify concentration polarization in ultrafiltration systems in which the membrane forms the base of a stirred, cylindrical container. The flow was approximated as a rigid-body rotation above a stationary surface (Bödewadt flow), with a filtration velocity that depended on the osmotic pressure of the retained solute, and therefore varied with radial position on the surface. Because the analysis was limited to moderate solute concentrations and filtrate

velocities, physical properties were assumed to be constant. Attention was restricted to large Reynolds and Schmidt numbers, so it was permissible to neglect radial diffusion and to use an analytical approximation for the velocity field. The axisymmetric convective-diffusion problem was solved using a finite difference method. One set of simulations focused on the osmotic reduction in filtration rate caused by a completely retained solute. The boundary layer results were compared with predictions based on a commonly used stagnant film model, and it was found that the latter consistently underestimated the reduction in filtration rate, although the discrepancies were no more than 21%. A comparison was also made with a "hybrid" model in which stagnant film theory was assumed to be valid locally and local mass transfer coefficients were calculated by the laminar boundary layer model. The hybrid model also underestimated the reduction in the filtration rate; however, discrepancies were no more than 15%. A second set of simulations concerned the effects of polarization on apparent sieving coefficients for permeable solutes. (The apparent sieving coefficient is the filtrate concentration divided by that in the bulk retentate, whereas the true sieving coefficient for the membrane is the filtrate concentration divided by that at the membrane surface.) A comparison of the boundary layer and stagnant film results showed that the latter consistently underestimated the effects of polarization on sieving. The magnitude of the discrepancy in the predicted ratio of true to observed sieving coefficient increased with increasing dimensionless filtration rate and with decreasing sieving coefficient, and was as much as 78% for the conditions considered. Thus, the stagnant film approach was found to be much less satisfactory for correcting sieving coefficients than for predicting mean filtrate velocities. It was found that the hybrid model performed considerably better than the stagnant film model in estimating the effect of polarization on sieving, especially at very small values of Θ. For the hybrid model, the maximum deviation from the boundary layer results was only 15%. The predictive capability of the boundary layer model was tested using filtration data with BSA in two commercial ultrafiltration cells. The agreement was found to be excellent, provided that an appropriate value was selected for the angular velocity of the bulk fluid.

Thesis Supervisor: William M. Deen
Title: Carbon P. Dubbs Professor of Chemical Engineering

ACKNOWLEDGEMENTS

I would like to thank my thesis advisor, Professor William Deen, for his guidance and support throughout the course of this work. His deep understanding of transport phenomena and his thoroughness have kept me honest and taught me much. Thanks are also due to the other members of my thesis committee, Professors Kenneth Smith and Alan Grodzinsky, for their encouragement and their constructive comments regarding the direction of my research.

I would also like to thank the other members, past and present, of my research group: Randy Lewis, Erin Johnson, Aurelie Edwards, Glen Bolton, Manish Keshive, Jeff White, Pat Gwynne, Bo Chen, Stephanie Stine, and Matt Lazzara. The many conversations, brain-storming sessions, and laughs we shared made my stay at MIT an enjoyable one and helped me maintain my perspective and my sanity.

Special thanks go to Bill and Tonya Grieco, great friends that over the past five years have become more like extended family. I believe it is no mistake that we will soon be neighbors again in Pennsylvania - it seems that life has a way of keeping those closest to you nearby.

All of this would not have been possible without the love and support of my parents. Mom and Dad, you have always done whatever you could to provide me with every opportunity possible. I have strived to live my entire life by your example.

Finally, my deepest appreciation goes to my wife Jolene. Thank you for always being there for me - you are truly my best friend in the world. Your encouragement and love has shown me that in our life together anything is possible. I look forward to spending the rest of my years as I have spent the last ten - sharing my greatest triumphs, worst defeats, and everything in between with you.

TABLE OF CONTENTS

LIST OF FIGURES

LIST OF TABLES

CHAPTER 1

Background

1.1 Introduction

Hydrogels enjoy many uses in chemical and biomedical research. Techniques such as liquid chromatography and electrophoresis rely on the use of gels as media, and therapeutic devices such as contact lenses and certain implantable drug delivery devices are composed of gels. Additionally, some body tissues display structures which are remarkably similar to hydrogels. A particularly interesting example is the glomerular basement membrane (GBM). The GBM is the most significant continuous barrier to the ultrafiltration of blood plasma across the glomerular capillary walls of the kidney, the first step in the formation of urine. The GBM is a fibrous structure consisting primarily of Type IV collagen and glycoprotein (Brenner and Rector, 1981). Robinson and Walton (1987) have suggested that because of its structure, the GBM can be accurately modeled as a random fiber matrix gel.

This widespread utilization of fibrous hydrogels makes it important to understand the transport of proteins and other macromolecules through these materials. Such an understanding would enable the rational design of synthetic media for chromatographic or membrane separations. An understanding of the transport of nutrients through synthetic gels would aid in the design of drug delivery devices in which gels are used to encapsulate cells that produce therapeutic agents (which must in turn be transported out of the gel). The development of an understanding of the transport of proteins and other macromolecules across barriers such as the GBM is an important step in understanding glomerular ultrafiltration and the failures in ultrafiltration associated with disease.

1.2 Darcy Permeability of Fibrous Media

An important part of evaluating hindered transport of solutes in fibrous gels is the understanding of low Reynolds number flow through such media. Experiments and theories related to Stokes flow through fibrous media have been summarized by Jackson and James (1986). The authors compared experimental data for a wide variety of media ranging from stainless steel wire crimps to collagen and solutions of hyaluronic acid. They found that the results for different media collapsed reasonably well if the appropriate dimensionless variables are employed, namely ϕ (the volume fraction of fibers) and the dimensionless permeability κ/r_f^2 where r_f is the fiber radius and κ is the Darcy permeability. Darcy's Law is stated as

$$\mathbf{v} = -\frac{\kappa}{\mu}\nabla P \tag{1-1}$$

where $\mathbf{v}$ is the fluid velocity, μ is the viscosity, and P is pressure.

Theories discussed in this summary involved solving Stokes' equation inside of a unit cell with zero velocity at a rod surface and zero velocity gradient at the edge of the cell. These theories were divided into three categories:

i.) flow parallel to an array of parallel rods

ii.) flow normal to an array of parallel rods

iii.) flow through three-dimensional arrays

The first group of theories were found to overpredict experimental permeabilities. The authors noted that such a result is to be expected since fibers randomly oriented across the flow would offer more resistance in experiments. The second group of theories were found to predict permeabilities that were roughly half as large as those predicted by considering flow parallel to an array of parallel rods.

The final group of theories consisted of two expressions, the first of which was derived by Spielman and Goren (1968) by modeling flow through fibrous media as the flow around a single

circular cylinder surrounded by an infinite homogeneous porous medium (a technique now referred to generally as "swarm" theory). Their expression for a three-dimensional array (for $\phi < 0.75$) was

$$\frac{1}{4\phi} = \frac{1}{3} + \frac{5}{6}\frac{\sqrt{\kappa}}{r_f}\frac{K_1\left(r_f/\sqrt{\kappa}\right)}{K_0\left(r_f/\sqrt{\kappa}\right)} \tag{1-2}$$

where K_0 and K_1 are modified Bessel functions of the second kind. The second expression was derived by Jackson and James (1982) using a cubical lattice model. In this work, it was argued that the permeability of a random media is equivalent to the permeability of a cubical lattice formed of the same material. Their expression was derived by adding the resistances of rods aligned both with and across the flow, calculated using the model of Drummond and Tahir (1984) for flow normal to a square array of cylinders. It took the form:

$$\frac{\kappa}{r_f^2} = \frac{3}{20\phi}\left[-\ln\phi - 0.931 + \mathrm{O}(\ln\phi)^{-1}\right] \tag{1-3}$$

The authors noted that the two models (Eqs. 1-2 and 1-3) agreed reasonably well with each other and with the experimental data obtained.

Noticeably missing from the experimental data collected by Jackson and James are data for high porosity hydrogels. Our laboratory provided the first experimental values for the permeability of agarose gels (Johnson and Deen, 1996). In these experiments, thin gel membranes were cast onto a rectangular polyester mesh approximately 70 μm thick in order to give them enough rigidity to withstand significant pressure drops. Using a commercial ultrafiltration cell, the permeabilities of gels ranging in concentration from 2% to 8% were measured. It was found that Eq. 1-3 significantly underpredicted the Darcy permeabilities of agarose gels, especially at lower values of ϕ.

More recently, the permeabilities for monomodal and bimodal periodic and random fibrous

media were calculated numerically by Clague and Phillips (1997). The authors calculated the hydrodynamic interactions between fibers by applying a numerical version of slender body theory to a collection of fibers in a cubic cell. Their model provided predictions for the Darcy permeabilities of agarose that were higher than those obtained with Eq. 1-3. However, the numerical estimates for the permeabilities were still smaller than the experimental values of Johnson and Deen (1996), especially at lower gel concentrations.

1.3 Hindered Transport Theory

1.3.1 Overview

In porous or fibrous materials where the pore diameter or interfiber spacing is comparable to the dimensions of a protein or other macromolecule, the rates of diffusion or convection of the macromolecule tend to be lower than in bulk solution. This phenomenon, termed "hindered transport," is explained in large part by a combination of steric and hydrodynamic interactions between the permeating molecule and the medium (Deen, 1987). The local flux of solute through an isotropic medium (or through a medium in which fluxes are one-dimensional) can be written as

$$\mathbf{N} = -K_d D_\infty \nabla C + K_c \mathbf{v} C \tag{1-4}$$

where C is the macromolecule concentration averaged over a volume that is small compared to the dimensions of the medium but large compared to the pore diameter or interfiber spacing, D_∞ is the free-solution diffusivity, and $\mathbf{v}$ is the superficial fluid velocity. The dimensionless coefficients K_d and K_c describe hindrances to diffusion and convection, respectively. The diffusive hindrance coefficient equals D/D_∞, where D is the apparent diffusivity within the porous or fibrous material. The convective hindrance coefficient may be interpreted as the ratio of the average solute velocity (in the absence of diffusion) to the superficial fluid velocity.

For the case of one-dimensional transport across a membrane of thickness L, the macroscopic flux equation can be obtained by integrating Eq. 1-4 over the membrane thickness subject to boundary conditions at the surfaces. These boundary conditions are established by the external solute concentrations:

$$\frac{C_0}{C_0'} = \frac{C_L}{C_L'} = \Phi \tag{1-5}$$

where primes denote external solute concentrations and Φ is the equilibrium partition coefficient. The resulting expression is

$$N = WvC_0' \frac{\left[1 - (C_L'/C_0')e^{-\mathrm{Pe}}\right]}{\left[1 - e^{-\mathrm{Pe}}\right]} \tag{1-6}$$

$$\mathrm{Pe} = \frac{WvL}{HD_\infty} \tag{1-7}$$

where $H = \Phi K_d$, $W = \Phi K_c$, and Pe is the membrane Péclet number. The limiting forms of Eq. 1-6 for the extremes of the Péclet number are:

$$N = \frac{HD_\infty}{L}(C_0' - C_L') \qquad (\mathrm{Pe} << 1) \tag{1-8}$$

$$N = WvC_0' \qquad (\mathrm{Pe} >> 1) \tag{1-9}$$

The coefficients Φ, K_d, and K_c are functions of solute size and charge, as well as the properties of the stationary medium. These coefficients are often expressed in terms of the "solute permeability," which equals HD_∞/L, and "reflection coefficient" for filtration:

$$\sigma_f = \lim_{Pe \to \infty} (1 - \Theta) = 1 - W \tag{1-10}$$

where Θ is the sieving coefficient (see Section 1.4 below). The filtration reflection coefficient can be interpreted as the fraction of solute "reflected" or rejected by the membrane when convection is dominant (Pe $\rightarrow \infty$).

1.3.2 Porous Media

The objective of research in hindered transport is to establish the relationships between the structural properties and the transport coefficients. Much of this research has focused on theoretical or experimental models for transport through arrays of straight pores of regular cross section. The hydrodynamic theory for hindered transport is well developed for such situations, especially for spherical macromolecules in long, cylindrical pores (Deen, 1987). One example of such a theory which is applicable to the entire range of $0 \leq \lambda < 1$, where λ is the ratio of the solute radius to the pore radius, is based on the hydrodynamic results of Bungay and Brenner (1973). These authors used singular perturbation techniques to solve the problem of flow around a sphere positioned eccentrically in a long cylindrical tube. The authors obtained asymptotic expansions for the torque, hydrodynamic force, and pressure drop for flow past a stationary sphere as well as for a sphere translating or rotating in a quiescent fluid. Using the results provided by these authors for the force on a sphere placed on the centerline of the tube, expressions for the coefficients H and W can be obtained (Deen, 1987). These results are shown in Figure 1.1. From these results the coefficients K_d and K_c are obtained by dividing H and W by Φ, which in the case of cylindrical pores can be evaluated from geometry:

$$\Phi = (1 - \lambda)^2 \tag{1-11}$$

The resulting values of K_d and K_c are shown graphically in Figure 1.2. In pores, the diffusivity of

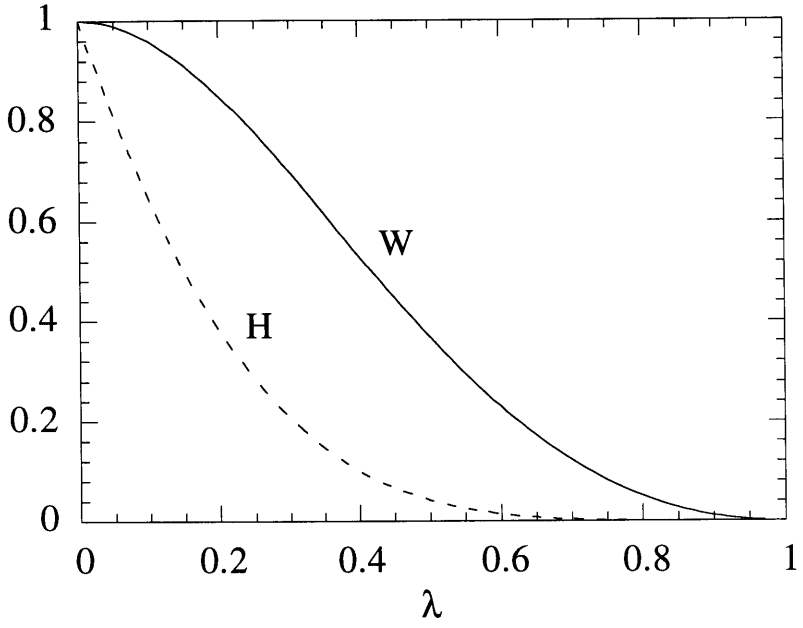

FIGURE 1.1: Results of Deen (1987) for $W = \Phi K_c$ and $H = \Phi K_d$ in cylindrical pores as functions of $\lambda = r_s/r_p$. The solid and dotted lines are coefficients governing convection and diffusion, respectively.

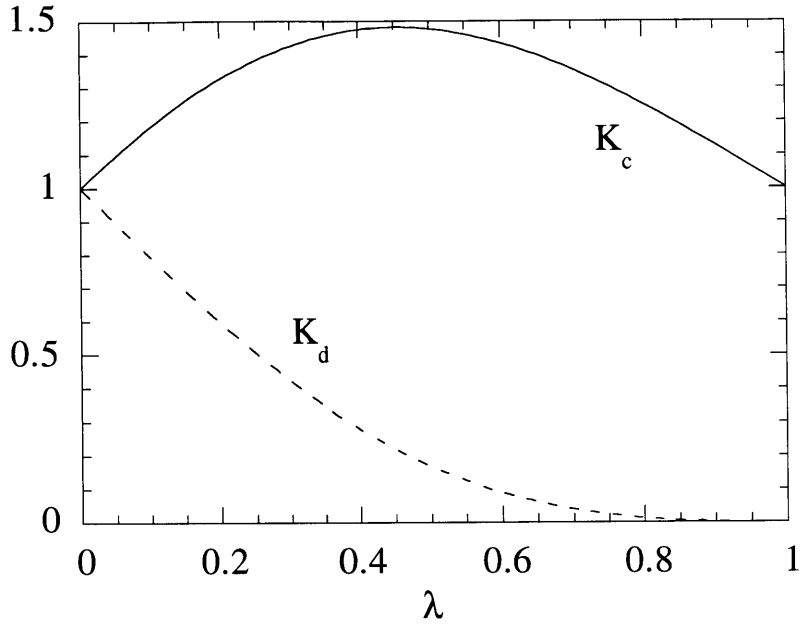

FIGURE 1.2: Results for hindered transport coefficients K_d and K_c in cylindrical pores as functions of $\lambda = r_s/r_p$. Curves were obtained by dividing the results of Deen (1987) (Figure 1.1) by Eq. 1-11. The solid and dotted lines are coefficients governing convection and diffusion, respectively.

a solute is always hindered ($K_d < 1$) due to hydrodynamic interactions between the solute and the pore wall. However, the convective hindrance coefficient, K_c, is always greater than one. This is due to steric interactions which prevent the solute from sampling the regions of lowest fluid velocity near the pore walls.

The filtration reflection coefficient, σ_f, for cylindrical pores can be evaluated by using the result for W (Figure 1.1) in Eq. 1-10. The result is shown graphically in Figure 1.3, where σ_f is plotted as a function of λ. Also shown in this figure is the Anderson and Malone (1974) result for the osmotic reflection coefficient, σ_o, for cylindrical pores. This reflection coefficient describes the reduction in the osmotic contribution to flow across a membrane separating two solutions of different concentration caused by only partial exclusion of solute by the membrane. The volume flux, J_v, across such a "leaky" membrane is given by

$$J_v = L_p\left(\Delta P_\infty - \sigma_o \Delta \Pi_\infty\right) \tag{1-12}$$

where L_p is the hydraulic permeability of the membrane, P and Π are pressure and osmotic pressure, respectively, and the subscript ∞ denotes bulk solution conditions on each side of the membrane. Anderson and Malone (1974) found that for the case of rigid, spherical molecules and a membrane consisting of long, cylindrical pores

$$\sigma_o = (1-\Phi)^2 \tag{1-13}$$

Anderson (1981) found that for such a system Eq. 1-13 provided a good approximation for the filtration reflection coefficient as well. As can be seen in Figure 1.3, the two expressions (Eqs. 1-10 and 1-13) provide very similar results.

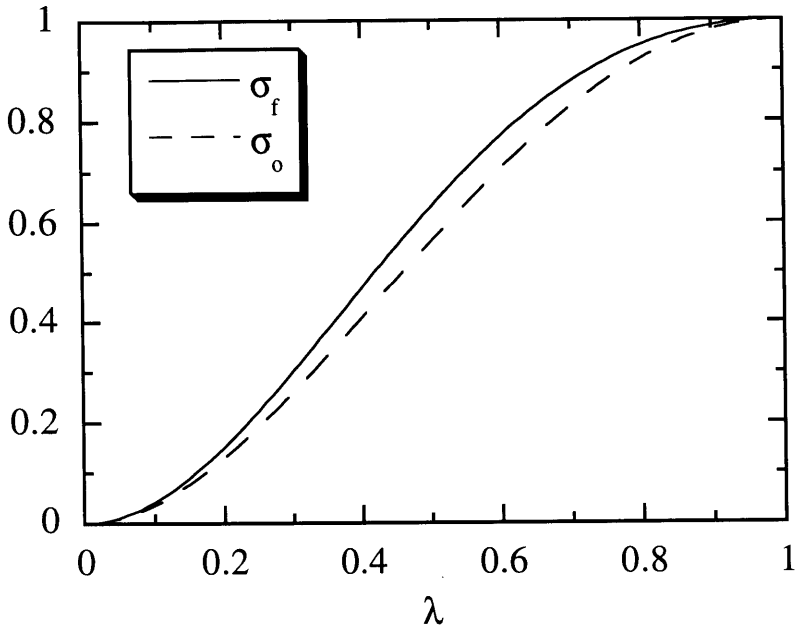

FIGURE 1.3: Filtration and osmotic reflection coefficients for membranes consisting of long, cylindrical pores. Values for σ_f were calculated by using the result for W (Figure 1.1) in Eq. 1-10. Values for σ_o were calculated from Eq. 1-13.

1.3.3 Fibrous Media

Although hydrodynamic theory developed for straight, cylindrical pores has been successful in many cases in correlating transport data in membranes, this theory provides little insight into the structure-function relationships for fibrous materials, such as crosslinked, polymeric gels. As stated in Section 1.1, hydrogels are widely used in chromatographic separations and in therapeutic devices, and a number of body tissues (e.g., capillary basement membranes) have gel-like properties. Thus, there is ample motivation to develop a better understanding of hindered transport in gels.

Ogston (1958) was among the first to suggest that a solution of linear polymers, or the polymeric component of a gel, might be represented as a randomly oriented array of straight cylindrical fibers. The parameters which characterize the fiber array in this model are the fiber radius, r_f, and the volume fraction of fibers, ϕ. This concept is the basis for much of the theoretical work on hindered transport in gels, which has focused mainly on equilibrium partitioning and diffusion. Ogston (1958) predicted partition coefficients for macromolecules in fiber arrays by determining probability distributions of interfiber spacings. His result is given by

$$\Phi = \exp\left[-\phi(1+\lambda)^2\right] \equiv \exp(-f) \tag{1-14}$$

where for the case of fibrous media $\lambda = r_s/r_f$. Stochastic-jump arguments were used later to derive an expression for the diffusivity within a fibrous medium (Ogston et al., 1973). These and other results was adapted by Curry and co-workers for the modeling of microvascular permeability properties (Curry and Michel, 1980; Curry, 1984). The diffusion theory of Ogston does not include solute-fiber hydrodynamic interactions, which will reduce the mobility of a permeating macromolecule. Hydrodynamic interactions were considered by Phillips et al. (1989; 1990), who used Stokesian dynamics and generalized Taylor dispersion theory to compute the apparent diffusivity and the convective velocity of a spherical molecule moving through a parallel array of

cylinders. Those authors proposed that diffusivities could be estimated for other fiber arrangements by treating the fiber array as a homogeneous medium characterized by its Darcy permeability, κ. An extension of that idea to account for steric restrictions was described by Johnson et al. (1996). Their expression for K_d took the form:

$$K_d = F\left(r_s/\sqrt{\kappa}\right)S(f) \tag{1-15}$$

where F describes the effect of hydrodynamic interactions and S is a steric or tortuosity factor (see Section 2.3.3). Clague and Phillips (1996) calculated hydrodynamic interactions for the case of a spherical solute moving through a random array of cylinders by representing the sphere as a collection of point singularities and accounting for the fibers using a numerical version of slender-body theory. There are as yet no theoretical results for convection of macromolecules through random arrays of fibers.

Several methods have been used to measure hindered diffusivities of proteins and other macromolecules in polymer solutions and gels. Recent work has taken advantage of such techniques as pulsed-field-gradient NMR (Gibbs et al., 1992), holographic interferometry (Kosar and Phillips, 1995), and fluorescence recovery after photobleaching (FRAP) (Johnson et al., 1995; 1996). In contrast, very little is known about convective hindrance factors. In what appears to be the only relevant study to date, Kapur et al. (1997) studied diffusive and convective transport of two proteins, ribonuclease A and bovine serum albumin (BSA) through poly(vinylidine fluoride) membranes whose pores were filled with polyacrylamide gel.

1.4 Summary of Thesis Work

The primary purpose of this thesis work was to provide experimental values of K_c as a function of solute size and gel concentration. To complement previous results for K_d from our laboratory (Johnson et al., 1995; 1996), globular proteins and Ficoll, a crosslinked copolymer of

sucrose and epichlorohydrin, were employed with agarose gels. The advantage of agarose, beyond its ready availability, is that it possesses fibers (consisting of aggregates of α-helical polysaccharide chains) that exhibit undetectable Brownian motion (Mackie et al., 1978) and have little net charge. Thus, agarose gels appear to approximate the structural assumptions of the aforementioned fiber-matrix theories. Values of K_c were determined experimentally by measuring the sieving coefficients (Θ, the ratio of the filtrate to retentate concentration) of several macromolecules in agarose gel membranes. The rationale behind the experimental design is seen by rearranging Eq. 1-6. Given that

$$N = vC_L' \tag{1-14}$$

and defining the sieving coefficient (Θ) as

$$\Theta = \frac{C_L'}{C_0'} \tag{1-15}$$

the sieving coefficient is found to be related to the hindrance factors by

$$\Theta = \frac{\Phi K_c}{1-(1-\Phi K_c)\exp(-\mathrm{Pe})} \tag{1-16}$$

$$\mathrm{Pe} = \frac{(\Phi K_c)vL}{(\Phi K_d)D_\infty} \tag{1-17}$$

Equations 1-16 and 1-17 show that sieving coefficients can be used to determine K_c, provided that Φ and K_d can be determined independently. Values for K_d were estimated from previous data (Johnson et al., 1996), whereas the model of Ogston (1958) was used to calculate Φ. The sieving experiments and the results for the convective hindrance coefficient are discussed in detail in Chapter 2.

In order to correctly interpret experimental sieving results, it was necessary to correct these results for the effect of "concentration polarization," or the tendency of retained solutes to accumulate near the upstream surface of the membrane (see Section 3.1). In other words, experimentally what is measured is an "apparent" sieving coefficient:

$$\Theta' = \frac{C_f}{C_b} \tag{1-18}$$

where C_f is the concentration of the solute in the filtrate and C_b is the molecule concentration in the bulk retentate solution. However, what is needed in Eq. 1-16 is the "true" sieving coefficient:

$$\Theta = \frac{C_f}{C_m} \tag{1-19}$$

where C_m is the concentration of the solute at the upstream surface of the membrane. In order to correct experimental sieving results for the concentration polarization phenomenon, a model was developed in which laminar boundary layer theory was used to describe polarization in stirred ultrafiltration cells. The flow in the cell was approximated as a rigid-body rotation above a stationary surface (Bödewadt flow), with a filtration velocity that depended on the osmotic pressure of the retained solute, and therefore varied with radial position on the surface. The resulting axisymmetric convective-diffusion problem was solved using a finite difference method. The development of this model is discussed in Chapter 3. The results from the model are compared with the predictions of a stagnant film model in which the apparent and true sieving coefficients are related by

$$\Theta = \frac{\Theta'}{(1-\Theta')\exp\left(v_f / k_{sf}\right) + \Theta'} \tag{1-20}$$

where v_f is the filtration rate and k_{sf} is the stagnant film mass transfer coefficient. In evaluating the

usefulness of the stagnant film model, several methods were used to determine k_{sf}. First, the quantities in Eq. 1-20 were taken to be area averages and the area-averaged mass transfer coefficient calculated using the boundary layer model was used, in the limit of vanishing filtration rate. In other words, as might be attempted in practice, k_{sf} was obtained using mass transfer data from the same system in the absence of filtration. Second, a "hybrid" model was developed in which Eq. 1-20 was assumed to be valid locally, and local mass transfer coefficients were calculated by the boundary layer model, again in the absence of filtration. Finally, again taking the quantities in Eq. 1-20 to be area averages, the area-averaged k_{sf} was determined experimentally by measuring the reduction in filtration rate that occurred across commercial regenerated cellulose membranes when a concentrated amount of protein was added to an initially protein-free buffer. Comparisons between these results and those from the rigorous boundary layer model are presented in Chapter 3.

CHAPTER 2

Experimental Determination of Convective Hindrances in Gels

2.1 Introduction

The primary purpose of this thesis work was to provide the experimental data for the convective hindrance coefficient, K_c, for particular gel/solute combinations. To complement previous results for K_d from our laboratory (Johnson et al., 1995; 1996), globular proteins and Ficoll, a crosslinked copolymer of sucrose and epichlorohydrin, were employed with agarose gels. It was desired to determine the dependence of K_c on solute size and on gel concentration.

2.2 Methods

2.2.1 Macromolecules

Four globular proteins, bovine immunoglobulin G (IgG), bovine serum albumin (BSA), ovalbumin, and lactalbumin and a polydisperse preparation of Ficoll with a weight-average molecular weight of 70,000 (Type 70) were obtained from Sigma (St. Louis, MO) and used without further purification. The Ficoll was labelled with 5-([4,6-dichlorotriazin-2-yl]amino) fluorescein (DTAF) (Sigma) using the procedure described by De Belder and Granath (1973). Unreacted DTAF was removed by elution through 10 ml disposable desalting columns (Econo-Pac® 10 DG, Bio-Rad, Hercules, CA). Labelled Ficoll was concentrated in a 200 ml ultrafiltration cell (Model 8200, Amicon, Beverly, MA) with a 5 kD molecular weight cutoff regenerated cellulose membrane (PLCC 062 10, Millipore, Bedford, MA). Concentrated samples were freeze-dried until usage.

Fresh aqueous solutions were prepared by dissolving the macromolecules in buffer

consisting of 0.01 M sodium phosphate and 0.1 M KCl at pH 7.0. The solute concentration in all solutions was 2 mg/mL, and solutions were filtered using a 0.22 μm syringe filter (Millex®-GV Filter Unit, Millipore) prior to use in sieving experiments. All four proteins are anionic at neutral pH, but it was confirmed for three of these proteins (BSA, ovalbumin, and lactalbumin) that at this ionic strength their diffusivities are not significantly affected by electrostatic interactions, even in highly charged, sulfated agarose gels (Johnson et al., 1995). Thus, molecular charge was not expected to be a factor. To confirm this, sieving experiments using ovalbumin were performed in phosphate buffer containing 1.0 M KCl. The sieving coefficients measured in these experiments were not significantly different from those measured in buffer containing 0.1 M KCl.

2.2.2 Gel Membranes

Agarose membranes were prepared on polyester mesh supports, as done previously (Johnson et al., 1996). Slurries were produced by dissolving a measured amount of agarose powder (Type VI: high gelling temperature, Sigma, St. Louis, MO) in 10 ml 0.01 M sodium phosphate buffer containing 0.1 M KCl. They were then heated in a 90°C oven for 4.5 to 5.5 hours and shaken by hand periodically to ensure adequate mixing; an extra hour was needed for the most concentrated solutions to allow all air bubbles to escape. Membranes were cast by placing a 25 mm-diameter piece of polyester mesh (Spectra/Mesh Polyester Filters, Spectrum Medical Industries, Inc., Houston, TX) on a glass plate (also heated to 90°C) and pouring the hot agarose slurry onto it. The dimensions of the polyester mesh are shown in Figure 2.1. A second hot glass plate was placed on top, and any air was squeezed out. The plates were clamped together, placed in buffer, and stored overnight at 4°C. Membranes were prepared with agarose concentrations of 4, 6, and 8% (w/v). The volume fraction of agarose was obtained by dividing the mass fraction by 1.025 (Johnson et al., 1996).

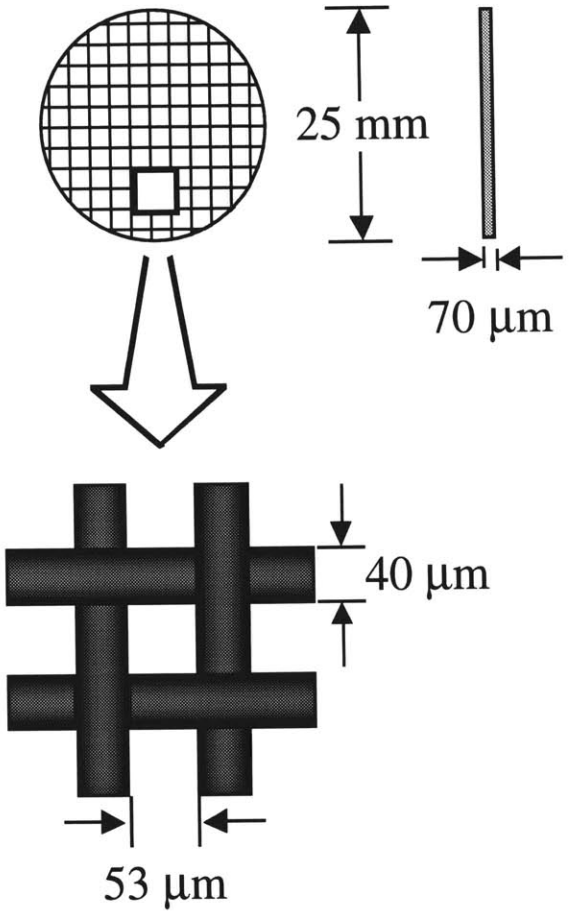

FIGURE 2.1: Dimensions of polyester mesh support for agarose membranes.

2.2.3 Darcy Permeability Measurements

The Darcy permeability of each agarose sample was determined by measuring the hydraulic permeability of the mesh-supported membrane. Membranes were mounted in a 10 mL ultrafiltration cell (Model 8010, Amicon, Beverly, MA) which was filled with the sodium phosphate/KCl buffer. The transmembrane pressure, applied using compressed nitrogen, was chosen to yield similar filtration rates for all experiments ($v_f \cong 10^{-5}$ cm/s). The pressure drop was monitored using a pressure transducer (Model DP15, Validyne Engineering, Northridge, CA), and corrections were made to account for hydrostatic pressure. The flow rate of solution through the membrane was determined by weighing the filtrate. To minimize transient effects, collections were started 10 to 30 minutes after the application of pressure. The thickness of each hydrated membrane (L) was measured using a micrometer, by placing the membrane between two glass microslides of known thickness. These measurements indicated that thicknesses were not significantly different from that of the polyester supports used (70 μm). The Darcy permeability was calculated as

$$\kappa = \frac{\mu Q L}{\beta A \Delta P} \tag{2-1}$$

where μ is the viscosity of the buffer, Q is the volumetric flow rate of buffer through the membrane, β is a factor that accounts for the presence of the polyester mesh (Johnson et al., 1996), A is the exposed membrane area, and ΔP is the pressure drop across the membrane.

The value of β for the polyester mesh supports used in this work was calculated by solving Laplace's equation for the pressure field in the gel (Johnson and Deen, 1996):

$$\nabla^2 P = 0 \tag{2-2}$$

For these calculations, the gel membrane was modeled as shown in Figure 2.2. The woven

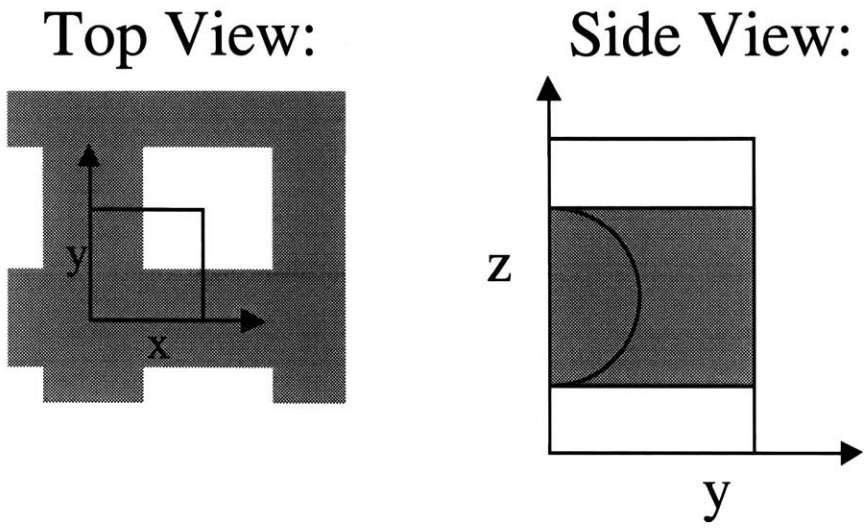

FIGURE 2.2: Model idealization of polyester mesh.

polyester mesh was modeled as a square array of intersecting cylinders 40 μm in diameter, and the total thickness of the model membrane was brought to 70 μm by adding additional "gel" above and below the mesh fibers. It was found previously (Johnson and Deen, 1996) that the value of β that is calculated is insensitive to whether this extra thickness of gel is placed above or below the mesh or distributed on either side. One quarter of the mesh opening was modeled due to symmetry, and the boundary conditions used were:

$$\mathbf{n} \cdot \nabla P = 0 \qquad \text{(on fiber surfaces and symmetry planes)} \tag{2-3}$$

$$P = \Delta P \qquad \text{(on top membrane surface)} \tag{2-4}$$

$$P = 0 \qquad \text{(on bottom membrane surface)} \tag{2-5}$$

Calculations were performed on a Silicon Graphics Indy workstation using FIDAP, a commercial finite element package (Fluent, Inc., Evanston, IL), and were based on the Galerkin method using quadratic basis functions. The FIDAP code used is located in Appendix A. Using 7,290 mesh elements it was found that $\beta = 0.510$, with an estimated error of $< 0.1\%$.

2.2.4 Sieving Measurements

Following the determination of Darcy permeability for a particular membrane, the ultrafiltration cell was emptied and refilled with sodium phosphate/KCl buffer containing 2 mg/mL solute. The stirring rate, calibrated using a strobe, was set at 220 rpm and pressure was applied again. Pressures were chosen to provide filtration rates that would result in membrane Péclet numbers of order unity for solutes (see Eq. 1-17). After a delay of 30 to 60 minutes to minimize transient effects and purge the collection line, the filtrate was collected for an additional 30 to 60 minutes. The retentate was then removed from the cell, which was rinsed and again filled with protein-free buffer. A second measurement of Darcy permeability was performed following the sieving experiment, and data from an experiment were retained only if the hydraulic permeability

changed by < 5 %. Each membrane was used only for a single sieving experiment using either one protein or the polydisperse Ficoll preparation.

For the protein experiments, solute concentrations were measured in the initial and final retentates and in the filtrate by absorbance at 280 nm with a UV spectrophotometer (Shimadzu, Columbia, MD). Retentate and filtrate samples from Ficoll experiments were analyzed using gel filtration chromatography. The column (XK 16, Pharmacia, Piscataway, NJ) was packed with an agarose/dextran composite gel (Superdex® 200, Pharmacia) and fed at 90 ml/h with a high precision pump (P-500, Pharmacia). The eluent was analyzed with a spectrofluorometric detector (RF-551, Shimadzu). Molecular size of Ficolls was related to elution time by calibrating the gel chromatography column with four narrow fractions of Ficoll (2.97, 3.77, 4.64, and 5.87 nm) obtained by special order from Pharmacia. The apparent sieving coefficient for all solutes was calculated as

$$\Theta' = \frac{C_f}{C_b} \tag{2-6}$$

where C_f and C_b are the protein concentrations of the filtrate and the bulk retentate, respectively. The value of C_b was calculated as the arithmetic average of the initial and final retentate concentrations, which differed by an average of 9.4% for all sieving experiments.

Analysis of Ficoll samples yielded a sieving curve for a continuous range of Ficoll sizes. Figure 2.3 shows example chromatograms of an initial solution, final retentate and filtrate from a sieving experiment with a 6% gel membrane. Shown in this figure is the fluorescence intensity as a function of elution time. Using the calibration information obtained from the narrow fractions of Ficoll, the same data is plotted in Figure 2.4 as a function of Ficoll size. To determine the size range over which reliable sieving coefficients could be calculated, elution profiles for each experiment were shifted by the standard deviation in the pump flow rate. The standard deviation (0.4% at 90 ml/h) was determined by pumping solute-free buffer through the column and

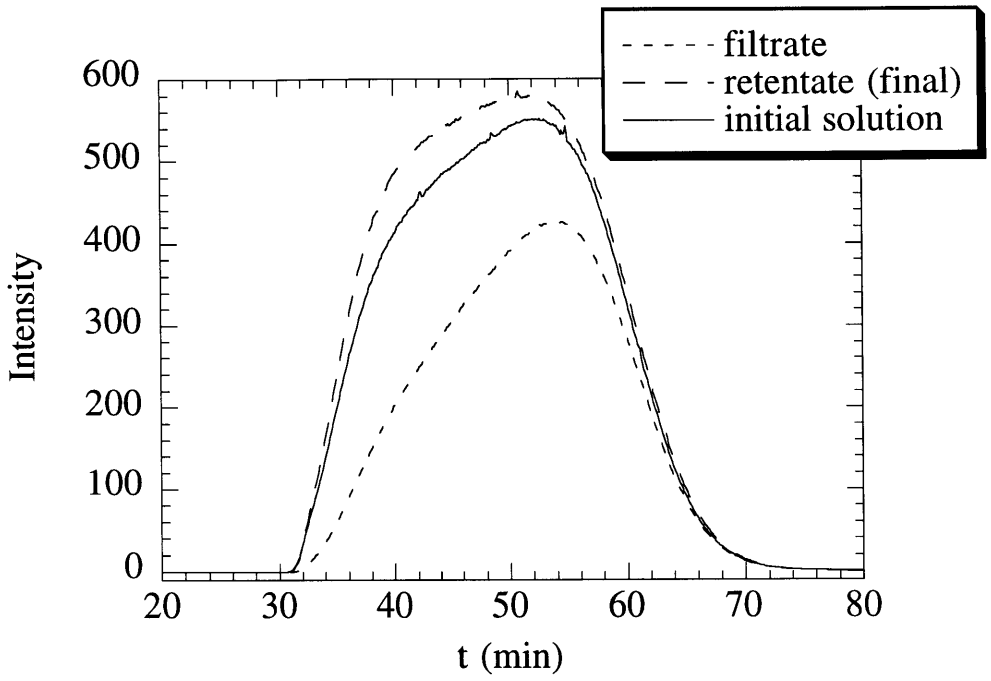

FIGURE 2.3: Example chromatograms from a Ficoll sieving experiment with a 6% agarose gel. Plotted is the fluorescence intensity in arbitrary units as a function of elution time in minutes.

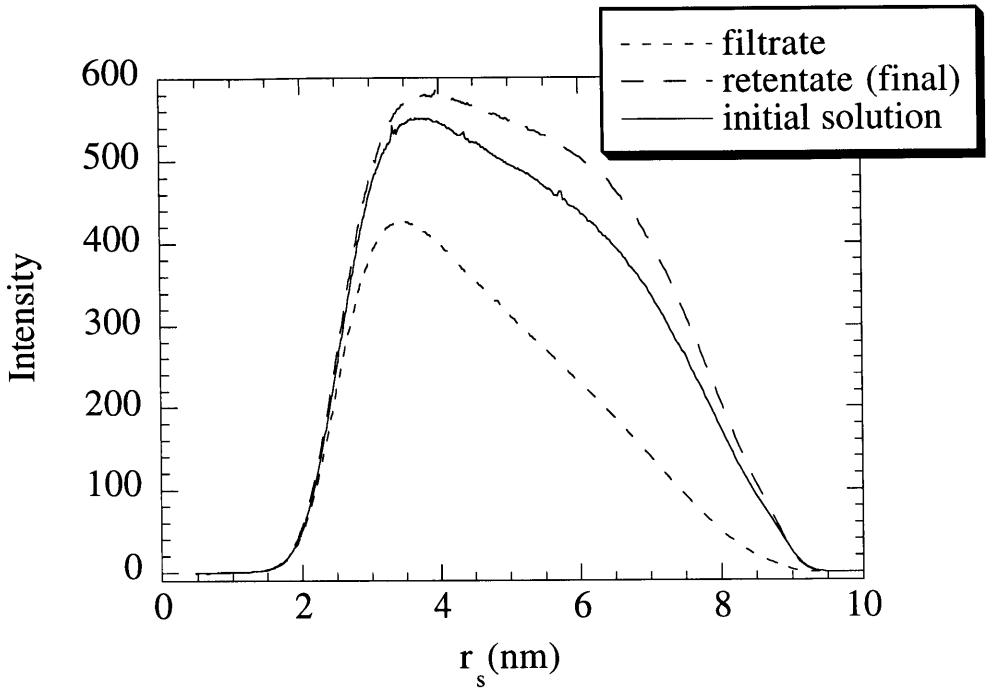

FIGURE 2.4: Example chromatograms from a Ficoll sieving experiment with a 6% agarose gel. Plotted is the fluorescence intensity in arbitrary units as a function of Ficoll Stokes-Einstein radius (nm).

repeatedly collecting and weighing the eluent. To maximize the effect of this deviation on the measured sieving coefficient, filtrate samples were shifted in one direction by this amount and initial solutions and retentates were shifted in the opposite direction. The effect of these shifts on the resulting values of the measured sieving coefficient were calculated. The percentage change in Θ' caused by these shifts for all experiments with 6% gels are shown in Figure 2.5 as a function of Ficoll molecular size. From this it was determined that for the size range of approximately 2.5 to 7 nm the uncertainty in the pump flow rate resulted in a change in the measured sieving coefficient of 5% or less. Sieving coefficients were calculated only for this range of molecular sizes.

Concentration polarization caused the protein concentration at the membrane surface (C_m) to exceed that in the bulk retentate. As stated in Section 1.4, true sieving coefficients ($\Theta = C_f/C_m$) were calculated using several methods. First, a model was developed from laminar boundary layer theory to quantify concentration polarization in stirred ultrafiltration cells. In this model the fluid flow in the cell is approximated as a rigid-body rotation above a stationary surface (Bödewadt flow), and the axisymmetric convection-diffusion problem is solved using a finite difference method. It was assumed that solutions were sufficiently dilute so that the effect of osmotic pressure on the filtration velocity at the surface was negligible. The validity of this assumption is addressed below. Given this, the filtration rate (and therefore the sieving coefficient; see Eqs. 1-16 and 1-17) used in the model was uniform over the surface of the membrane. To calculate true sieving coefficients, C_b was set equal to its measured value and Θ was varied until the mixing cup average of the filtration concentration calculated by the model was equal to the measured value of C_f.

In another approach, values for the stagnant film mass transfer coefficient, k_{sf}, were determined experimentally for the stirred cells and used in Eq. 1-20. True sieving coefficients calculated in this way for BSA, ovalbumin, and lactalbumin were reported in Johnston and Deen

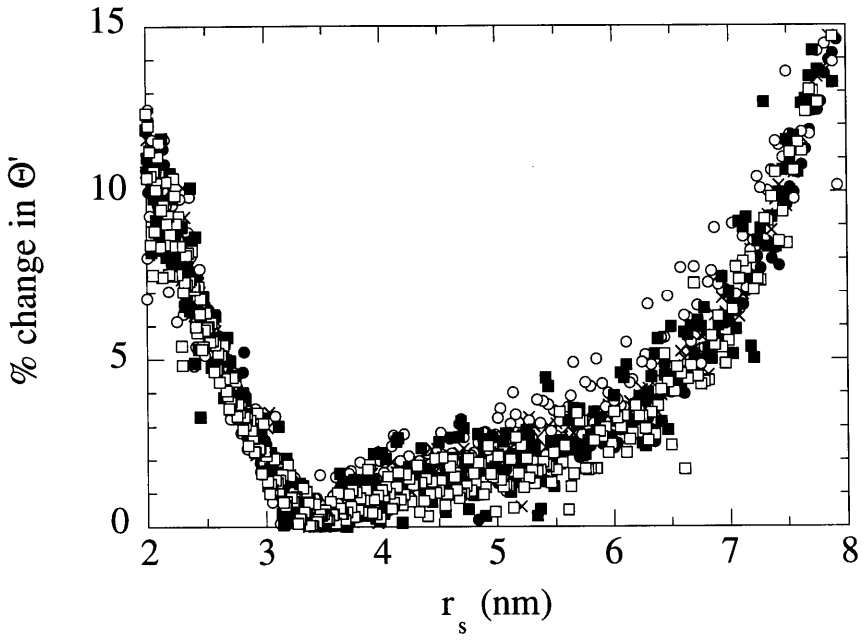

FIGURE 2.5: The percentage change in measured sieving coefficient caused by shifting experimental results by the uncertainty in the pump flow rate for all Ficoll experiments with 6% agarose gels. Results are plotted as a function of Ficoll molecular size.

(1999).[1] As seen in this paper and in Section 3.3.5, the experimentally measured stagnant film mass transfer coefficient was found to be a strong function of the filtration rate. It was found that if k_{sf} in Eq. 1-20 was corrected for the different diffusivities of the solutes and allowed to vary with the filtration rate, the stagnant film values for Θ calculated from Eq. 1-20 differed from those computed by the laminar boundary layer model by an average of only 0.9% and a maximum of 2.7%. Values of K_c calculated from these sieving coefficients were also reported in Johnston and Deen (1999).[2] It was found that these stagnant film values for K_c differed from those computed by the laminar boundary layer model by an average of only 1.2% and a maximum of 4.8%. Because of these findings and for the sake of clarity, all of the results presented here for the true sieving coefficients and for the convective hindrance factors are those obtained from the full 2-D laminar boundary layer model.

To confirm the validity of the sieving coefficient results, the mass balances for the solutes were checked. These balances were found to close to within an average of 2.2% for all nine solutes in all three gel concentrations. To verify that charge effects were absent, sieving measurements using ovalbumin and 6% agarose were also carried out in a buffer containing 1.0 M KCl. There was no significant difference between the results with 1.0 and 0.1 M KCl, indicating that electrostatic interactions were negligible. The validity omitting the effect of osmotic pressure on filtration rate in the laminar boundary layer model was tested using experiments with BSA, where the relationship between solution concentration and osmotic pressure has been reported (Vilker et al., 1981). Experiments in which sieving coefficients were lowest ($\phi = 0.078$) were considered in order to maximize the influence of osmotic pressure. The osmotic pressure

---

[1] In Johnston and Deen (1999), the apparent and true sieving coefficients for ovalbumin in 8% agarose are incorrectly given as 0.60 and 0.55, respectively. The correct values are 0.62 and 0.57. Standard deviations are reported correctly.

[2] In Johnston and Deen (1999), the K_c value for ovalbumin in 8% agarose is incorrectly given as 0.88 ± 0.10. The correct value is 0.92 ± 0.11.

difference across membranes was calculated for these experiments and compared to the applied transmembrane pressure. The concentration at the membrane surface calculated by the model (and therefore the contribution of osmotic pressure) was greatest in the center of the ultrafiltration cell (see Section 3.3.2). It was determined that the local transmembrane osmotic pressure difference never exceeded 0.6% of the applied transmembrane pressure, indicating that omitting its effect was justified.

2.3 Results and Discussion

2.3.1 Darcy Permeability

The average pressures used and the resulting filtration rates for all permeability measurements are listed in Table 2.1. The Darcy permeabilities of the agarose gels (calculated using Eq. 2-1) are listed in this table and shown graphically as a function of agarose volume fraction in Figure 2.6. For the range of volume fractions examined ($0.039 \leq \phi \leq 0.078$), κ varied by more than a factor of ten. Plotted in Figure 2.6 for comparison are the results of Johnson and Deen (1996), which are seen to be in excellent agreement with the present data. As reported in this previous paper, substantial variations in permeability were observed between nominally identical membranes, including those from the same agarose solution. Permeabilities of 4% gels ranged from 71.5 to 121.5 nm^2. Permeabilities of 6% gels ranged from 10.8 to 30.1 nm^2, while permeabilities of 8% gels ranged from 4.2 to 9.0 nm^2.

The effect of the applied transmembrane pressure on the Darcy permeabilities of the gels was investigated. This was done by preparing 4 additional membranes of each gel concentration (4, 6, and 8%) and measuring the Darcy permeabilities of these gels at five different pressures ranging from approximately 2 to 20 kPa. The results of these experiments are presented graphically in Figure 2.7. The present results indicate less of a dependence of κ on the applied pressure than suggested by Johnson and Deen (1996). In this previous study, the results of a

TABLE 2.1: Darcy permeabilities of agarose gels. Values are given as mean ± SE for 25 measurements, except for those marked with * (n = 23).

ϕ	ΔP (kPa)	v (10^{-5} cm/s)	κ (nm^2)
0.039	1.94 ± 0.05	14.20 ± 0.50	95.1 ± 2.8
0.059	5.15 ± 0.04	8.07 ± 0.35	20.3 ± 0.9
0.078	14.55 ± 0.19	6.41 ± 0.26	5.7 ± 0.2

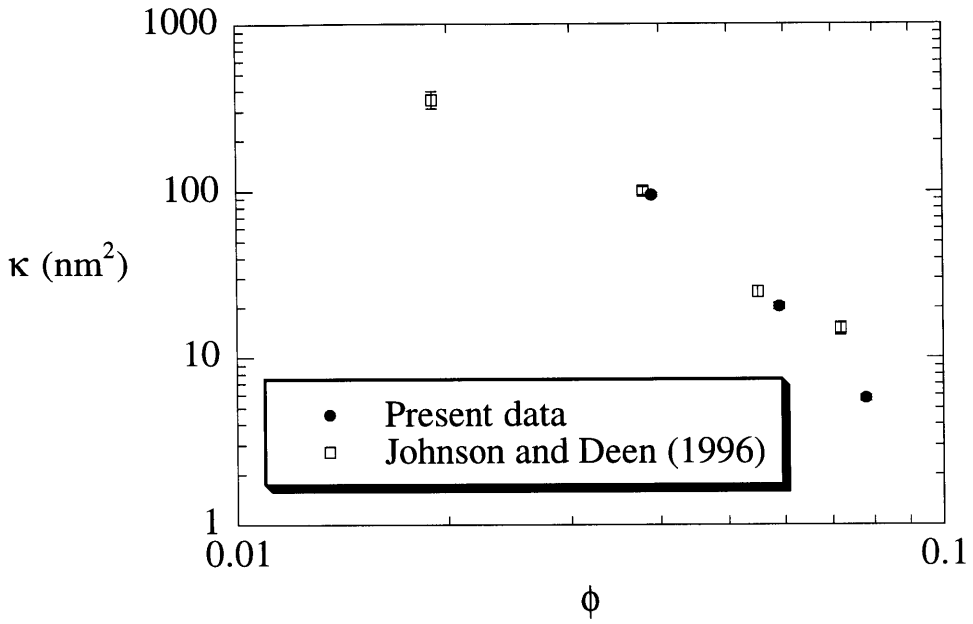

FIGURE 2.6: Darcy permeability of agarose gels, κ, as a function of the volume fraction of fibers, ϕ. Symbols show the mean ± SE (n = 5 for the data of Johnson and Deen, for present data n = 25 for 6% and 8% gels, n = 23 for 4% gels).

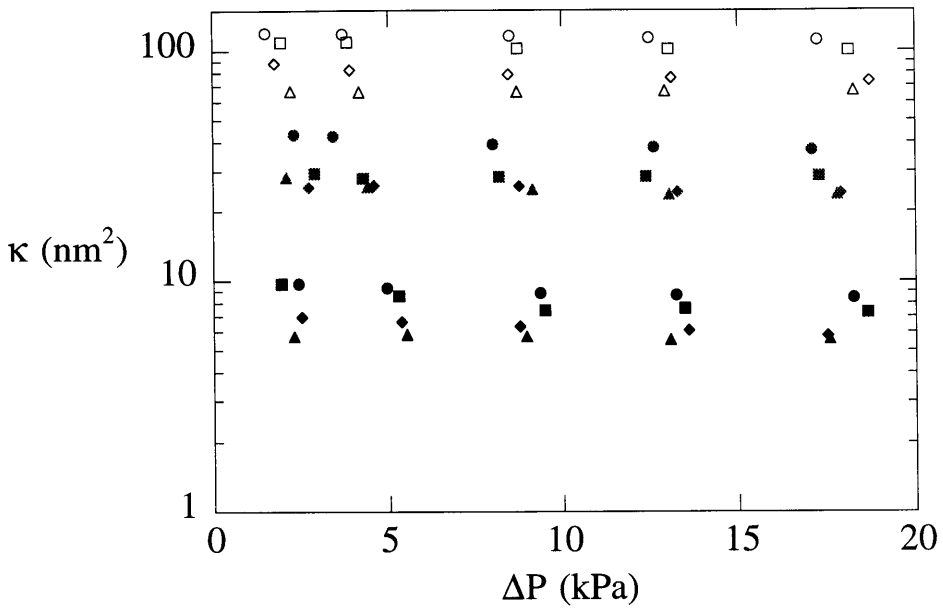

FIGURE 2.7: Darcy permeability of agarose gels, κ, as a function of the applied transmembrane pressure, ΔP. Open symbols represent 4% gels, gray symbols are 6% gels, and black symbols are 8% gels.

single gel at each of four different values of ϕ were presented. Darcy permeabilities for each gel were measured at five different pressures in the range stated above. It was found that for each gel the permeability varied roughly linearly with the applied pressure. The slopes of the fitted lines (in nm^2/kPa) were given as -1.59, -1.35, and -0.488 for ϕ = 0.038, 0.055, and 0.072, respectively. In the present study these slopes (given as mean ± SE, also in nm^2/kPa) were calculated as -0.46 ± 0.18, -0.21 ± 0.09, and -0.08 ± 0.02 for ϕ = 0.039, 0.059, and 0.078, respectively. One explanation for the difference in these results is the fact that in the previous study (Johnson, 1995), it was stated that the thickness of gel membranes (prepared on the same 70 μm mesh as in the present study) was as much as 100 μm. This indicates the presence of an additional gel layer either above or below (or on both sides) of the polyester mesh. It is possible that this extra gel is more easily compressed by applied pressure than the gel within the polyester mesh. As stated in Section 2.2.3, the thickness of gel membranes prepared in this study was not found to be significantly more than the 70 μm mesh thickness.

2.3.2 Sieving Coefficient

The sieving data for the four globular proteins are summarized in Table 2.2. Sieving data for five selected sizes of Ficoll are summarized in Table 2.3. The Stokes-Einstein radii (r_s) of BSA, ovalbumin, and lactalbumin are those determined by Johnson et al. (1996) from measurements of D_∞ by FRAP. The Stokes-Einstein radius of IgG is taken from Potschka (1986). Molecular sizes of Ficoll were calculated from elution time as described in Section 2.2.4. All of the true sieving coefficients presented here were calculated from the full numerical laminar boundary layer model (see Chapter 3) as described above in Section 2.2.4.

As expected, the apparent sieving coefficient (Θ') and true sieving coefficient (Θ) both decreased with increasing r_s or increasing ϕ. The correction for concentration polarization was modest for most gel/solute combinations, such that Θ' exceeded Θ by an average of only 11%. The difference between measured and true sieving coefficients increased with increasing solute size

TABLE 2.2: Sieving coefficient results for proteins. Sieving coefficients are given as mean ± SE for 5 measurements, except for * (n = 3).

Protein	r_s (nm)	ϕ	Θ'	Θ
lactalbumin	2.1	0.039	1.01 ± 0.002 *	1.00 ± 0.003 *
		0.059	0.95 ± 0.005	0.93 ± 0.006
		0.078	0.81 ± 0.014	0.79 ± 0.014
ovalbumin	3.0	0.039	0.97 ± 0.002	0.95 ± 0.002
		0.059	0.83 ± 0.011	0.80 ± 0.010
		0.078	0.62 ± 0.023	0.58 ± 0.023
BSA	3.6	0.039	0.94 ± 0.005	0.90 ± 0.007
		0.059	0.68 ± 0.018	0.63 ± 0.018
		0.078	0.44 ± 0.032	0.40 ± 0.028
IgG	5.2	0.039	0.85 ± 0.008	0.77 ± 0.010
		0.059	0.41 ± 0.026	0.36 ± 0.021
		0.078	0.28 ± 0.016	0.22 ± 0.013

TABLE 2.3: Sieving coefficient results for selected Ficolls. Sieving coefficients are given as mean ± SE for 5 measurements.

r_s (nm)	ϕ	Θ'	Θ
3.0	0.039	0.96 ± 0.009	0.94 ± 0.012
	0.059	0.80 ± 0.023	0.76 ± 0.022
	0.078	0.68 ± 0.017	0.63 ± 0.012
4.0	0.039	0.92 ± 0.008	0.88 ± 0.011
	0.059	0.67 ± 0.031	0.62 ± 0.028
	0.078	0.49 ± 0.022	0.43 ± 0.014
5.0	0.039	0.88 ± 0.012	0.82 ± 0.016
	0.059	0.55 ± 0.037	0.49 ± 0.032
	0.078	0.33 ± 0.025	0.28 ± 0.015
6.0	0.039	0.83 ± 0.012	0.74 ± 0.014
	0.059	0.43 ± 0.040	0.37 ± 0.033
	0.078	0.21 ± 0.022	0.17 ± 0.012
7.0	0.039	0.77 ± 0.012	0.65 ± 0.013
	0.059	0.32 ± 0.038	0.26 ± 0.028
	0.078	0.13 ± 0.016	0.09 ± 0.008

and increasing gel concentration due to increased extent of polarization. For the largest Ficoll at ϕ = 0.078, Θ' exceeded Θ by an average of 35%. True sieving coefficients are plotted for all solutes in the least concentrated 4% gel in Figure 2.8. Results for 6% and 8% agarose are plotted in Figures 2.9 and 2.10, respectively. As can be seen in these three figures, the agreement between sieving coefficients of Ficolls and proteins of similar size was very good. Some of the differences between the proteins and Ficolls may have been due to differences in the Darcy permeabilities of the gels used in each set of experiments. For example, in Figure 2.9 the average sieving coefficient for IgG appears to be low compared to that for Ficolls of similar size. However, the average permeability of the 6% gels used in the IgG experiments was 15.7 nm^2, while the average permeability of the 6% gels used in the Ficoll experiments was over 30% higher at 20.6 nm^2.

2.3.3 Convective Hindrance Coefficient

To calculate K_c from Θ using Eq. 1-10, it was necessary to estimate Φ and K_d. Following Ogston (1958), partition coefficients were calculated for each gel-protein combination using

$$\Phi = \exp\left[-\phi\left(1+\frac{r_s}{r_f}\right)^2\right] \equiv \exp(-f) \tag{2-7}$$

where r_f is the number-average radius of an agarose fiber, calculated from the SAXS data of Djabourov et al. (1989) to be 1.9 nm. The use of Eq. 2-7 is justified by its success in correlating experimental data for the partitioning of proteins and Ficoll in agarose gels with concentrations ranging from 2 to 8% (Johnson, 1995). Diffusive hindrance coefficients for all solutes except IgG were evaluated using the data of Johnson et al. (1996) for these macromolecules in agarose gels. Values of K_d for selected sizes of Ficoll were obtained by curve fitting the data for Ficoll in this previous paper. Due to the lack of data for the hindered diffusion of IgG, it was assumed that K_d for this protein was equal to that obtained for a Ficoll molecule of identical size.

Because the gel properties obtained previously did not exactly match those of the present

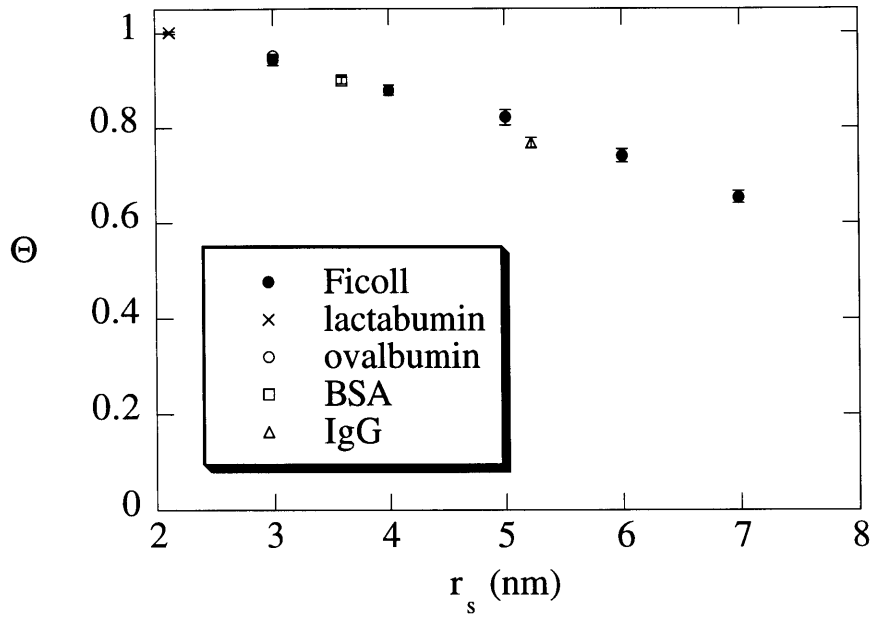

FIGURE 2.8: True sieving coefficients, Θ, for solutes as a function of the solute size, r_s, in 4% agarose gels. Symbols show the mean ± SE (n = 5, except for lactalbumin, where n = 3).

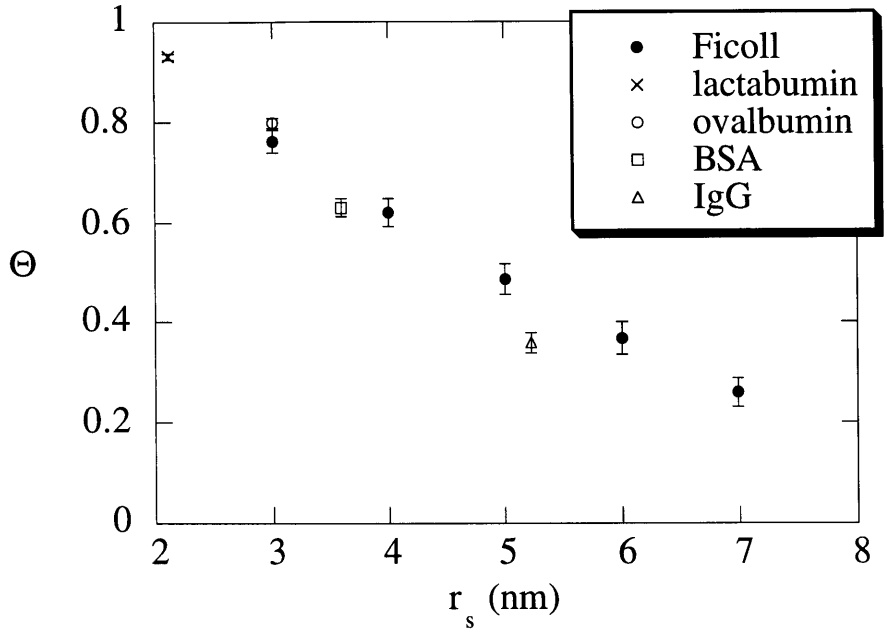

FIGURE 2.9: True sieving coefficients, Θ, for solutes as a function of the solute size, r_s, in 6% agarose gels. Symbols show the mean ± SE (n = 5).

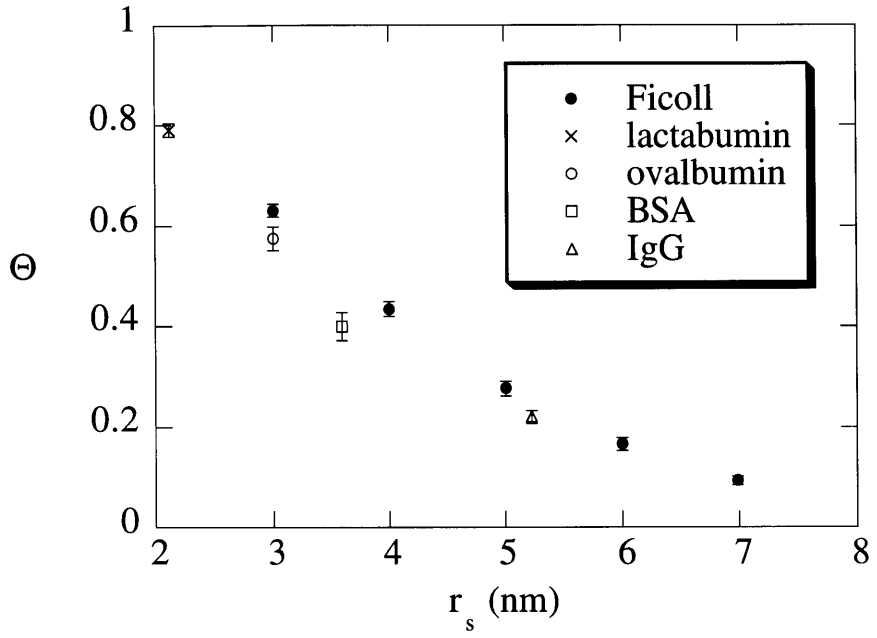

FIGURE 2.10: True sieving coefficients, Θ, for solutes as a function of the solute size, r_s, in 8% agarose gels. Symbols show the mean ± SE (n = 5).

study, the experimental results for K_d were adjusted by using the effective medium theory of Johnson et al. (1996) to describe the dependence on κ and ϕ. The expressions used were

$$K_d = F\left(r_s / \sqrt{\kappa}\right) S(f) \tag{2-8}$$

$$F\left(r_s / \sqrt{\kappa}\right) = \left[1 + \left(r_s / \sqrt{\kappa}\right) + \frac{1}{9}\left(r_s / \sqrt{\kappa}\right)^2\right]^{-1} \tag{2-9}$$

$$S(f) = \exp\left(-0.84 f^{1.09}\right) \tag{2-10}$$

where F describes the reduction in diffusivity due to solute-fiber hydrodynamic interactions (based on Brinkman's equation) and S is a steric or tortuosity factor. The expression for F is from Solomentsev and Anderson (1996). Their result (as given by Eq. 2-9) represents a correction to the Brinkman factor employed by Johnson et al. (1996) and others; the difference is the coefficient "1/9" instead of "1/3." The expression for S comes from the results of Brownian dynamics simulations of Johansson and Löfroth (1993).

The results for K_c for the four globular proteins and selected Ficolls are shown in Tables 2.4 and 2.5, respectively, together with the corresponding values of ϕ, κ, Φ, and K_d. Again, all of the results presented here for the convective hindrance coefficient were calculated from true sieving coefficients obtained using the full 2-D laminar boundary layer model. The agreement between K_c values calculated for globular proteins and Ficolls of similar size is good. However, this agreement was not as good as that observed in the case of the true sieving coefficients. In other words, small differences in true sieving coefficients resulted in larger differences in convective hindrance coefficients. Similar agreement between K_d values for proteins and Ficolls was observed by Johnson et al. (1996). Determination of convective hindrance coefficients allowed for the final calculation of membrane Péclet numbers for the sieving experiments (Eq. 1-17). As stated in Section 2.2.4, a Péclet number of order unity was desired for all experiments.

TABLE 2.4: Partition and hindrance coefficients for proteins. Hindrance coefficients are given as mean ± SE for 5 measurements, except for those marked with * (n = 3).

Protein	ϕ	κ (nm^2)	Φ	K_d	K_c
lactalbumin	0.039	82.1 ± 6.1	0.84	0.65 ± 0.005 *	1.19 ± 0.004 *
	0.059	22.7 ± 2.0	0.77	0.45 ± 0.006	1.18 ± 0.012
	0.078	5.1 ± 0.3	0.71	0.28 ± 0.005	1.05 ± 0.030
ovalbumin	0.039	111.0 ± 2.3	0.77	0.62 ± 0.001	1.23 ± 0.003
	0.059	22.7 ± 1.4	0.68	0.40 ± 0.006	1.14 ± 0.024
	0.078	5.6 ± 0.4	0.60	0.24 ± 0.005	0.92 ± 0.047
BSA	0.039	88.2 ± 4.2	0.72	0.63 ± 0.004	1.24 ± 0.010
	0.059	20.0 ± 1.2	0.61	0.36 ± 0.006	0.97 ± 0.039
	0.078	5.1 ± 0.5	0.52	0.21 ± 0.008	0.68 ± 0.074
IgG	0.039	97.6 ± 6.8	0.58	0.43 ± 0.006	1.33 ± 0.018
	0.059	15.7 ± 1.7	0.44	0.27 ± 0.011	0.78 ± 0.060
	0.078	6.8 ± 0.1	0.33	0.22 ± 0.002	0.65 ± 0.041

TABLE 2.5: Partition and hindrance coefficients for selected Ficolls. Hindrance coefficients are given as mean ± SE for 5 measurements.

r_s (nm)	ϕ	κ (nm^2)	Φ	K_d	K_c
	0.039	91.5 ± 3.1	0.77	0.58 ± 0.003	1.21 ± 0.017
3.0	0.059	20.6 ± 2.6	0.67	0.44 ± 0.013	1.04 ± 0.057
	0.078	6.1 ± 0.8	0.59	0.30 ± 0.012	1.01 ± 0.032
	0.039		0.69	0.51 ± 0.003	1.28 ± 0.016
4.0	0.059	same	0.57	0.38 ± 0.014	1.04 ± 0.068
	0.078		0.47	0.26 ± 0.012	0.89 ± 0.039
	0.039		0.60	0.44 ± 0.003	1.38 ± 0.027
5.0	0.059	same	0.46	0.31 ± 0.013	1.04 ± 0.081
	0.078		0.36	0.22 ± 0.011	0.76 ± 0.047
	0.039		0.51	0.37 ± 0.003	1.46 ± 0.028
6.0	0.059	same	0.36	0.25 ± 0.011	1.01 ± 0.096
	0.078		0.26	0.18 ± 0.010	0.63 ± 0.051
	0.039		0.43	0.30 ± 0.003	1.54 ± 0.031
7.0	0.059	same	0.27	0.19 ± 0.009	0.94 ± 0.105
	0.078		0.18	0.15 ± 0.009	0.51 ± 0.049

Because all sizes of Ficoll were run in a single filtration experiment, this necessarily resulted in a range of Péclet numbers. Overall, Péclet numbers ranged from 0.9 to 15.8.

The results for K_c as a function of solute size for all solutes in 4% agarose are shown graphically in Figure 2.11. Similar results for 6% and 8% agarose are shown in Figures 2.12 and 2.13, respectively. Although Φ and K_d decrease monotonically with increasing molecular size or gel concentration, the convective hindrance coefficient does not display this monotonic behavior. In 4% agarose (Figure 2.10), K_c increases with increasing solute size from a theoretical value of 1 for a point-sized solute to as high as 1.54 for the largest Ficoll reported here. In 6% agarose (Figure 2.11), K_c was found first to increase from unity with increasing solute size and then decrease as solute size was increased further. This trend is slightly more apparent in the globular proteins studied. Although the same behavior was observed for the Ficolls, none of the K_c values calculated for Ficoll were significantly different from unity in this gel concentration. In 8% agarose (Figure 2.13), $K_c > 1$ for only the smallest molecule studied (lactalbumin). Otherwise, K_c was observed to decrease with increasing solute size down to an average of 0.51 for the largest Ficoll studied.

Also plotted in Figures 2.11 through 2.13 for comparison are the theoretical predictions for K_c for a parallel array of fibers from Phillips et al. (1990). The data and theory are in qualitative agreement; in particular, note the prediction that $K_c > 1$ for intermediate values of ϕ. This is due to the fact that the finite size of the solute prevents it from sampling regions near solid boundaries, where the fluid velocity is lowest. Both the data and the theory show that as molecular size and/or gel concentration increases, K_c decreases to values below 1. This behavior is a result of the hindering effect of the fibers, which causes the solute velocity to fall below the average fluid velocity. However, although the theory predicts this decline in K_c at $\phi = 0.039$, experimental values of K_c are continually increasing with increasing solute size at this gel concentration, even for the largest solutes studied. This decline in K_c is not observed in the data from agarose until the gel becomes more concentrated. Note also that the theory predicts that as solute size is increased at a

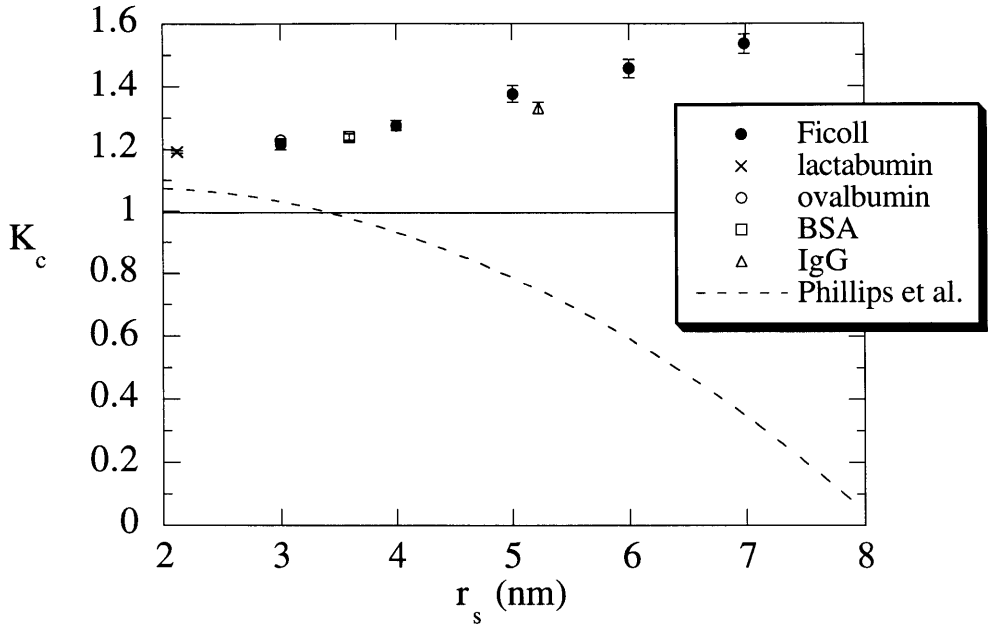

FIGURE 2.11: Values of the convective hindrance coefficient, K_c, for solutes as a function of molecular size, r_s, in 4% agarose gels. The dotted line is the result of the Phillips et al. (1990) theory for parallel arrays of fibers.

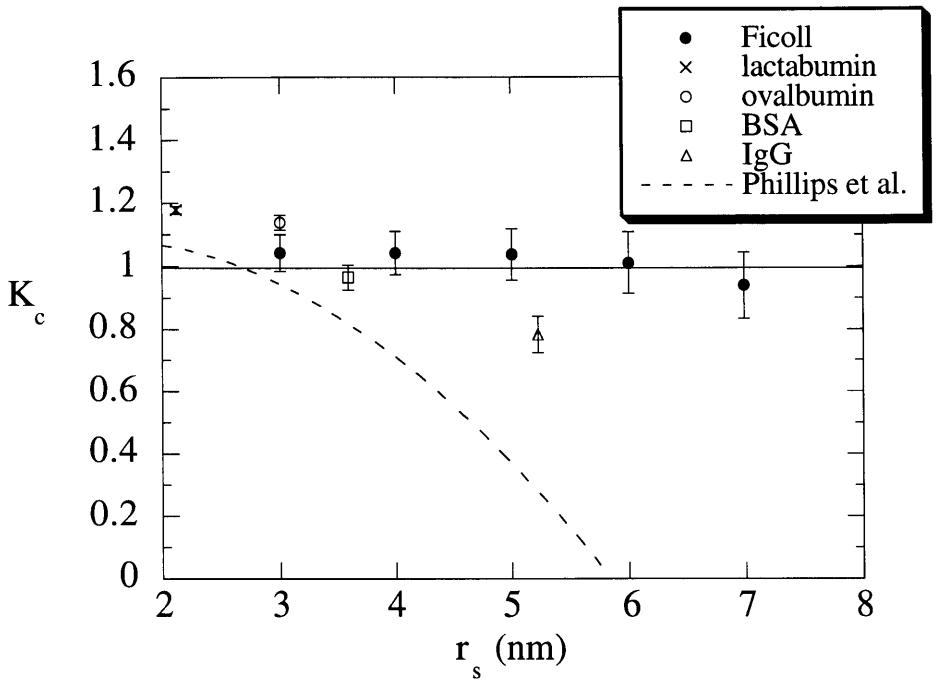

FIGURE 2.12: Values of the convective hindrance coefficient, K_c, for solutes as a function of molecular size, r_s, in 6% agarose gels. The dotted line is the result of the Phillips et al. (1990) theory for parallel arrays of fibers.

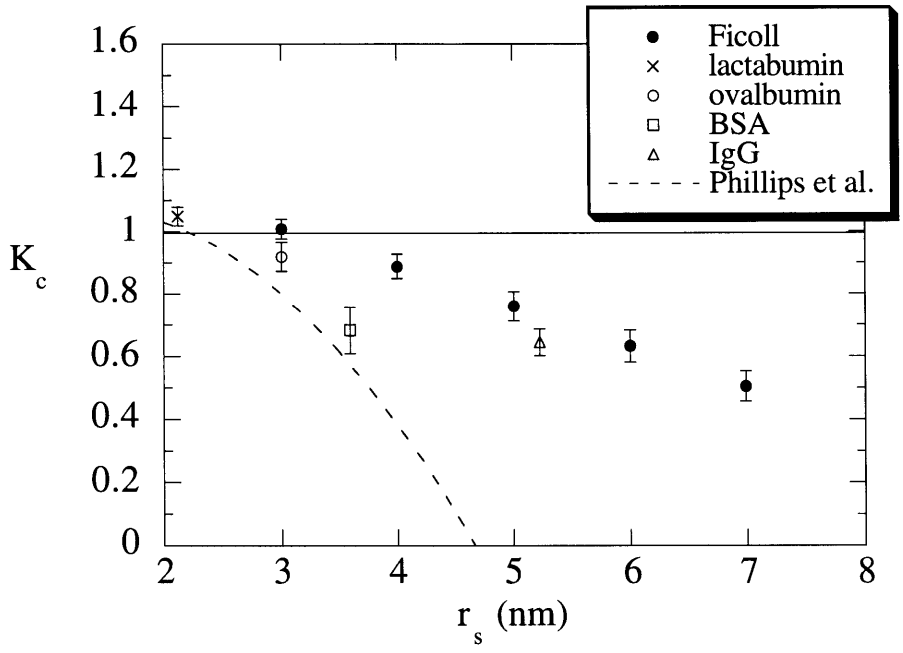

FIGURE 2.13: Values of the convective hindrance coefficient, K_c, for solutes as a function of molecular size, r_s, in 8% agarose gels. The dotted line is the result of the Phillips et al. (1990) theory for parallel arrays of fibers.

given ϕ, eventually $K_c \rightarrow 0$. This is due to the fact that the fiber array considered by the theory is oriented in a parallel lattice. As solute size increases, eventually the permeating molecule becomes too large to fit through the space size of the lattice. Because the fibers of agarose gels are randomly oriented, this behavior is not observed experimentally since there inevitably exist gaps in the gel which are large enough to permit passage of even the largest solutes. The lack of quantitative agreement between the data and the theory is not surprising due to the random orientation of agarose fibers. Indeed it has also been found that the diffusivities of proteins and Ficoll in agarose gels are more accurately explained by a model with random fiber orientation. Although the theory for parallel fibers also predicts that $K_d \rightarrow 0$ at a given ϕ, this behavior was not observed in experiments with agarose gels (Johnson et al., 1996).

The discussion thus far has viewed ϕ as the primary variable that distinguishes one agarose membrane from another. However, one might also regard the Darcy permeability as the distinguishing characteristic; κ and ϕ are, of course, inversely related (see Figure 2.6). Because of the variations in κ from sample to sample, a plot of K_c versus κ might be expected to reveal a more continuous trend. Such a plot is shown for the globular proteins studied in Figure 2.14, where it is seen that for all four proteins, K_c increased with increasing Darcy permeability. At smaller values of κ, K_c values were smallest for the largest protein (IgG). In other words, the hindering effect of the fibers had the greatest impact on the transport of the largest solute. Similar behavior was observed with the Ficolls studied. At larger values of κ the trend was reversed, with K_c values being smallest for the smallest protein (lactalbumin). In this region, $K_c > 1$ and the deviation from unity was caused by the fibers excluding the solute from the regions of lowest fluid velocity. This inaccessible region was largest for the largest solutes, causing K_c to deviate more from unity as solute size was increased. Again, similar behavior was observed with the Ficolls studied. Finally, it seemed that K_c for all solutes was more sensitive to changes in κ at smaller values of the Darcy permeability. In principle, $K_c \rightarrow 0$ for all macromolecules as $\kappa \rightarrow 0$. As κ was increased from zero, K_c increased rapidly with increasing Darcy permeability such that $K_c > 1$

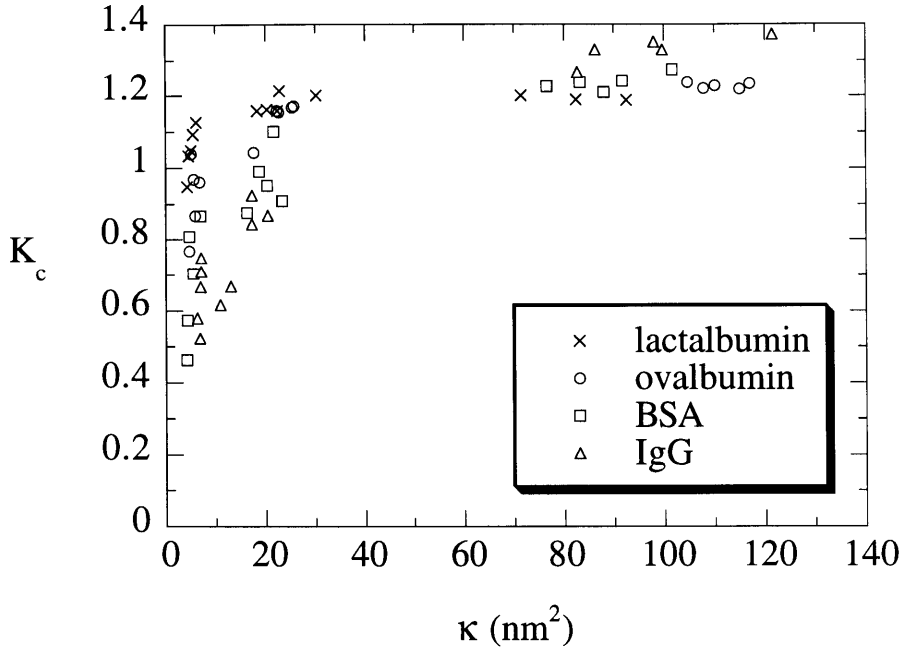

FIGURE 2.14: Values of the convective hindrance coefficient, K_c, for proteins as a function of the agarose Darcy permeability, κ.

for all solutes by $\kappa \cong 30$ nm^2. At larger values of the Darcy permeability, K_c was much less sensitive to changes in κ. For example, studies with IgG in 4% agarose showed only an 8.5% increase in K_c when κ was increased 46.9% from 83 to 122 nm^2. Just as $K_c \to 1$ as $r_s \to 0$, it is expected that $K_c \to 1$ as $\kappa \to \infty$. However at the Darcy permeabilities studied this eventual decrease in K_c with increasing κ was not observed.

The effect of uncertainties in estimates for Φ and K_d on the calculation of K_c were investigated. This was done by taking all of the data for sieving coefficients of solutes, changing the calculated values of either Φ or K_d by a specified amount and recalculating K_c. Increasing Φ by 10% resulted in an average decrease in K_c of 9.9%. Decreasing Φ by 10% resulted in an average increase in K_c of 12.0%. The convective hindrance coefficient was much less sensitive to changes in K_d. Increasing K_d by 10% resulted in an average decrease in K_c of only 0.9%. Decreasing K_d by 10% resulted in an average increase in K_c of only 0.8%. These results are not surprising given the form of Eqs. 1-16 and 1-17.

The current results can be compared with some previous work on hindered convection of solutes in pores by considering the filtration reflection coefficient, σ_f, which is given by Eq. 1-10. As stated in Section 1.3.2, Anderson and Malone (1974) derived an expression for the osmotic reflection coefficient (σ_o) for neutral spheres in cylindrical pores (Eq. 1-13), and Anderson (1981) found that result to be a good approximation also for the filtration reflection coefficient in cylindrical pores, and for either reflection coefficient in straight pores of noncircular cross-section. Indeed, as seen in Figure 1.3, the filtration and osmotic reflection coefficients for membranes consisting of long, cylindrical pores are very similar. Curry and Michel (1980) speculated that Eq. 1-13 may be applied also to fiber-matrix membranes. To test whether that is true for agarose, the present results are compared with the predictions of Eq. 1-13 in Figures 2.15 through 2.17. Equation 1-13 did a remarkably good job of predicting values of σ_f for solutes in 4% agarose gels (see Figure 2.15). However, as ϕ was increased, the experimental behavior of σ_f as a function of Φ changed, and the agreement between the data and Eq. 1-13 worsened. Two possibilities exist

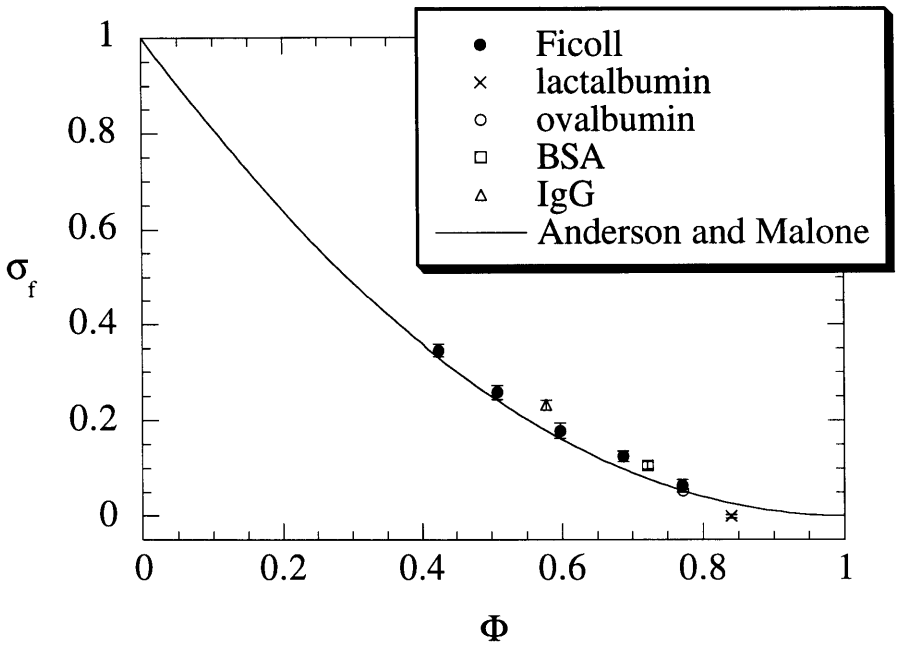

FIGURE 2.15: Values of the filtration reflection coefficient, σ_f, for solutes as a function of the partition coefficient, Φ in 4% agarose membranes. The solid line is the theoretical expression developed by Anderson and Malone (1974) (Eq. 1-13).

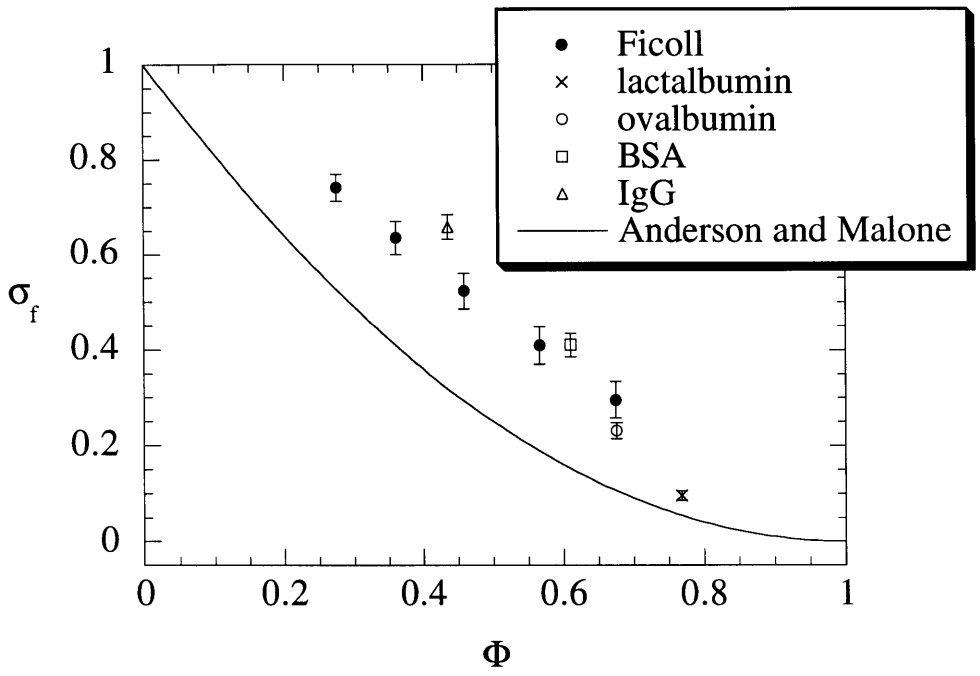

FIGURE 2.16: Values of the filtration reflection coefficient, σ_f, for solutes as a function of the partition coefficient, Φ in 6% agarose membranes. The solid line is the theoretical expression developed by Anderson and Malone (1974) (Eq. 1-13).

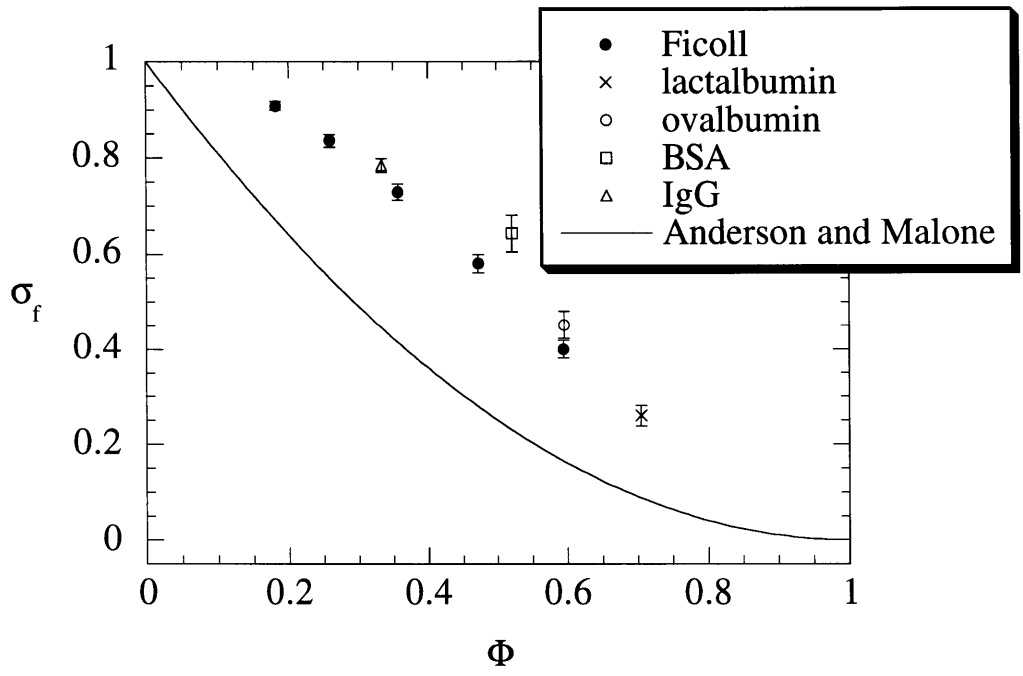

FIGURE 2.17: Values of the filtration reflection coefficient, σ_f, for solutes as a function of the partition coefficient, Φ in 8% agarose membranes. The solid line is the theoretical expression developed by Anderson and Malone (1974) (Eq. 1-13).

pertaining to the agreement between Eq. 1-13 and the experimental data for solutes in 4% agarose membranes. The first is that something in the structure of agarose causes the gel membranes to present the same hindrances to solutes as porous membranes in the limit of small gel concentration. Testing gels where $\phi < 0.039$ would provide information as to whether or not the behavior observed in 4% agarose represents an asymptotic lower limit. However, agarose membranes with $\phi < 0.039$ were not studied due to the lack of data for hindered diffusion at lower gel concentrations and the lack of structural integrity of the gels. Also, it was believed that with the solutes used this would not provide useful information as in most cases it is likely that the reflection coefficient would be very close to zero. The second possible explanation is that the agreement observed in Figure 2.15 is coincidental. Although it is possible that the data obtained for 4% agarose does represent an asymptotic limit in the behavior of the filtration reflection coefficient, it seems more likely that the agreement between this data and Eq. 1-13 is largely coincidental.

Kapur et al. (1997) measured the reflection coefficients of ribonuclease A (RNAse) and BSA using poly(vinylidine fluoride) membranes whose pores were filled with polyacrylamide gel. The polyacrylamide fiber volume fraction was varied from 0.04 to 0.09. Estimating partition coefficients from hindered diffusion studies carried out using these same membranes, they found good agreement between their data for BSA and the prediction of Eq. 1-13. However, their data for RNAse deviated significantly from this model. In this paper the authors presented the following empirical equation which was a fit to their experimental data for both solutes:

$$1-\sigma_f = \left\{1+127\left[\left(\frac{r_s}{r_f}\right)\phi\right]^4\right\}^{-1} \tag{2-11}$$

The present experimental data is plotted in Figure 2.18 along with Eq. 2-11. Although it appears that the data may be expressed entirely as a function of the proposed variable $((r_s/r_f)\phi)$, the agreement between the present data and Eq. 2-11 is poor. An analogous fit to the present data is

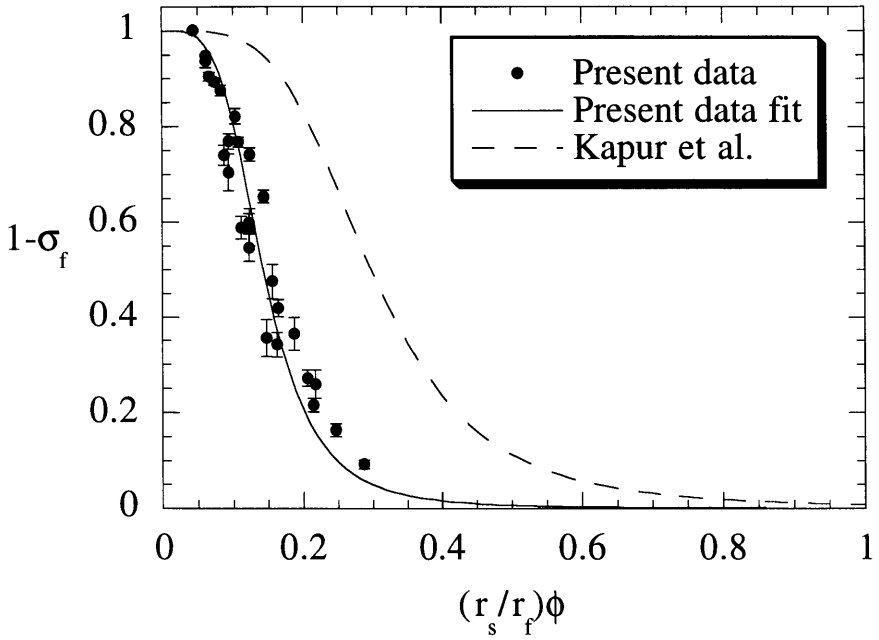

FIGURE 2.18: The sieving coefficient in the limit of infinite membrane Péclet number ($1-\sigma_f$) for solutes in agarose gels. The solid line is the fit of the present data (Eq. 2-12). The dotted line is the empirical correlation of Kapur et al. (1997) (Eq. 2-11).

given by

$$1-\sigma_f = \left\{1+2400\left[\left(\frac{r_s}{r_f}\right)\phi\right]^4\right\}^{-1} \tag{2-12}$$

The lack of quantitative agreement between the two sets of data is not surprising considering the structural differences between the membranes prepared here and the polyacrylamide/poly(vinylidine fluoride) membranes prepared in this previous work. Kapur et al. (1997) also found differences between the diffusive hindrance coefficient behavior they observed in their membranes and that reported by Johnson et al. (1996) for agarose.

2.4 Conclusions

Novel data were obtained for the convective hindrance coefficients of proteins and Ficolls in agarose gels of varying concentration. Aside from qualitative trends, these results are not represented well by the available theories either for parallel arrays of fibers (Figures 2.10 through 2.12) or for straight pores (Figures 2.14 through 2.16). Given evidence from previous partitioning and diffusion data that an agarose gel is better represented as a randomly oriented array of fibers, the large quantitative discrepancies between the data and models are not entirely surprising. Thus, the present results suggest that there is a need to extend theories of hindered convection to random arrays of fibers. Given the paucity of data on the convective transport of macromolecules in gels, additional experiments using well-characterized materials would also be of value.

CHAPTER 3

Concentration Polarization in Stirred Ultrafiltration Cells

3.1 Introduction

A well-known phenomenon in ultrafiltration, termed "concentration polarization," is the tendency of retained solutes to accumulate near the upstream surface of a membrane. High solute concentrations at the membrane surface reduce filtration rates (either osmotically or by surface blockage), and also tend to increase solute passage through the membrane. Thus, concentration polarization both degrades separations and complicates efforts to use sieving measurements to characterize membranes.

The simplest description of concentration polarization is derived from a stagnant film model, used by Sherwood et al. (1965) to analyze reverse osmosis and first applied to ultrafiltration by Michaels (1968). The stagnant film model has been used in many subsequent ultrafiltration studies (e.g., Opong and Zydney, 1991; Zydney, 1997; Johnston and Deen, 1999). In this approach, attention is focused on a thin layer of fluid next to the membrane, and a one-dimensional problem is obtained by assuming that the solute concentration depends only on distance from the membrane surface. Only convection and diffusion normal to the membrane are considered explicitly. The effects of convective transport parallel to the membrane surface are embedded in the value of the effective film thickness (δ). The analytical solution to this one-dimensional problem yields an expression for what is termed the "polarization factor" (B),

$$B \equiv \frac{C_m - C_f}{C_b - C_f} = \exp\left(\frac{v_f}{k_{sf}}\right) \tag{3-1}$$

where C_m, C_f, and C_b are concentrations at the membrane surface, in the filtrate, and in the bulk

retentate solution, respectively, and v_f is the filtrate velocity (i.e., the volume flux relative to the membrane). The mass transfer coefficient for the stagnant film model (k_{sf}) is related to the solute diffusivity (D) and film thickness by $k_{sf} = D/\delta$. Equation 3-1 captures the essential feature of concentration polarization, which is that it is worsened as v_f/k_{sf} is increased. Only for $v_f/k_{sf} \to 0$ does $B \to 1$, indicating that polarization is negligible.

Equation 3-1 is attractive because of its simplicity, but its predictive ability is limited by the unknown nature of δ for many systems. Although δ can be estimated from experimental information on the mass transfer coefficient for a given solute and a given filtration rate, there is no guarantee that the same value of δ will be applicable to other conditions, as one might hope. Indeed, an analysis of ultrafiltration data for bovine serum albumin (BSA) solutions in small stirred cells yielded apparent values of k_{sf} (and hence δ) that were quite sensitive to v_f (see Section 3.2 and Johnston and Deen, 1999). Moreover, even for mass transfer in systems without filtration, scaling arguments based on laminar boundary layer theory show that effective film thicknesses must vary with D (e.g., Deen, 1998, p. 422-425).

More rigorous analyses of concentration fields in ultrafiltration are complicated by the fact that such problems are usually made nonlinear by the dependence of v_f on the solute concentration. That is, the osmotic pressure opposing filtration is determined by the solute concentration at the upstream membrane surface. Unless the osmotic pressure is much smaller than the applied transmembrane pressure, this precludes attempts to compute the velocity field without simultaneously addressing the mass transfer problem. In concentrated solutions, the complexity may be exacerbated by variable viscosities and/or diffusivities. Nonetheless, detailed analyses are available for certain geometries. A number of authors have computed two-dimensional concentration fields for laminar crossflow ultrafiltration in tubes or parallel-plate channels (Shen and Probstein, 1977; Gill et al., 1988; Denisov, 1994; Bhattacharjee et al., 1999). Other systems for which there have been detailed analyses include spiral wound membrane modules (Madireddi et al., 1999) and two-dimensional stagnation flow (Kozinski and Lightfoot, 1971). Some authors

have employed a "hybrid" approach, which applies the stagnant film model locally, in combination with theoretical information on mass transfer coefficients in the absence of filtration. This approach, which has been applied mainly to crossflow systems, avoids having to assume that δ is spatially uniform and thereby allows v_f and C_m to vary with position (Blatt et al., 1970; Zydney, 1997). The hybrid approach appears to be most useful when a simple expression is available for the mass transfer coefficient, as in the entrance region of a tube or parallel-plate channel.

Systems in which the membrane forms the base of a stirred cylindrical cell are often used experimentally, but have received relatively little theoretical attention. In what appears to be the only detailed analysis of convective diffusion in this type of ultrafiltration system, Saksena and Zydney (1997) approximated the flow as a rigid-body rotation above a stationary surface (known as Bödewadt flow), and included filtration by superimposing on the main flow a small velocity normal to the surface. A very similar fluid dynamical model was used previously by Smith and Colton (1972), who analyzed mass transfer to the base of a stirred cylindrical container in the absence of filtration (e.g., a dialysis cell). For the ultrafiltration problem, Saksena and Zydney used a similarity transformation to reduce the axisymmetric species conservation equation to an ordinary differential equation, which was solved numerically. This transformation was made possible by assuming that the product of $v_f(r)$ and concentration boundary layer thickness was a constant, where r is radial position. Although not emphasized by those authors, it was necessary also that the filtrate concentration be independent of radial position. The main objective of that work was to examine the effects of solute-solute diffusional interactions in concentrated solutions, but the same assumptions would be required to apply the similarity transformation to dilute solutions. Those approximations limit the generality of that approach.

The purpose of the present study was to investigate further the Bödewadt flow model for stirred cell ultrafiltration. By solving the axisymmetric species conservation equation numerically, restrictions on the radial variations of v_f and filtrate concentration were avoided. The analysis is limited to laminar flow at high Reynolds number and high Schmidt number. [In stirred cells the

transition from laminar to turbulent flow occurs at a Reynolds number of approximately 3×10^4 (Colton and Smith, 1972), and Schmidt numbers for protein solutions are typically $>10^4$.] Solute concentrations were assumed to be moderate, as is typical of membrane characterization experiments, allowing the viscosity and diffusivity to be regarded as constants. The boundary layer formulation and solution methods are described first. Then, certain general results are discussed in comparison with predictions of stagnant film and hybrid models. Finally, the predictions of the boundary layer model are tested using data on the filtration of BSA solutions in commercial ultrafiltration cells.

3.2 Model Development

3.2.1 Overview

The system of interest is depicted schematically in Figure 3.1. An ultrafiltration membrane forms the base of a cylindrical cell of radius R. The cell is partially filled with a macromolecule solution, which is stirred by an impeller that rotates at an angular velocity ω_s. A desired filtration rate is set by controlling the gas pressure, and the liquid volume is assumed to be sufficiently large that the process is pseudo-steady. This system was modeled as shown in Figure 3.2b, in which a semi-infinite solution undergoes rigid-body rotation above a stationary surface, with the angular velocity of the bulk liquid denoted as ω. This representation was motivated by the fact that rotational flow above an impermeable, planar surface (Bödewadt flow) has been well characterized (Schlicting, 1979, pp. 225-230; Rogers and Lance, 1960), and the observation that those velocity results are readily modified to include moderate rates of filtration (Saksena and Zydney, 1997). In the model the membrane is considered to occupy a circular area of radius R within a larger surface. Because the stirrer must overcome the torques exerted on the fluid by the side and bottom of the cell, the rotation rate of the stirrer must exceed that of the bulk fluid; that is, $\omega/\omega_s < 1$, as will be seen in the discussion of the experimental results.

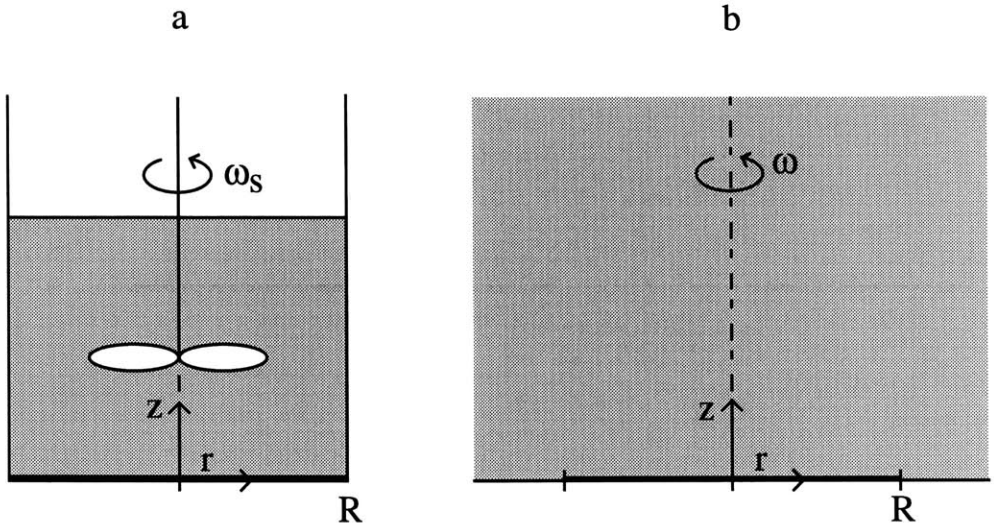

FIGURE 3.1: The flow in a typical stirred ultrafiltration cell (panel a) is modeled as a semi-infinite fluid rotating above a surface (panel b). The membrane radius is R. The angular velocity of the stirrer (ω_s) differs from that of the bulk fluid in the model (ω).

The omission of the impeller from the model system (Fig. 3.1b) is justified by the fact that the momentum and concentration boundary layer thicknesses in such systems are often much smaller than the impeller-surface separation. For laminar flow at high Reynolds number (Re), the momentum boundary layer thickness (δ_m) is expected to scale as

$$\frac{\delta_m}{R} \sim \mathrm{Re}^{-1/2} \tag{3-2}$$

where $\mathrm{Re} = \omega R^2/\nu$ and ν is the kinematic viscosity (Deen, 1998, p. 338). If the Schmidt number ($\mathrm{Sc} = \nu/D$) is also large, the concentration boundary layer thickness (δ_c) will vary as

$$\frac{\delta_c}{R} \sim \mathrm{Re}^{-1/2}\,\mathrm{Sc}^{-1/3} \tag{3-3}$$

(Deen, 1998, p. 424). Thus, even for $\mathrm{Re} = 10^3$ and $\mathrm{Sc} = 10^4$, which are not particularly large values for protein solutions in stirred cells, δ_c would be only about 0.1% of R. This indicates that it is sufficient to focus on the region very near the membrane surface. The pressure and velocity fields in this thin region are discussed next, followed by a description of the convective diffusion problem.

3.2.2 Pressure Field

It was assumed that the dynamic pressure in the liquid ($\mathcal{P}$) is approximately that for a fluid undergoing rigid-body rotation,

$$\mathcal{P}(r) = \frac{1}{2}\rho\omega^2 r^2 \tag{3-4}$$

where ρ is density. Here the arbitrary constant in the dynamic pressure was chosen so that $\mathcal{P} = 0$ at $r = 0$. The radial variation in pressure described by Eq. 3-4, when imposed on the boundary

layer, results in a flow near the membrane that is directed inward (i.e., toward the axis of rotation). It follows that the concentration boundary layer begins to develop at the outer edge of the membrane ($r = R$).

To calculate the filtrate velocity, an expression was needed also for the transmembrane pressure difference. Adding static pressure variations to those in Eq. 3-4, the actual liquid pressure (P) was found to be

$$P(r,z) = \mathcal{P}(r) - \rho g z + c = \frac{1}{2}\rho\omega^2 r^2 - \rho g z + c \tag{3-5}$$

The constant c was determined by returning to the system in Figure 3.1, equating pressures at the gas-liquid interface, and specifying the total volume of liquid. This was sufficient to define the height of the gas-liquid interface, which was found to be parabolic in r with a minimum at the center. The transmembrane pressure difference (ΔP) was then evaluated as

$$\Delta P \equiv P(r,0) - P_f = P_0 - P_f + \rho g h_0 + \frac{1}{2}\rho\omega^2 R^2\left[\left(\frac{r}{R}\right)^2 - \frac{1}{2}\right] \tag{3-6}$$

where P_0 is the gas pressure, h_0 is the liquid height under static conditions, and P_f is the pressure in the filtrate (assumed constant). The last term in Eq. 3-6 is usually a small fraction of ΔP, so that in all simulations ΔP was assumed to be independent of r. For the experimental conditions discussed later, it was calculated that the radial variations in ΔP never exceeded 0.6% of its mean value.

3.2.3 Velocity Field

The equations of motion for this system can be reduced to a set of ordinary differential equations by assuming a solution of the form

$$v_r = r\omega F(\zeta), \quad v_\theta = r\omega G(\zeta), \quad v_z = \sqrt{\nu\omega}H(\zeta) - v_f(r) \tag{3-7}$$

where $v_f(r)$ is the local velocity normal to the membrane surface (> 0 for filtration) and

$$\zeta \equiv z\sqrt{\frac{\omega}{\nu}} \tag{3-8}$$

The dimensionless axial coordinate ζ is of order unity at the edge of the momentum boundary layer (Rogers and Lance, 1960). The inclusion of v_f as an additive term in v_z follows Saksena and Zydney (1997). Using primes to denote derivatives with respect to ζ, the continuity equation becomes

$$H' + 2F = 0 \tag{3-9}$$

and the r- and θ-components of the Navier-Stokes equation transform to

$$F'' - F^2 + G^2 - HF' + \frac{v_f(r)}{\sqrt{\nu\omega}}F' = 1 \tag{3-10}$$

$$G'' - 2FG - HG' + \frac{v_f(r)}{\sqrt{\nu\omega}}G' = 0 \tag{3-11}$$

The z-component of the Navier-Stokes equation is not needed. The boundary conditions which express no slip at the membrane surface, $v_z = -v_f$ at the surface, and rigid-body rotation far from the surface, are

$$F(0) = G(0) = H(0) = 0, \quad F(\infty) = 0, \quad G(\infty) = 1 \tag{3-12}$$

Equations 3-9 through 3-12 reduce to those applicable in the absence of filtration, provided

that

$$\frac{v_f(r)}{\sqrt{\nu\omega}} << 1 \tag{3-13}$$

Therefore, if Eq. 3-13 is satisfied, previous results for $F(\zeta)$, $G(\zeta)$, and $H(\zeta)$ can be used for the filtration problem.[3] Equation 3-13 is not difficult to satisfy; for the experiments discussed later, $\langle v_f \rangle / \sqrt{\nu\omega} \sim 10^{-4}$, where $\langle v_f \rangle$ is the filtrate velocity averaged over the membrane surface.

The thinness of the concentration boundary layer, relative to the momentum boundary layer, allowed the velocity field to be simplified by using expressions valid for small ζ. Thus, $F(\zeta)$ was approximated by its Maclaurin series expansion,

$$F(\zeta) = F'(0)\zeta + \frac{1}{2}F''(0)\zeta^2 + \ldots \tag{3-14}$$

(note the omission of $F(0)$, see Eq. 3-12). From Rogers and Lance (1960), $F'(0) = -0.94197$, indicating that the radial flow near the surface is directed inward, as already mentioned.[4] By fitting a curve to other results for $F(\zeta)$ tabulated in Schlichting (1979, p. 228), with the values of $F(0)$ and $F'(0)$ fixed as just described, it was found that $F''(0) = 1.10$. From continuity (Eq. 3-9), $H(\zeta)$ was expressed as

$$H(\zeta) = -F'(0)\zeta^2 - \frac{1}{3}F''(0)\zeta^3 + \ldots \tag{3-15}$$

---

[3] The functions defined here as $F(\zeta)$, $G(\zeta)$, and $H(\zeta)$ are those denoted in Rogers and Lance (1960) as $\mathcal{F}(\xi)$, $\mathcal{G}(\xi)$, and $\mathcal{H}(\xi)$, respectively. In their analysis the bulk fluid and the surface were assumed to have angular velocities ω and $\sigma\omega$, respectively, so that Bödewadt flow corresponds to their special case of $\sigma = 0$.

[4] Following Eq. 21 of Saksena and Zydney (1997), the constant 0.94197 is given incorrectly as 0.525.

An expression for $G(\zeta)$ was not needed to compute the axisymmetric concentration field.

The filtration velocity was calculated from the transmembrane pressure drop and the osmotic pressure difference ($\Delta\Pi$) using

$$v_f = L_p(\Delta P - \sigma\Delta\Pi) \tag{3-16}$$

where L_p is the membrane hydraulic permeability and σ is the reflection coefficient. As discussed later, $\Delta\Pi$ was related to the solute concentration by using either the Van't Hoff equation or certain empirical expressions.

3.2.4 Concentration Field

The steady, axisymmetric species conservation equation for the stirred cell is

$$v_r\frac{\partial C}{\partial r} + v_z\frac{\partial C}{\partial z} = D\left[\frac{\partial^2 C}{\partial z^2} + \frac{1}{r}\frac{\partial}{\partial r}\left(r\frac{\partial C}{\partial r}\right)\right] \tag{3-17}$$

where $C(r,z)$ is the solute concentration. The boundary conditions used were

$$C(R,z) = C_b \tag{3-18}$$

$$\frac{\partial C(r,\infty)}{\partial z} = 0 \tag{3-19}$$

$$\frac{\partial C(r,0)}{\partial z} = -\frac{v_f(r)}{D}(1-\Theta)C(r,0) \tag{3-20}$$

where $\Theta = C_f(r)/C(r,0)$ is the local value of the membrane sieving coefficient. Equation 3-18 requires that the concentration at the outer edge of the membrane (the "leading edge" for the concentration boundary layer) equal the bulk concentration. Equation 3-19 specifies that axial

gradients in concentration vanish in the bulk solution, far from the surface. Equation 3-20 was derived by equating the axial flux at the membrane surface with the flux of solute in the filtrate.

In all of the present calculations Θ was regarded as a constant. Thus, to the extent that the concentration at the upstream membrane surface varied with radial position, the filtrate concentration did also. In general, for a given membrane-solute combination, Θ will depend on v_f. Constancy of Θ requires either that v_f be constant or that the membrane Péclet number be large (see Section 1.4 and Deen, 1998, p. 67).

The species conservation equation was made dimensionless by introducing the following quantities:

$$Y = 1 - \frac{r}{R} \tag{3-21}$$

$$Z = \mathrm{Sc}^{1/3}\zeta = \mathrm{Sc}^{1/3} z \sqrt{\frac{\omega}{\nu}} \tag{3-22}$$

$$\Psi = \frac{C}{C_b} \tag{3-23}$$

$$\alpha(Y) = \frac{v_f(Y)}{\sqrt{\nu\omega}} \mathrm{Sc}^{2/3} \tag{3-24}$$

The reversed radial coordinate (Y) allows the numerical solution to proceed from the outer edge of the membrane, where the concentration is known. The new axial coordinate (Z) is scaled for the concentration boundary layer; that is, its order of magnitude is unity within that region. The function $\alpha(Y)$ is a dimensionless filtration rate, scaled as shown by $\mathrm{Sc}^{2/3}$ in order to remove the Schmidt number from the boundary condition at the membrane surface. Substitution of these variables and the expansions for v_r and v_z in Eq. 3-17 gives

$$-(1-Y)\left[F'(0)Z+\frac{1}{2}F''(0)Z^2\mathrm{Sc}^{-1/3}\right]\frac{\partial\Psi}{\partial Y}-\left[F'(0)Z^2+\frac{1}{3}F''(0)Z^3\mathrm{Sc}^{-1/3}+\alpha(Y)\right]\frac{\partial\Psi}{\partial Z} \quad (3\text{-}25)$$

$$=\frac{\partial^2\Psi}{\partial Z^2}+\frac{1}{\mathrm{ReSc}^{2/3}}\left[\frac{\partial^2\Psi}{\partial Y^2}-\frac{1}{(1-Y)}\frac{\partial\Psi}{\partial Y}\right]$$

Because the present analysis was restricted to the case of high Re and Sc, the radial diffusion term in Eq. 3-25 was neglected. Preliminary calculations revealed that for the large values of Sc of interest here ($> 10^4$), the $F''(0)$ terms in the velocity components had a negligible effect on the model results. For example, for $\mathrm{Sc} = 1.5 \times 10^4$, inclusion of these higher order terms resulted in $< 0.5\%$ changes in both the area-averaged mass transfer coefficient and the area-averaged surface concentration calculated by the model. Accordingly, Eq. 3-25 was simplified to

$$-(1-Y)F'(0)Z\frac{\partial\Psi}{\partial Y}-\left[F'(0)Z^2+\alpha(Y)\right]\frac{\partial\Psi}{\partial Z}=\frac{\partial^2\Psi}{\partial Z^2} \quad (3\text{-}26)$$

The boundary conditions for $\Psi(Y,Z)$ are

$$\Psi(0,Z)=1 \quad (3\text{-}27)$$

$$\frac{\partial\Psi(Y,\infty)}{\partial Z}=0 \quad (3\text{-}28)$$

$$\frac{\partial\Psi(Y,0)}{\partial Z}=-\alpha(Y)[1-\Theta]\Psi(Y,0) \quad (3\text{-}29)$$

Note that with the scaling employed, which is valid for asymptotically large Sc, neither Re nor Sc appears in Eqs. 3-26 through 3-29. Thus, Ψ is dependent only on position (Y,Z) and the parameter α.

The local mass transfer coefficient is defined as

$$k \equiv -\frac{D}{(C_m - C_b)} \frac{\partial C}{\partial z}\bigg|_{z=0} \tag{3-30}$$

Given the functional dependence of Ψ and the relationship between Z and z (Eq. 3-22), it follows that the local Sherwood number is of the form

$$\mathrm{Sh} = \frac{kR}{D} = f(Y,\alpha)\mathrm{Re}^{1/2}\mathrm{Sc}^{1/3} \tag{3-31}$$

where the coefficient $f(Y,\alpha)$ is computed from the values of Ψ and $\partial\Psi/\partial Z$ at $Z = 0$. In general, those results must be obtained numerically. However, for the region near the outer edge of the membrane and for small filtration rates, an analytical solution can be found, which provides a useful check on the numerical results. That solution (using similarity) is described next, and then the numerical procedure is outlined.

3.2.5 Similarity Solution Near Membrane Outer Edge

As pointed out in Smith and Colton (1972), at the outer edge of the membrane axial convection is negligible for $\alpha = 0$. This suggests that for $Y << 1$ and $\alpha \rightarrow 0$, Eq. 3-26 can be approximated as

$$-F'(0)Z\frac{\partial\Psi}{\partial Y} = \frac{\partial^2\Psi}{\partial Z^2} \tag{3-32}$$

For $\alpha \rightarrow 0$ and a fixed value of Θ, Eq. 3-29 also reduces to a simpler form, corresponding to specification of a constant value of $\partial\Psi/\partial Z$ at the membrane surface. For the calculation of mass transfer coefficients, the magnitude of that constant is immaterial. Thus, the simplified boundary condition at the membrane surface was written as

$$\frac{\partial \Psi(Y,0)}{\partial Z} = -1 \tag{3-33}$$

The other boundary conditions, given by Eqs. 3-27 and 3-28, remain the same. This problem was solved by assuming that $\Psi = \Psi(s)$ only, where

$$s \equiv Z\left(-\frac{9Y}{F'(0)}\right)^{-1/3} \tag{3-34}$$

Using this similarity solution, the coefficient in the Sherwood number was found to be

$$f(Y,0) = \Gamma(2/3)\left[\frac{-F'(0)}{9}\right]^{1/3} Y^{-1/3} = 0.6381 Y^{-1/3} \qquad (Y << 1) \tag{3-35}$$

In order to provide a second check of the validity of the numerical method employed (discussed below), the similarity solution was also determined for the case of a constant concentration at the membrane surface. To obtain this solution, the boundary condition in Eq. 3-29 was replaced with

$$\Psi(Y,0) = 2 \tag{3-36}$$

As with the constant flux boundary condition mentioned above, the value of the concentration at the membrane surface was immaterial. Using the similarity variable in Eq. 3-34, the coefficient in the Sherwood number for the constant concentration case was found to be

$$f(Y,0) = \frac{3}{\Gamma(1/3)}\left[\frac{-F'(0)}{9}\right]^{1/3} Y^{-1/3} = 0.5277 Y^{-1/3} \qquad (Y << 1) \tag{3-37}$$

3.2.6 Numerical Solution

The complete boundary value problem given by Eqs. 3-26 through 3-29 was solved using a modified Crank-Nicolson method. Using this method, each step in Y was broken down into two half-steps. If j and k are indices for the Y and Z directions, respectively, beginning at (j, k) the first half-step was taken to (j+1/2, k). At this point, the finite difference representation of Eq. 3-26 used was

$$-\left(1-Y_{j+1/2}\right)F'(0)Z_k\left[\frac{2\left(\Psi_{j+1/2,k}-\Psi_{j,k}\right)}{\Delta Y}\right]-\left[F'(0)Z_k^2+\alpha\left(Y_{j+1/2}\right)\right]\left[\frac{\Psi_{j,k+1}-\Psi_{j,k-1}}{2(\Delta Z)}\right] \qquad (3\text{-}38)$$

$$=\frac{\Psi_{j+1/2,k+1}-2\Psi_{j+1/2,k}+\Psi_{j+1/2,k-1}}{(\Delta Z)^2}$$

The second half step was then taken to (j+1, k). The finite difference equation used for this half-step was

$$-\left(1-Y_{j+1}\right)F'(0)Z_k\left[\frac{\Psi_{j+1,k}-\Psi_{j,k}}{\Delta Y}\right]-\left[F'(0)Z_k^2+\alpha\left(Y_{j+1}\right)\right]\left[\frac{\Psi_{j+1/2,k+1}-\Psi_{j+1/2,k-1}}{2\Delta Z}\right] \qquad (3\text{-}39)$$

$$=\frac{1}{2}\left[\frac{\Psi_{j+1,k+1}-2\Psi_{j+1,k}+\Psi_{j+1,k-1}}{(\Delta Z)^2}+\frac{\Psi_{j,k+1}-2\Psi_{j,k}+\Psi_{j,k-1}}{(\Delta Z)^2}\right]$$

The FORTRAN code that was written to perform this solution is located in Appendix B. For simulations involving dilute solutions it was assumed that $\Delta\Pi = 0$, making v_f a constant that could be specified in advance. With v_f independent of the concentration field, the latter could be computed in one step. For more concentrated solutions ($\Delta\Pi$ not negligible), an iterative procedure was required. An initial guess of a constant filtration rate was entered, and the concentration field was computed using this initial v_f. The osmotic pressure at the membrane surface was then calculated, and Eq. 3-16 was used to update $v_f(r)$ for use in the next iteration. The filtration rate was updated according to

$$v_f^{i+1} = v_f^i + f\left\{v_f\left[C^i(r,0)\right] - v_f^i\right\} \tag{3-40}$$

where the superscripts indicate the iteration. Depending on the value chosen for the "relaxation factor" f in Eq. 3-40, the filtration rate used in iteration i+1 was somewhere between that used in iteration i and that calculated from the concentration profile determined by iteration i. Iteration continued until the area-averaged filtration rate converged to within a relative tolerance of $< 10^{-5}$. For most simulations $f = 0.5$ was sufficiently small to ensure convergence.

To accommodate a finite grid, the boundary condition at $Z = \infty$ (Eq. 3-28) was usually imposed at $Z = 10$. Increasing this value to 20 resulted in only a 0.5% change in the average surface concentration calculated by the model, confirming that 10 was sufficiently large. A 100×100 grid was found to provide results for the average surface concentration that were accurate to within 0.1%.

3.3 Results and Discussion

3.3.1 Mass Transfer Coefficient

Smith and Colton (1972) investigated the problem of mass transfer in Bödewadt flow in the absence of filtration. They included radial diffusion, and computed the steady state solution as the large-time limit of a transient problem, using an alternating-difference implicit procedure. Three types of boundary conditions were considered. The present results were compared with those of Smith and Colton by setting $\alpha(Y) = 0$ in Eq. 3-26 and replacing Eq. 3-29 with a constant concentration condition (Eq. 3-36). The results from the current model and the results from Smith and Colton (1972) are plotted in Figure 3.2 as $\mathrm{Sh}\ \mathrm{Re}^{-1/2}\ \mathrm{Sc}^{-1/3}$ versus dimensionless radial position. Also plotted in this figure is the similarity solution for the constant concentration boundary condition (Eq. 3-37). Both models show good agreement with the similarity solution for $Y << 1$. Instabilities in the present model were observed for small values of Y when the constant

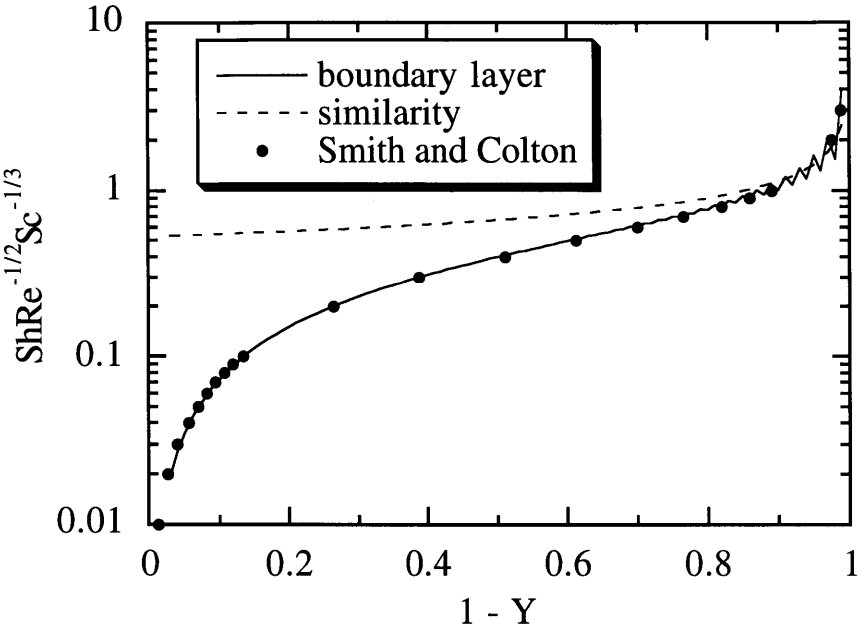

FIGURE 3.2: Dimensionless mass transfer coefficient as a function of radial position for the constant concentration boundary condition (Eq. 3-36). Results from the boundary layer model are shown along with the results of Smith and Colton (1972). The curve labeled "similarity" was calculated from Eq. 3-37.

concentration boundary condition (Eq. 3-36) was used. This was due to the singularity at $Y = Z = 0$. That is, the boundary conditions in Eqs. 3-27 and 3-36 impose two different values of Ψ at this point. For the conditions used ($Re = 10^4$ and $Sc = 10^5$), the two sets of mass transfer coefficients were indistinguishable in the range $0 \leq Y \leq 0.97$. The present model did not allow calculation of mass transfer coefficients for larger values of Y, due to instabilities in the concentration field that appeared as $Y \rightarrow 1$. A likely reason for failure of the numerical solution in this region is that the radial convection term in Eq. 3-26 vanishes, so that the partial differential equation loses its parabolic character. It should be noted also that the present formulation becomes inaccurate for $Y \rightarrow 1$, because the neglect of radial diffusion makes it impossible to impose the symmetry condition at the axis of rotation, namely, $\partial\Psi/\partial Y = 0$ at $Y = 1$. The numerical difficulties notwithstanding, it was possible in all simulations to obtain stable concentration values over 99.9% of the membrane area.

The behavior of the local mass transfer coefficient in the presence of filtration was investigated using several constant values of the dimensionless filtration rate, α. (As noted earlier, α is constant when osmotic effects are negligible.) The results are plotted in Figure 3.3, again as $Sh\ Re^{-1/2}\ Sc^{-1/3}$ versus dimensionless radial position. Shown for comparison is the similarity result for the constant flux boundary condition given by Eq. 3-35. In all cases, there was a rapid decline in mass transfer coefficient when moving inward from the outer edge of the membrane, a consequence of the increasing thickness of the concentration boundary layer (see below). For a given radial position, the mass transfer coefficient decreased as the filtration rate was reduced. The asymptotic limit reached for $\alpha \rightarrow 0$ was in excellent agreement with the similarity solution for the outer 10-15% of the membrane radius. The results for $\alpha = 0.001$ (not shown) were indistinguishable on this plot from those for $\alpha = 0.01$. As shown in Figure 3.3, the agreement with the analytical result was much worse for $\alpha = 1$. For filtration rates of that magnitude, the region in which axial convection may be neglected is much smaller ($Y^{1/3} << 1$). This is seen by performing an order of magnitude analysis of Eq. 3-26. The orders of magnitude of each term are:

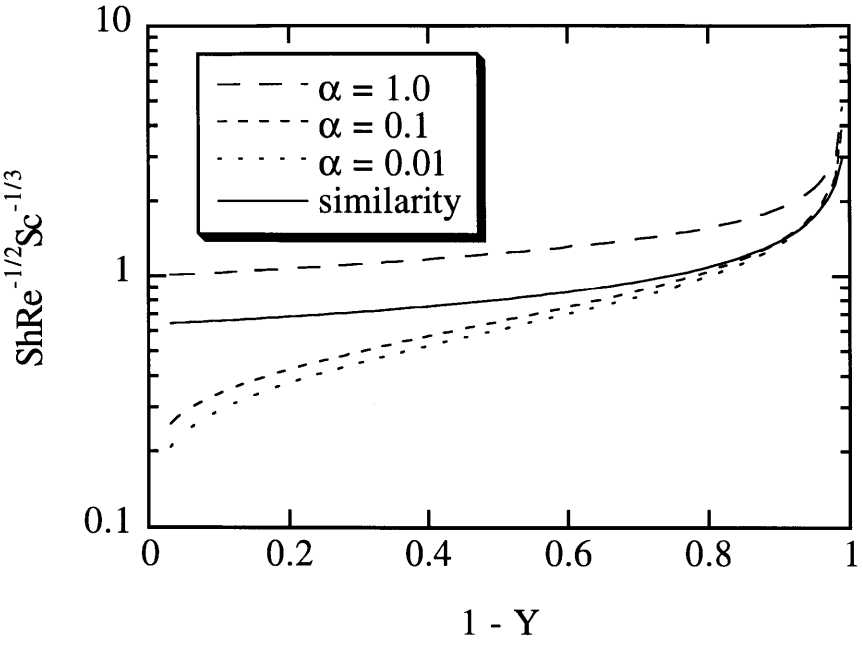

FIGURE 3.3: Dimensionless mass transfer coefficient as a function of radial position for the constant flux boundary condition (Eq. 3-33). Results from the boundary layer model are shown for several values of the dimensionless filtration rate (α). The curve labeled "similarity" was calculated from Eq. 3-35.

$$-(1-Y)F'(0)Z\frac{\partial \Psi}{\partial Y} \sim \delta_c \frac{\Delta \Psi}{Y} \tag{3-41}$$

$$-\left[F'(0)Z^2 + \alpha(Y)\right]\frac{\partial \Psi}{\partial Z} \sim \left(\delta_c^2 + \alpha\right)\frac{\Delta \Psi}{\delta_c} \tag{3-42}$$

$$\frac{\partial^2 \Psi}{\partial Z^2} \sim \frac{\Delta \Psi}{\delta_c^2} \tag{3-43}$$

where δ_c is the thickness of the concentration boundary layer. Equating the orders of magnitude of radial convection (Eq. 3-41) and axial diffusion (Eq. 3-43) gives

$$\delta_c \sim Y^{1/3} \tag{3-44}$$

In order for axial convection (Eq. 3-42) to be negligible

$$\left(\delta_c^3 + \alpha\delta_c\right) << 1 \tag{3-45}$$

For the case of $\alpha \to 0$, Eq. 3-45 is equivalent to setting $Y << 1$. For $\alpha \sim 1$, the requirement for neglecting axial convection becomes $Y^{1/3} << 1$.

The area-averaged mass transfer coefficients for the case of constant concentration (Figure 3.2) and constant flux as $\alpha \to 0$ (Figure 3.3) at the membrane surface were determined. In doing so the mass transfer coefficient for $Y < 0.1$ was calculated from the corresponding similarity result (Eq. 3-37 for constant concentration, Eq. 3-35 for constant flux). The results, given in the form of Eq. 3-31, were

$$\langle \mathrm{Sh} \rangle = \frac{\langle k \rangle R}{D} = 0.775 \mathrm{Re}^{1/2} \mathrm{Sc}^{1/3} \tag{3-46}$$

for the case of constant concentration and

$$\langle \mathrm{Sh} \rangle = \frac{\langle k \rangle R}{D} = 1.01 \mathrm{Re}^{1/2} \mathrm{Sc}^{1/3} \tag{3-47}$$

for the case of constant flux ($\alpha \to 0$). It was observed for both cases that the difference between the numerically determined mass transfer coefficient and the similarity result was approximately linear in Y. A least-squares fit to the numerical results lead to

$$f(Y,0) \cong 0.5277 Y^{-1/3} - 0.53Y \tag{3-48}$$

for the case of constant concentration

$$f(Y,0) \cong 0.6381 Y^{-1/3} - 0.41Y \tag{3-49}$$

for the case of constant flux ($\alpha \to 0$). Equations 3-48 and 3-49 are sufficiently accurate that, when averaged over the membrane area, they give 0.773 and 1.01 for the coefficients in Eqs. 3-46 and 3-47, respectively. The numerical results for $f(Y,0)$ for each case are plotted along with Eqs. 3-48 and 3-49 in Figures 3.4 and 3.5.

3.3.2 Concentration Field

Concentration contours representative of the behavior at moderate filtration rates are plotted in Figure 3.6. These calculations were performed for an ideal semipermeable membrane (i.e., $\sigma = 1$ in Eq. 3-16 and $\Theta = 0$ in Eq. 3-29) and assumed that $\Pi \propto C$, as in the Van't Hoff equation. Under these conditions the only remaining dimensionless parameters are

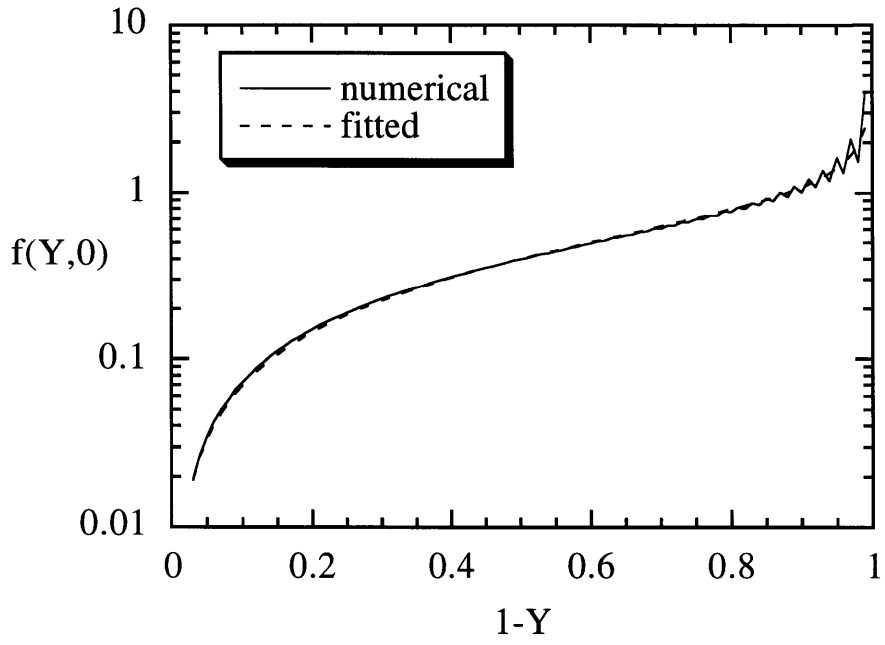

FIGURE 3.4: Dimensionless mass transfer coefficient as a function of radial position for the constant concentration boundary condition (Eq. 3-36). The curve labeled "numerical" is the result of the boundary layer model (Figure 3.2). The curve labeled "fitted" is given by Eq. 3-48.

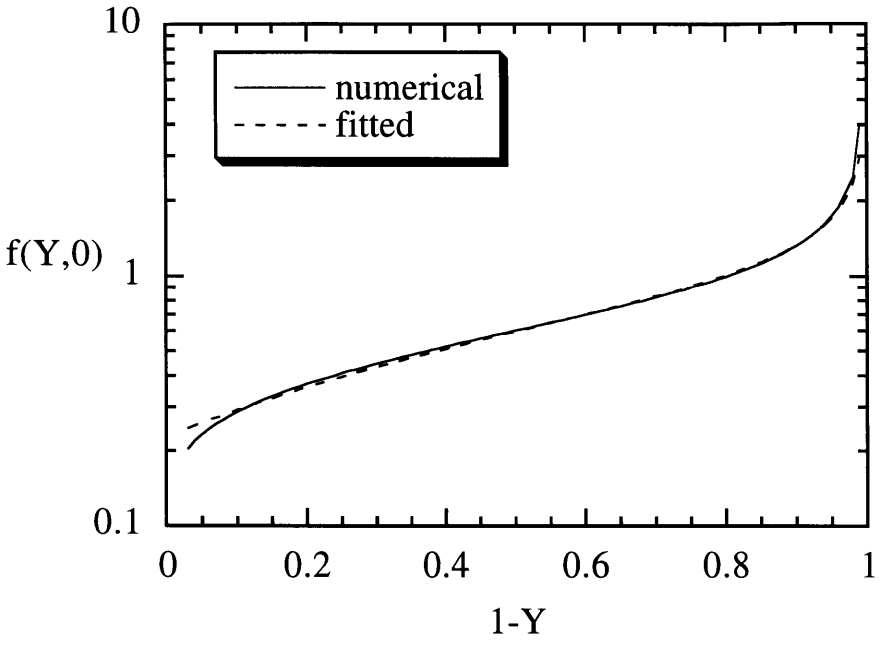

FIGURE 3.5: Dimensionless mass transfer coefficient as a function of radial position for the constant flux boundary condition (Eq. 3-33). The curve labeled "numerical" is the result of the boundary layer model for $\alpha \rightarrow 0$ (Figure 3.3). The curve labeled "fitted" is given by Eq. 3-49.

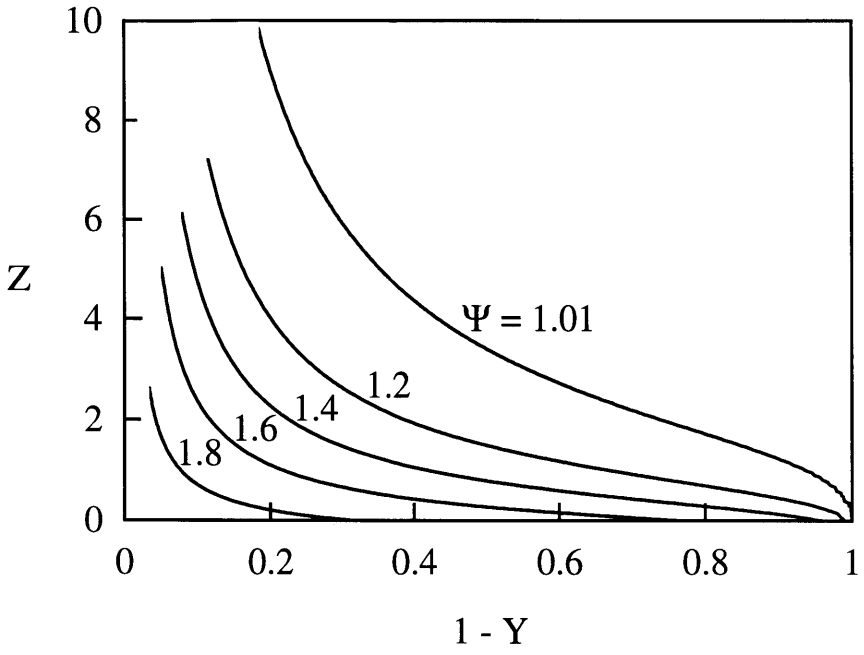

FIGURE 3.6: Contours of constant concentration computed for $\alpha_0 = 1$ and $\beta = 0.5$.

$$\alpha_0 \equiv \frac{v_{f0}}{\sqrt{\nu\omega}}\mathrm{Sc}^{2/3} = \frac{L_p\left(\Delta P - \Pi_b\right)}{\sqrt{\nu\omega}}\mathrm{Sc}^{2/3} \tag{3-50}$$

$$\beta \equiv \frac{\Pi_b}{\Delta P} \tag{3-51}$$

where v_{f0} and Π_b are the filtration velocity and osmotic pressure, respectively, based on the bulk solute concentration. The parameter α_0 is a scaled filtration velocity, and β is a measure of the importance of osmotic effects. For the results shown in Figure 3.6, $\alpha_0 = 1$ and $\beta = 0.5$. As seen, each concentration contour had an inflection point. Taking the $\Psi = 1.01$ contour as an index of the boundary layer thickness, there was a rapid increase in thickness near the outer edge of the membrane, a leveling off at intermediate positions, and then another rapid increase near the center of the cell. The initial increase and tendency to level off are typical of boundary layers developing along surfaces (e.g., for flow parallel to a flat plate), whereas the final increase is due to the upward axial velocities that become dominant as the axis of rotation is approached. The plume-like behavior of the concentration field near the center of a stirred cell was examined in more detail by Smith and Colton (1972). As already mentioned, numerical instabilities precluded the calculation of the concentration field all the way to $Y = 1$. The size of the unstable region varied from the inner 3% of the cell radius at the membrane ($Z = 0$) to about the inner 20% of the cell radius at $Z = 10$, as indicated by the termination of the contours in Figure 3.6. For these conditions the product of dimensionless filtration rate (α) and dimensionless boundary layer thickness (Z for $\Psi = 1.01$) was 0 at $Y = 0$, 0.84 at $Y = 0.4$, and 1.24 at $Y = 0.8$. This indicates that the similarity transformation of Saksena and Zydney (1997), which requires that product to be constant, would not have been applicable.

3.3.3 Effect of Polarization on Filtration Rate

The next set of simulations illustrates the effects of concentration polarization on the filtration rate averaged over the membrane surface. As with the calculations for Figure 3.6, it was

assumed for simplicity that the membrane was perfectly semipermeable and the solution was ideal. The results were expressed by dividing the area-averaged filtration rate by that which would exist if polarization were absent. Thus, the quantity examined was

$$\frac{\langle v_f \rangle}{v_{f0}} = \frac{\Delta P - \langle \Pi_m \rangle}{\Delta P - \Pi_b} \tag{3-52}$$

where the brackets denote averages over membrane area and $\Pi_m = \Pi(C_m) = \Pi[C(r,0)]$. This relative filtration rate is plotted in Figure 3.7 as a function of α_0, for several values of β. As indicated by the solid curves, increasing α_0 at constant β decreased the relative filtration rate, because concentration polarization was enhanced. At a given α_0, increasing β also decreased the relative filtration rate, because it amplified the effects of osmotic pressure and thereby allowed polarization to play a greater role. For $\beta = 0$ (no solute in the system), polarization would be absent, and the relative filtration rate would remain at unity for all values of α_0.

The dashed curves in Figure 3.7 represent predictions based on the stagnant film theory. To obtain these curves, all stagnant-film variables were interpreted as area averages. Setting $C_m = \langle C_m \rangle$ and $v_f = \langle v_f \rangle$, and using $C_f = 0$ and $\Pi \propto C$ as before, Eq. 3-1 becomes

$$\frac{\langle \Pi_m \rangle}{\Pi_b} = \exp\left(\frac{\langle v_f \rangle}{k_{sf}}\right) \tag{3-53}$$

To evaluate k_{sf} in Eq. 3-53 in a self-consistent manner, the area-averaged mass transfer coefficient calculated using the boundary layer model was used, in the limit of vanishing filtration rate (Eq. 3-47). In other words, as might be attempted in practice, k_{sf} was obtained using mass transfer data from the same system in the absence of filtration. If k_{sf} is set equal to $\langle k \rangle$, Eq. 3-53 becomes

$$\frac{\langle \Pi_m \rangle}{\Delta P} = \beta \exp\left[\frac{\alpha_0}{1.01(1-\beta)}\left(1 - \frac{\langle \Pi_m \rangle}{\Delta P}\right)\right] \tag{3-54}$$

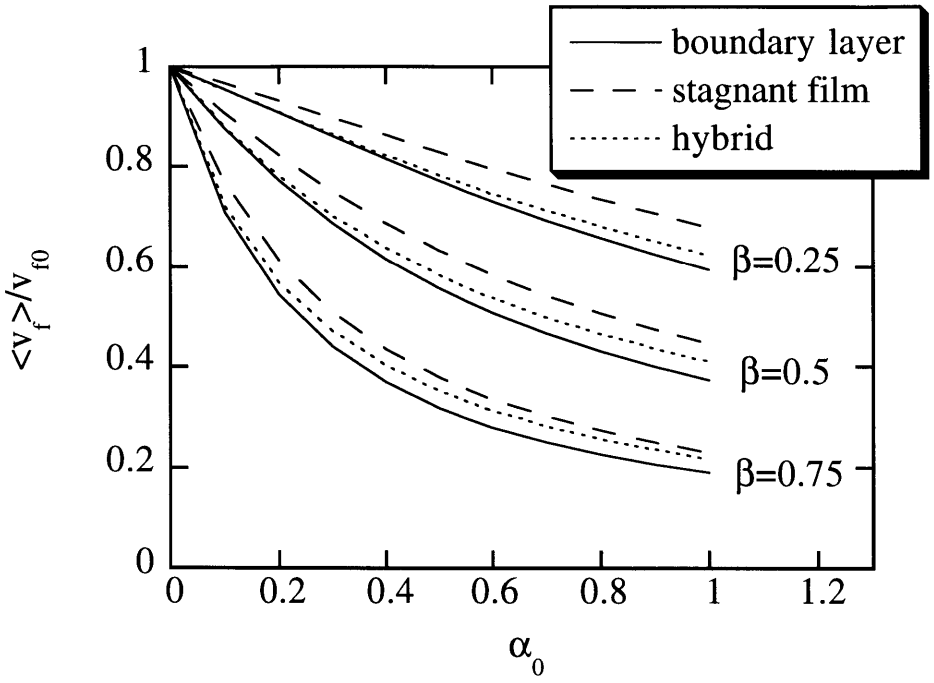

FIGURE 3.7: Ratio of average filtration rate to that in the absence of concentration polarization, as a function of the dimensionless filtration rate without polarization (α_0), for the boundary layer, stagnant film, and hybrid models. The results are for an ideal semipermeable membrane.

Equation 3-54 was solved iteratively to determine $\langle \Pi_m \rangle / \Delta P$. This allowed direct comparisons to be made between the stagnant film and boundary layer results. As seen in Figure 3.7, the relative filtration velocity predicted by the stagnant film model exceeded that obtained from the more rigorous boundary layer theory for all values of α_0 and β. In other words, the stagnant film approach always underestimated the effects of concentration polarization on filtration velocity. However, the difference between the two predictions was relatively small, the stagnant film value being at most 21% higher than that from the boundary layer theory. Similar trends were observed when the osmotic pressure was assumed to be a quadratic function of solute concentration. That is, it appears that there is always a small to moderate overestimation of filtration rate by the stagnant film model, whether or not the solution is thermodynamically ideal.

The dotted curves in Figure 3.7 were obtained from a hybrid model, which was derived as follows. Letting $g(Y) = \Pi_m / \Pi_b$, the assumptions of an ideal semipermeable membrane and ideal solution lead to

$$\frac{\langle v_f \rangle}{v_{f0}} = \frac{1 - \beta \langle g \rangle}{1 - \beta} \tag{3-55}$$

$$\langle g \rangle = 2 \int_0^1 g(Y)(1 - Y) dY \tag{3-56}$$

Assuming that the stagnant film result (Eq. 3-1) is valid locally, and interpreting k_{sf} now as the local mass transfer coefficient in the absence of filtration, the following expression for g was obtained:

$$g = \exp\left[\frac{\alpha_0}{f(Y,0)} \left(\frac{1 - \beta g}{1 - \beta} \right) \right] \tag{3-57}$$

Using Eq. 3-49 to evaluate $f(Y,0)$, Eq. 3-57 was solved iteratively to determine $g(Y)$, from which the average filtration velocity was found. As shown in Figure 3.7, the hybrid model yielded

predictions which were somewhat more accurate than those of the stagnant film model, although it too consistently overestimated the relative filtration velocity. For the hybrid model, the maximum deviation from the boundary layer results in Figure 3.7 was 15%.

3.3.4 Effect of Polarization on Sieving

The objective of the next set of simulations was to determine the relationship between the apparent sieving coefficient ($\Theta' = C_f/C_b$) and the actual sieving coefficient ($\Theta = C_f/C_m$), as a function of filtration conditions. As discussed in connection with Eq. 3-20, Θ was regarded as a constant. What is ordinarily measured is the concentration in the mixed filtrate divided by that in the bulk retentate, or $\langle\Theta'\rangle = \langle v_f C_f\rangle/\langle v_f\rangle C_b$. However, in the simulations to be discussed the osmotic pressure was assumed to be negligible ($\beta \rightarrow 0$), making the filtration velocity independent of radial position. That is, the macromolecule solutions were assumed to be dilute, as is the case in membrane characterization experiments using tracers. Consequently, the apparent sieving coefficient could be calculated simply as $\langle\Theta'\rangle = \langle C_f\rangle/C_b$. Figure 3.8 shows the ratio of actual to apparent sieving coefficient as a function of the dimensionless filtration rate (α), for values of Θ ranging from 0.01 to 0.75. The results for $\Theta = 0.01$ represent lower limits, in that they were indistinguishable on this plot from those for $\Theta = 0.001$. The boundary layer results are shown by the solid curves. As the filtration rate was increased at a given value of Θ, polarization was augmented and $\Theta/\langle\Theta'\rangle$ fell more and more below unity. At a given filtration rate, smaller values of Θ resulted in larger percentage differences between the apparent and actual sieving coefficient. In other words, the more effectively the solute is retained by the membrane, the greater is the influence of polarization on sieving.

To obtain comparable sieving predictions from the stagnant film theory, Eq. 3-1 was rearranged to give

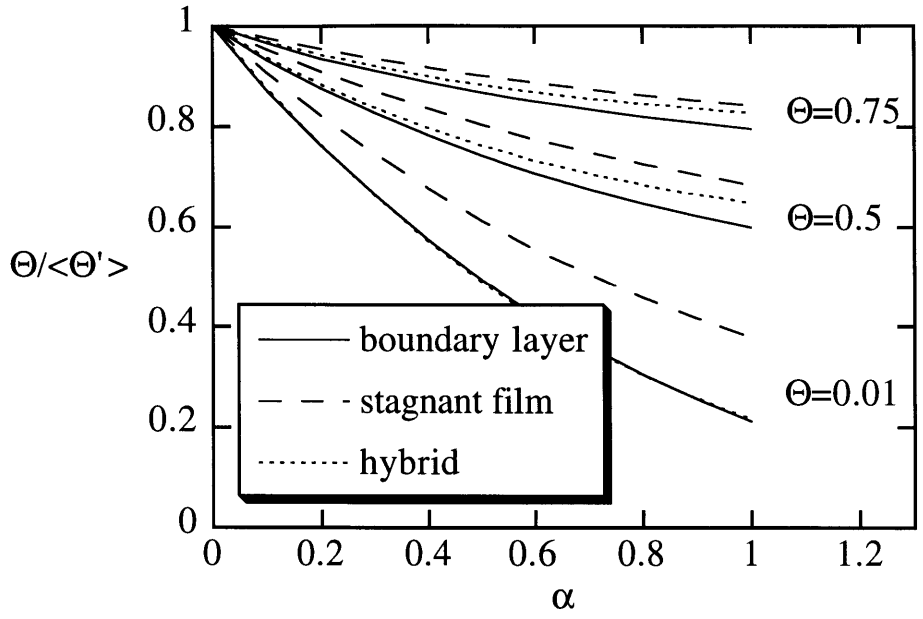

FIGURE 3.8: Ratio of actual sieving coefficient (Θ) to apparent sieving coefficient (Θ') as a function of dimensionless filtration rate (α), for the boundary layer, stagnant film, and hybrid models. The effects of osmotic pressure were neglected ($\beta = 0$).

$$\frac{\Theta'}{\Theta} = \frac{B}{1-\Theta(1-B)} \tag{3-58}$$

and assumed that $\Theta' = \langle\Theta'\rangle$ and $B = \exp(\langle v_f\rangle/\langle k\rangle)$. As shown by the dashed curves in Figure 3.8, the values of $\Theta/\langle\Theta'\rangle$ from the stagnant film model always exceeded those from the boundary layer theory. The magnitude of this overestimate increased with increasing filtration rate or with decreasing sieving coefficient. At $\alpha = 1$ and $\Theta = 0.01$, the stagnant film prediction for $\Theta/\langle\Theta'\rangle$ was 78% too large. Thus, using the stagnant film model to correct measured (apparent) sieving coefficients may lead to systematic errors that are much larger than those made in estimating filtration rates.

The corresponding hybrid model was derived by using the local values of v_f and k to evaluate the polarization factor. From Eqs. 3-1 and 3-49, the following expression for B was obtained:

$$B(Y) \equiv \frac{C_m(Y) - C_f(Y)}{C_b - C_f(Y)} = \exp\left[\frac{\alpha}{0.6381Y^{-1/3} - 0.410Y}\right] \tag{3-59}$$

Averaging Eq. 3-58 over the membrane surface then gives

$$\frac{\langle\Theta'\rangle}{\Theta} = 2\int_0^1 \frac{B(Y)(1-Y)}{1-\Theta[1-B(Y)]}dY \tag{3-60}$$

As shown by the dotted curves in Figure 3.8, the predictions of the hybrid model were significantly more accurate than those of the stagnant film approach. A particularly dramatic improvement was seen for very small sieving coefficients (e.g., $\Theta = 0.01$). For the hybrid model, the maximum deviation from the boundary layer results in Figure 3.8 was 15% (for $\Theta = 0.1$ - 0.2).

3.3.5 Comparisons with Experimental Data

Before the development of the laminar boundary layer model, the first approach taken to correct measured sieving coefficients for the effects of concentration polarization was to determine the value of the stagnant film mass transfer coefficients (k_{sf}) for the stirred cell in a separate set of experiments (Johnston and Deen, 1999). Filtration rates across regenerated cellulose membranes were measured in the presence and absence of BSA. The reduction in filtration rate caused by osmotic pressure was related to the concentration of BSA at the membrane surface, using a semiempirical correlation from the literature (Vilker et al., 1981). This allowed k_{sf} to be computed for BSA. The stagnant film mass transfer coefficients for the other proteins were calculated from this value by using laminar boundary layer theory to correct for differences in the diffusivities.

These experiments were performed using the same 10 ml ultrafiltration cell employed in the sieving studies, and also a 3 ml cell (Model 3, Amicon, Beverly, MA). Scale drawings of the two cells are shown in Figure 3.9. The solution used was 0.15 M NaCl, either protein-free or containing 4 g/dl BSA, with the pH adjusted to 7.4 using 0.1 N NaOH and 0.1 N HCl. The membranes were regenerated cellulose with a molecular weight cutoff of 30 kD (Amicon, Beverly, MA, and Millipore, Bedford, MA). Pressure drops ranging from 2.7 to 13.3 kPa were applied using compressed nitrogen and measured with a pressure transducer. In all experiments the angular velocity of the impeller (ω_s) was maintained at 220 rpm, resulting in Reynolds numbers of approximately 880 and 2690 for the 3 ml and 10 ml cells, respectively. The filtration rate was measured first using the protein-free buffer, then using the BSA solution, and then again with the protein-free buffer. After a 10 to 30 minute equilibration period following each change, the filtrate was collected for 30 minutes and weighed. With the BSA solution, the concentrations of BSA in the filtrate and retentate were measured.

The hydraulic permeability (L_p) of the membrane is related to the filtrate velocity (v_f) by Eq. 3-16. The value of L_p was determined from the protein-free filtrations by dividing the filtration rate by ΔP. Data from an experiment were retained only if the values of L_p in the first

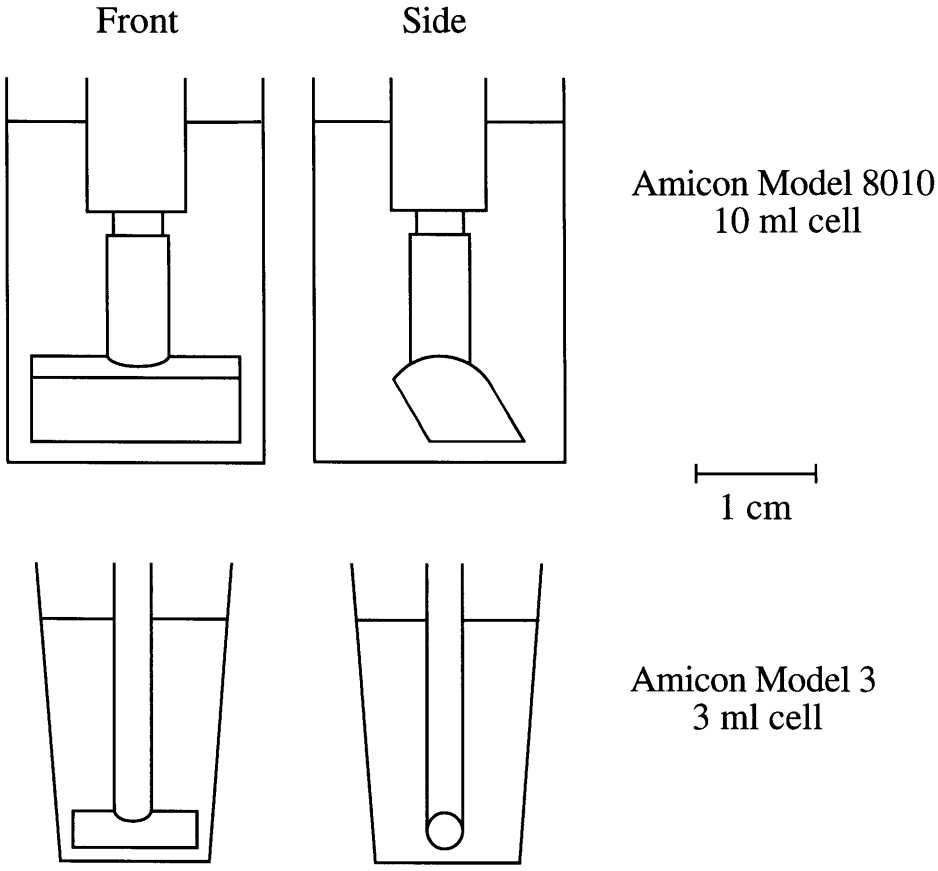

FIGURE 3.9: Scale drawings of the Amicon stirred cells used in the filtration experiments with BSA. The fluid levels indicated correspond to the nominal capacities. The values of R and the impeller-membrane separation were 1.05 and 0.14 - 0.18 cm, respectively, for the 10 ml cell, and 0.6 and 0.10 cm, respectively, for the 3 ml cell.

and third periods differed by less than 5%. To determine the concentration of BSA at the upstream surface of the membrane, the following semiempirical correlation was used (Vilker et al., 1981):

$$\Pi_{BSA} = RT\left\{2\left[\left(\frac{zC_{BSA}}{2M_{BSA}}\right)^2 + m_s^2\right]^{1/2} - 2m_s\right\} + \frac{RT}{M_{BSA}}\left(C_{BSA} + A_2C_{BSA}^2 + A_3C_{BSA}^3\right) \tag{3-61}$$

where R is the gas constant, T is temperature, z is the charge number for BSA (z = -20.4 at pH = 7.4), C_{BSA} is the concentration of BSA in g/l, M_{BSA} is the molecular weight of BSA (68,000 g/mol), and m_s is the molar salt concentration. The coefficients A_2 and A_3 are equal to -1.089 $\times$ 10^{-2} and 1.243 $\times$ 10^{-4}, respectively, for the conditions used here.

To obtain the concentration of BSA at the upstream membrane surface, Eqs. 3-16 and 3-61 were solved simultaneously for $\Delta\Pi$ and C_{BSA} (= C_m). In this calculation it was assumed that the membrane Péclet number was large, so that σ = (1- Θ). Because $\Theta \cong 10^{-3}$, this assumption caused little error. Rearranging Eq. 3-1, the mass transfer coefficient was calculated as

$$k_{sf} = v_f\left[\ln\left(\frac{C_m - C_f}{C_b - C_f}\right)\right]^{-1} \tag{3-62}$$

The results for the stagnant film mass transfer coefficient for BSA are shown in Figure 3.10. For filtration rates ranging from 0.3 to 1.8 μm/s, the results for both ultrafiltration cells were in good agreement. A linear increase in k_{sf} with v_f was observed. The best-fit line is given by k_{sf} = 1.36 + 2.40v_f, where k_{sf} and v_f are both in μm/s. The mass transfer coefficients for the other proteins were calculated by assuming that $k_{sf} \propto (D_\infty)^{2/3}$, as suggested by laminar boundary layer theory (Eq. 3-31).

The ability of the laminar boundary layer model to predict the reduction in filtration rate observed in these experiments was tested. As stated above, nearly perfect rejection of the 68 kD

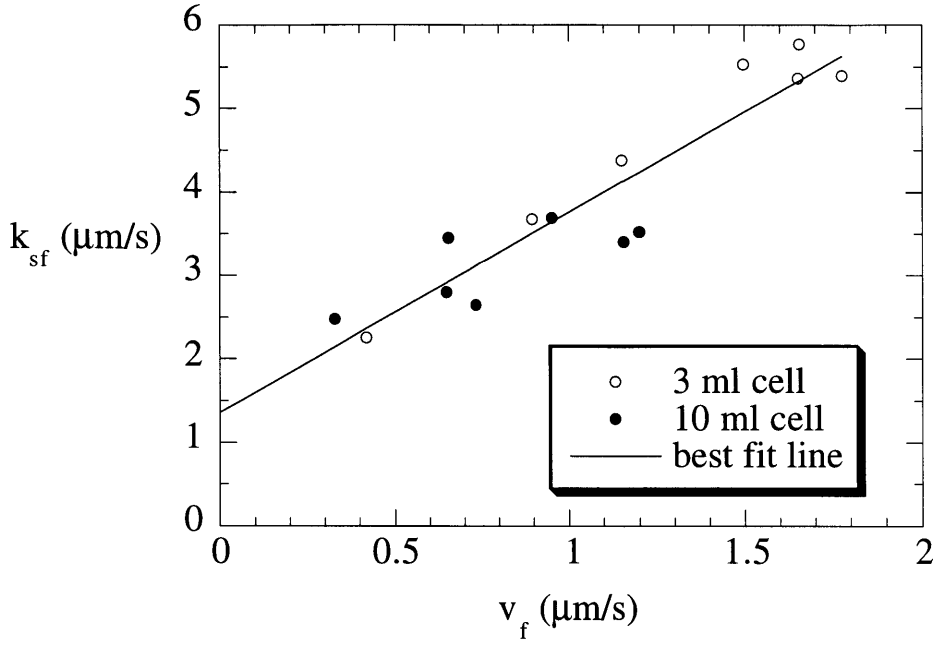

FIGURE 3.10: Experimental values of the stagnant film mass transfer coefficient, k_{sf}, as a function of filtration velocity, v_f, for BSA.

BSA was observed ($\langle\Theta'\rangle \cong 10^{-3}$), so the membranes were modeled as ideally semipermeable. The osmotic pressure was related to the BSA concentration using Eq. 3-61. The predicted and measured filtration rates for the 10 ml cell are compared in Figure 3.11. Values of β for this data set ranged from 0.37 to 0.66; values of α calculated using ω_s ranged from 0.07 to 0.27. When the angular velocity of the bulk fluid was equated with that of the stirrer ($\gamma \equiv \omega/\omega_s = 1$), the filtration rates predicted by the model exceeded the measured values by approximately 20%. However, as mentioned earlier, to impart a torque that will balance those exerted on the fluid by the bottom and side of the cell, the angular velocity of the stirrer must exceed that of the bulk fluid. In other words, it is expected that $\gamma < 1$. As shown in Figure 3.11, when it was assumed that $\gamma = 0.25$, the predicted filtration rates underestimated the measured values, whereas $\gamma = 0.36$ was found to minimize the sum of the squared errors. Colton and Smith (1972) measured the rate of benzoic acid dissolution from the base of a different stirred cell and compared the results with boundary layer predictions for a constant concentration boundary condition, thereby concluding that $\gamma = 0.49$. Inasmuch as γ must depend on the cell and impeller geometry, this difference in angular velocity factors is not surprising.

The results for the 3 ml cell, where the best-fit value was $\gamma = 0.87$, are shown in Figure 3.12. Values of β for this data set were similar to those for the 10 ml cell, ranging from 0.39 to 0.62. Values of α, calculated using ω_s, were also similar (0.06 - 0.26). However, in this case the agreement between the model and data was somewhat less satisfactory than for the 10 ml cell. In particular, for the 3 ml cell a fixed value of γ did not match the data equally well over the entire range of filtration rates, larger values of γ tending to work better at the higher filtration rates. Possibly contributing to this trend is the fact that the mean fluid heights were significantly lower at the higher values of $\langle v_f \rangle$, due to the small volume of this cell. By reducing the wetted area, this would have lowered the torque exerted on the fluid by the side of the cell, and thereby reduced the value of $\omega_s - \omega$ needed to balance that torque. A reduction in $\omega_s - \omega$ corresponds, of course, to values of γ closer to unity.

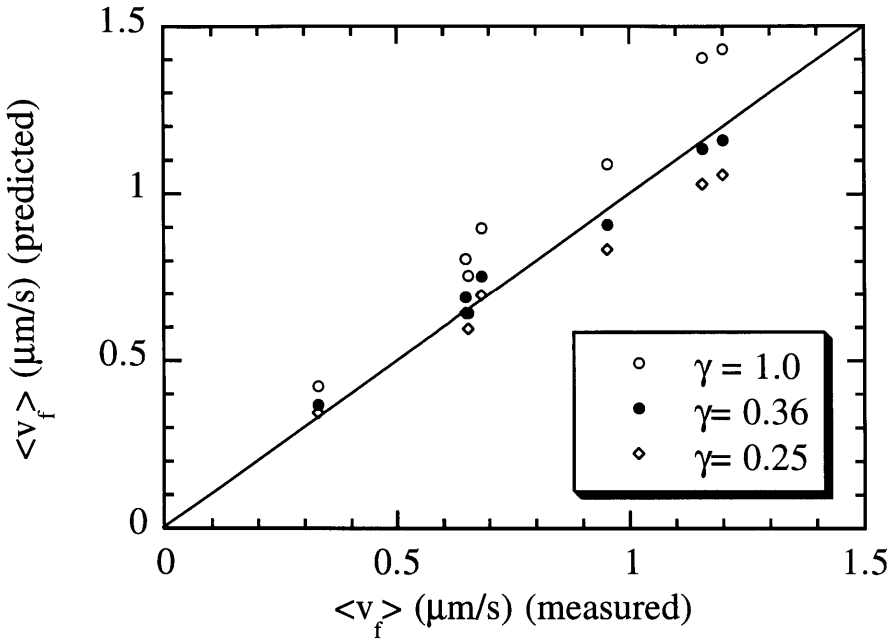

FIGURE 3.11: Comparison of average filtration rates predicted by the boundary layer model with those measured in the 10 ml cell. Predictions are shown for three assumed values of $\gamma = \omega/\omega_s$; the best-fit value was $\gamma = 0.36$.

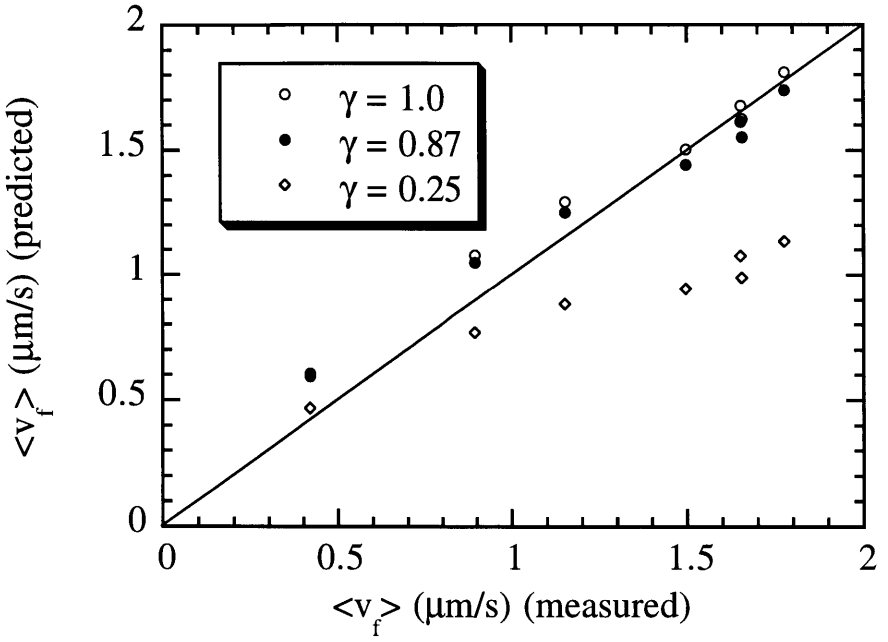

FIGURE 3.12: Comparison of average filtration rates predicted by the boundary layer model with those measured in the 3 ml cell. Predictions are shown for three assumed values of $\gamma = \omega/\omega_s$; the best-fit value was $\gamma = 0.87$.

As shown above, the stagnant film model can be fitted to the BSA data if k_{sf} is allowed to be a strong function of the filtration rate. However, the results from the boundary layer model indicate that the true area-average mass transfer coefficients (calculated by averaging local values obtained from Eq. 3-30) are not strongly dependent on the filtration rate. For example, the mass transfer coefficients calculated by the boundary layer model for BSA in the 10 ml cell ranged only from 4.2 to 4.5 μm/s, while the empirical expression for k_{sf} yields values ranging from 2.1 to 4.2 μm/s. Evidently, most of the empirical dependence of k_{sf} on $\langle v_f \rangle$ is needed merely to compensate for errors made in using area-averages for the various individual quantities in Eq. 3-1.

Finally, the true sieving coefficients calculated by the stagnant film model using the empirical expression for k_{sf} and those calculated from the laminar boundary layer model with γ= 0.36 were compared for a subset the experiments described in Chapter 2. Again, the values for Θ listed in Johnston and Deen (1999) for three of the proteins studied were calculated using Eq. 3-1 in conjunction with the expression for k_{sf} shown by the solid line in Figure 3.10. The corresponding values for Θ listed in Chapter 2 were calculated using the laminar boundary layer model with γ= 0.36. As stated in Chapter 2, these values differed only by an average of 0.9% and a maximum of 2.7%. Apparently, although the mass transfer coefficients calculated using these two methods are not in good agreement, the extents of polarization predicted are very similar. The errors involved in these predictions were minimized due to the small amount of polarization in the experiments. For this reason, only the values calculated using the laminar boundary layer model (γ = 0.36) were listed in Chapter 2.

3.4 Conclusions

A laminar boundary layer analysis based on Bödewadt flow was used to quantify concentration polarization in stirred, cylindrical ultrafiltration cells. The predictive capability of the boundary layer model was tested using filtration data with BSA solutions, and the agreement was found to be excellent, provided that an appropriate value was selected for the angular velocity of

the bulk fluid. Comparisons of the boundary layer results with those obtained from a conventional stagnant film model showed that the latter gave reasonably accurate values for mean filtrate velocities, but made substantial errors in converting apparent sieving coefficients to actual membrane sieving coefficients. The errors were lessened by use of a hybrid model, where the mass transfer coefficient was allowed to vary with position according to boundary layer theory. It appears that the main difficulty with the stagnant film model arises from the implicit averaging of concentrations and filtrate velocities over the membrane surface. Of course, the use of such position-independent quantities is what was needed to yield a one-dimensional problem with a simple analytical solution. It is concluded that the one-dimensional nature of the stagnant film model, which is its main strength, is also its main weakness.

APPENDIX A

FIDAP Code: Determination of the Polyester Mesh Correction Factor

The following Appendix contains the FIDAP code (FDREAD file) created in Fidap 7.6 (Fluent, Inc., Evanston, IL) to determine the value of the polyester mesh correction factor, β (see Section 2.2.3). The FDREAD file was created using the graphical user interface of the software package to manually draw the mesh and define the problem.

```
---------------------------------------------------------------------------------------------------------
TITLE(  )
Polyester Mesh Correction Factor
FI-GEN( ELEM = 1, POIN = 1, CURV = 1, SURF = 1, NODE = 0, MEDG = 1, MLOO = 1,
MFAC = 1, BEDG = 1, SPAV = 1, MSHE = 1, MSOL = 1, COOR = 1 )
WINDOW(CHANGE= 1, MATRIX )
    1.000000     .000000     .000000     .000000
     .000000    1.000000     .000000     .000000
     .000000     .000000    1.000000     .000000
     .000000     .000000     .000000    1.000000
   -10.00000    10.00000    -7.50000     7.50000    -7.50000     7.50000
WINDOW( CHAN = 1, MATR )
    1,     0,     0,     0
    0,     1,     0,     0
    0,     0,     1,     0
    0,     0,     0,     1
  -10,    10,  -7.5,   7.5,  -7.5,   7.5
POINT( ADD, COOR, X = 0.002, Y = 0.002, Z = 0.0035 )
POINT( ADD, COOR, X = 0, Y = 0, Z = 0.0055 )
POINT( ADD, COOR, X = 0, Y = 0, Z = 0.0015 )
POINT( ADD, COOR, X = 0, Y = 0, Z = 0.007 )
POINT( ADD, COOR, X = 0.0035, Y = 0.0035, Z = 0.007 )
POINT( ADD, COOR, X = 0, Y = 0, Z = 0 )
POINT( ADD, COOR, X = 0.0035, Y = 0.0035, Z = 0 )
POINT( SELE, ID = 2 )
POINT( SELE, ID = 1 )
POINT( SELE, ID = 3 )
CURVE( ADD, ARC )
```

```
POINT( SELE, ID = 4 )
POINT( SELE, ID = 2 )
CURVE( ADD, LINE )
POINT( SELE, ID = 3 )
POINT( SELE, ID = 6 )
CURVE( ADD, LINE )
POINT( SELE, ID = 5 )
POINT( SELE, ID = 7 )
CURVE( ADD, LINE )
POINT( SELE, ID = 4 )
POINT( SELE, ID = 5 )
CURVE( ADD, LINE )
POINT( SELE, ID = 6 )
POINT( SELE, ID = 7 )
CURVE( ADD, LINE )
WINDOW( CHAN = 1, MATR )
    1,      0,      0,      0
    0,      1,      0,      0
    0,      0,      1,      0
    0,      0,      0,      1
-0.0007, 0.0042, -9e-05, 0.00359, -0.00018, 0.00718
   45,     45,     45,     45
WINDOW( CHAN = 0, SIDE )
WINDOW( CHAN = 1, MATR )
   -1,      0,      0,      0
    0,      0,      1,      0
    0,      1,      0,      0
    0,      0,      0,      1
-0.00665, 0.00315, -0.00017, 0.00718, -9e-05, 0.00359
   45,     45,     45,     45
POINT( SELE, ID, WIND = 1 )
    2
    1
    3
CURVE( ADD, CIRC )
CURVE( SELE, ID, WIND = 1 )
    7
CURVE( DELE )
POINT( ADD, COOR, X = 0.001414, Y = 0.001414, Z = 0.004914 )
POINT( ADD, COOR, X = 0.001414, Y = 0.001414, Z = 0.002086 )
POINT( SELE, ID, WIND = 1 )
    2
    8
    1
CURVE( ADD, ARC )
POINT( SELE, ID, WIND = 1 )
    3
    9
    1
CURVE( ADD, ARC )
POINT( SELE, ID, WIND = 1 )
```

```
CURVE( SELE, ID, WIND = 1 )
    1
CURVE( DELE )
POINT( SELE, ID, WIND = 1 )
    8
    5
CURVE( ADD, LINE )
POINT( SELE, ID, WIND = 1 )
    9
    7
CURVE( ADD, LINE )
POINT( ADD, COOR, X = 0.0035, Y = 0.0035, Z = 0.0035 )
POINT( SELE, ID, WIND = 1 )
    1
   10
CURVE( ADD, LINE )
CURVE( SELE, ID, WIND = 1 )
    7
POINT( SELE, ID, WIND = 1 )
    8
CURVE( SPLI )
CURVE( SELE, ID, WIND = 1 )
    8
POINT( SELE, ID, WIND = 1 )
    9
CURVE( SPLI )
CURVE( SELE, ID, WIND = 1 )
    4
POINT( SELE, ID, WIND = 1 )
   10
CURVE( SPLI )
CURVE( SELE, ID, WIND = 1 )
    2
    9
   11
   10
    3
    5
   12
   13
   16
   17
   15
   14
    6
UTILITY( UNSE, ALL )
CURVE( SELE, ID, WIND = 1 )
    2
    9
   11
   10
```

```
    3
MEDGE( ADD, FRST, INTE = 9, RATI = 0.05, 2RAT = 0.05, PCEN = 0 )
MEDGE( SELE, ID, WIND = 1 )
    1
    2
    3
    4
    5
MEDGE( MODI, FRST, INTE = 9, RATI = 0.05, 2RAT = 0.05, PCEN = 0 )
CURVE( SELE, ID, WIND = 1 )
    5
   12
   16
   13
   17
   15
    6
   14
MEDGE( ADD, SUCC, INTE = 9, RATI = 0.05, 2RAT = 0.05, PCEN = 0 )
MEDGE( SELE, ID, WIND = 1 )
    6
    7
    8
    9
   10
   11
   12
   13
MEDGE( MODI, SUCC, INTE = 9, RATI = 0, 2RAT = 0, PCEN = 0 )
CURVE( SELE, ID, WIND = 1 )
    2
    5
    9
   12
UTILITY( UNSE, ALL )
MEDGE( SELE, ID, WIND = 1 )
    6
   12
MEDGE( MODI, FRST, INTE = 9, RATI = 0.05, 2RAT = 0.05, PCEN = 0 )
MEDGE( SELE, ID, WIND = 1 )
    7
   13
MEDGE( MODI, FRST, INTE = 9, RATI = 0.39, 2RAT = 0.39, PCEN = 0 )
CURVE( SELE, ID, WIND = 1 )
    2
    5
    9
   12
MFACE( WIRE, EDG1 = 1, EDG2 = 1, EDG3 = 1, EDG4 = 1 )
CURVE( SELE, ID, WIND = 1 )
    9
```

```
   16
   11
   13
MFACE( WIRE, EDG1 = 1, EDG2 = 1, EDG3 = 1, EDG4 = 1 )
CURVE( SELE, ID, WIND = 1 )
   10
   17
   11
   15
MFACE( WIRE, EDG1 = 1, EDG2 = 1, EDG3 = 1, EDG4 = 1 )
CURVE( SELE, ID, WIND = 1 )
    3
    6
   10
   14
MFACE( WIRE, EDG1 = 1, EDG2 = 1, EDG3 = 1, EDG4 = 1 )
POINT( ADD, COOR, X = 0.00465, Y = 0.002, Z = 0.0035 )
POINT( ADD, COOR, X = 0.00465, Y = 0, Z = 0.0055 )
POINT( ADD, COOR, X = 0.00465, Y = 0, Z = 0.0015 )
POINT( ADD, COOR, X = 0.00465, Y = 0, Z = 0.007 )
POINT( ADD, COOR, X = 0.00465, Y = 0.0035, Z = 0.007 )
POINT( ADD, COOR, X = 0.00465, Y = 0, Z = 0 )
POINT( ADD, COOR, X = 0.00465, Y = 0.0035, Z = 0 )
POINT( ADD, COOR, X = 0.00465, Y = 0.001414, Z = 0.004914 )
POINT( ADD, COOR, X = 0.00465, Y = 0.001414, Z = 0.002086 )
POINT( ADD, COOR, X = 0.00465, Y = 0.0035, Z = 0.0035 )
WINDOW( CHAN = 0, ISOM )
WINDOW( CHAN = 1, MATR )
-0.707107, -0.408248, 0.57735,     0
0.707107, -0.408248, 0.57735,     0
    0, 0.816497, 0.57735,     0
    0,     0,     0,     1
-0.00667, 0.00667, -0.00405, 0.00595, -0.00024, 0.00967
   45,    45,    45,    45
POINT( SELE, ID = 12 )
POINT( SELE, ID = 18 )
POINT( SELE, ID = 11 )
CURVE( ADD, ARC )
POINT( SELE, ID = 11 )
POINT( SELE, ID = 19 )
POINT( SELE, ID = 13 )
CURVE( ADD, ARC )
CURVE( SELE, ID, WIND = 1 )
   18
POINT( SELE, ID, WIND = 1 )
   18
CURVE( SPLI )
CURVE( SELE, ID, WIND = 1 )
   19
POINT( SELE, ID, WIND = 1 )
   19
```

```
CURVE( SPLI )
POINT( SELE, ID, WIND = 1 )
   14
   12
CURVE( ADD, LINE )
POINT( SELE, ID, WIND = 1 )
   14
   15
CURVE( ADD, LINE )
POINT( SELE, ID, WIND = 1 )
   15
   18
CURVE( ADD, LINE )
POINT( SELE, ID, WIND = 1 )
   15
   20
CURVE( ADD, LINE )
POINT( SELE, ID, WIND = 1 )
   20
   11
CURVE( ADD, LINE )
POINT( SELE, ID, WIND = 1 )
   20
   17
CURVE( ADD, LINE )
POINT( SELE, ID, WIND = 1 )
   17
   19
CURVE( ADD, LINE )
POINT( SELE, ID, WIND = 1 )
   17
   16
CURVE( ADD, LINE )
POINT( SELE, ID, WIND = 1 )
   16
   13
CURVE( ADD, LINE )
POINT( ADD, COOR, X = 0.002, Y = 0.00465, Z = 0.0035 )
POINT( ADD, COOR, X = 0, Y = 0.00465, Z = 0.0055 )
POINT( ADD, COOR, X = 0, Y = 0.00465, Z = 0.0015 )
POINT( ADD, COOR, X = 0, Y = 0.00465, Z = 0.007 )
POINT( ADD, COOR, X = 0.0035, Y = 0.00465, Z = 0.007 )
POINT( ADD, COOR, X = 0, Y = 0.00465, Z = 0 )
POINT( ADD, COOR, X = 0.0035, Y = 0.00465, Z = 0 )
POINT( ADD, COOR, X = 0.001414, Y = 0.00465, Z = 0.004914 )
POINT( ADD, COOR, X = 0.001414, Y = 0.00465, Z = 0.002086 )
POINT( SELE, ID, WIND = 1 )
   22
   28
   21
CURVE( ADD, ARC )
```

```
POINT( SELE, ID, WIND = 1 )
   21
   29
   23
CURVE( ADD, ARC )
CURVE( SELE, ID, WIND = 1 )
   33
POINT( SELE, ID, WIND = 1 )
   28
CURVE( SPLI )
CURVE( SELE, ID, WIND = 1 )
   34
POINT( SELE, ID, WIND = 1 )
   29
CURVE( SPLI )
POINT( SELE, ID, WIND = 1 )
   24
   22
CURVE( ADD, LINE )
POINT( SELE, ID, WIND = 1 )
   24
   25
CURVE( ADD, LINE )
POINT( SELE, ID, WIND = 1 )
   25
   28
CURVE( ADD, LINE )
POINT( ADD, COOR, X = 0.0035, Y = 0.00465, Z = 0.0035 )
POINT( SELE, ID, WIND = 1 )
   25
   30
CURVE( ADD, LINE )
POINT( SELE, ID, WIND = 1 )
   30
   21
CURVE( ADD, LINE )
POINT( SELE, ID, WIND = 1 )
   30
   27
CURVE( ADD, LINE )
POINT( SELE, ID, WIND = 1 )
   27
   29
CURVE( ADD, LINE )
POINT( SELE, ID, WIND = 1 )
   27
   26
CURVE( ADD, LINE )
POINT( SELE, ID, WIND = 1 )
   26
   23
```

```
CURVE( ADD, LINE )
CURVE( SELE, ID, WIND = 1 )
   25
   24
   20
   26
   21
   22
   23
   32
   31
   30
   29
   27
   28
   40
   41
   35
   39
   42
   43
   36
   37
   45
   44
   46
   47
   38
UTILITY( UNSE, ALL )
MEDGE( SELE, ID, WIND = 1 )
CURVE( SELE, ID, WIND = 1 )
   25
   20
   21
   27
   22
   23
   31
   29
   44
   42
   40
   46
   38
   37
   36
   35
MEDGE( ADD, SUCC, INTE = 9, RATI = 0, 2RAT = 0, PCEN = 0 )
CURVE( SELE, ID, WIND = 1 )
   24
   26
```

```
   22
UTILITY( UNSE, ALL )
CURVE( SELE, ID, WIND = 1 )
   24
   26
   28
   30
   32
   47
   45
   43
   41
   39
MEDGE( ADD, FRST, INTE = 9, RATI = 0.05, 2RAT = 0.05, PCEN = 0 )
CURVE( SELE, ID, WIND = 1 )
   24
   25
   26
   20
UTILITY( UNSE, ALL )
MEDGE( SELE, ID, WIND = 1 )
   14
   20
   25
   24
MEDGE( MODI, FRST, INTE = 9, RATI = 0.05, 2RAT = 0.05, PCEN = 0 )
MEDGE( SELE, ID, WIND = 1 )
   15
   19
   26
   29
MEDGE( MODI, FRST, INTE = 9, RATI = 0.39, 2RAT = 0.39, PCEN = 0 )
CURVE( SELE, ID, WIND = 1 )
   24
   25
   26
   20
MFACE( WIRE, EDG1 = 1, EDG2 = 1, EDG3 = 1, EDG4 = 1 )
CURVE( SELE, ID, WIND = 1 )
   26
   27
   28
   21
MFACE( WIRE, EDG1 = 1, EDG2 = 1, EDG3 = 1, EDG4 = 1 )
CURVE( SELE, ID, WIND = 1 )
   30
   29
   28
CURVE( SELE, ID, WIND = 1 )
   22
MFACE( WIRE, EDG1 = 1, EDG2 = 1, EDG3 = 1, EDG4 = 1 )
```

```
CURVE( SELE, ID, WIND = 1 )
   32
CURVE( SELE, ID, WIND = 1 )
   31
   30
   23
MFACE( WIRE, EDG1 = 1, EDG2 = 1, EDG3 = 1, EDG4 = 1 )
CURVE( SELE, ID, WIND = 1 )
   39
   40
   41
   35
MFACE( WIRE, EDG1 = 1, EDG2 = 1, EDG3 = 1, EDG4 = 1 )
CURVE( SELE, ID, WIND = 1 )
   41
   42
   43
   36
MFACE( WIRE, EDG1 = 1, EDG2 = 1, EDG3 = 1, EDG4 = 1 )
CURVE( SELE, ID, WIND = 1 )
   45
   44
   43
CURVE( SELE, ID, WIND = 1 )
   37
MFACE( WIRE, EDG1 = 1, EDG2 = 1, EDG3 = 1, EDG4 = 1 )
CURVE( SELE, ID, WIND = 1 )
   47
   46
   45
   38
MFACE( WIRE, EDG1 = 1, EDG2 = 1, EDG3 = 1, EDG4 = 1 )
POINT( SELE, ID = 11 )
POINT( SELE, ID = 1 )
CURVE( ADD, LINE )
POINT( SELE, ID = 12 )
POINT( SELE, ID = 2 )
CURVE( ADD, LINE )
POINT( SELE, ID = 13 )
POINT( SELE, ID = 3 )
CURVE( ADD, LINE )
POINT( SELE, ID = 14 )
POINT( SELE, ID = 4 )
CURVE( ADD, LINE )
POINT( SELE, ID = 15 )
POINT( SELE, ID = 5 )
CURVE( ADD, LINE )
POINT( SELE, ID = 16 )
POINT( SELE, ID = 6 )
CURVE( ADD, LINE )
POINT( SELE, ID = 17 )
```

```
POINT( SELE, ID = 7 )
CURVE( ADD, LINE )
POINT( SELE, ID = 18 )
POINT( SELE, ID = 8 )
CURVE( ADD, LINE )
POINT( SELE, ID = 19 )
POINT( SELE, ID = 9 )
CURVE( ADD, LINE )
POINT( SELE, ID = 20 )
POINT( SELE, ID = 10 )
CURVE( ADD, LINE )
POINT( SELE, ID = 21 )
POINT( SELE, ID = 1 )
CURVE( ADD, LINE )
POINT( SELE, ID = 22 )
POINT( SELE, ID = 2 )
CURVE( ADD, LINE )
POINT( SELE, ID = 23 )
POINT( SELE, ID = 3 )
CURVE( ADD, LINE )
POINT( SELE, ID = 24 )
POINT( SELE, ID = 4 )
CURVE( ADD, LINE )
POINT( SELE, ID = 25 )
POINT( SELE, ID = 5 )
CURVE( ADD, LINE )
POINT( SELE, ID = 26 )
POINT( SELE, ID = 6 )
CURVE( ADD, LINE )
POINT( SELE, ID = 27 )
POINT( SELE, ID = 7 )
CURVE( ADD, LINE )
POINT( SELE, ID = 28 )
POINT( SELE, ID = 8 )
CURVE( ADD, LINE )
POINT( SELE, ID = 29 )
POINT( SELE, ID = 9 )
CURVE( ADD, LINE )
POINT( SELE, ID = 30 )
POINT( SELE, ID = 10 )
CURVE( ADD, LINE )
CURVE( SELE, ID = 48 )
CURVE( SELE, ID = 49 )
CURVE( SELE, ID = 50 )
CURVE( SELE, ID = 51 )
CURVE( SELE, ID = 52 )
CURVE( SELE, ID = 53 )
CURVE( SELE, ID = 54 )
CURVE( SELE, ID = 55 )
CURVE( SELE, ID = 56 )
CURVE( SELE, ID = 57 )
```

```
CURVE( SELE, ID = 58 )
CURVE( SELE, ID = 59 )
CURVE( SELE, ID = 60 )
CURVE( SELE, ID = 61 )
CURVE( SELE, ID = 62 )
CURVE( SELE, ID = 63 )
CURVE( SELE, ID = 64 )
CURVE( SELE, ID = 65 )
CURVE( SELE, ID = 66 )
CURVE( SELE, ID = 67 )
MEDGE( ADD, SUCC, INTE = 9, RATI = 0, 2RAT = 0, PCEN = 0 )
CURVE( SELE, ID = 48 )
UTILITY( UNSE, ALL )
CURVE( SELE, ID = 51 )
CURVE( SELE, ID = 24 )
CURVE( SELE, ID = 49 )
CURVE( SELE, ID = 2 )
MFACE( WIRE, EDG1 = 1, EDG2 = 1, EDG3 = 1, EDG4 = 1 )
CURVE( SELE, ID = 49 )
CURVE( SELE, ID = 20 )
CURVE( SELE, ID = 55 )
CURVE( SELE, ID = 12 )
MFACE( WIRE, EDG1 = 1, EDG2 = 1, EDG3 = 1, EDG4 = 1 )
CURVE( SELE, ID = 55 )
CURVE( SELE, ID = 21 )
CURVE( SELE, ID = 48 )
CURVE( SELE, ID = 13 )
MFACE( WIRE, EDG1 = 1, EDG2 = 1, EDG3 = 1, EDG4 = 1 )
CURVE( SELE, ID = 48 )
CURVE( SELE, ID = 22 )
CURVE( SELE, ID = 56 )
CURVE( SELE, ID = 15 )
MFACE( WIRE, EDG1 = 1, EDG2 = 1, EDG3 = 1, EDG4 = 1 )
CURVE( SELE, ID = 56 )
CURVE( SELE, ID = 23 )
CURVE( SELE, ID = 50 )
CURVE( SELE, ID = 14 )
MFACE( WIRE, EDG1 = 1, EDG2 = 1, EDG3 = 1, EDG4 = 1 )
CURVE( SELE, ID = 61 )
UTILITY( UNSE, ALL )
CURVE( SELE, ID = 50 )
CURVE( SELE, ID = 32 )
CURVE( SELE, ID = 53 )
CURVE( SELE, ID = 3 )
MFACE( WIRE, EDG1 = 1, EDG2 = 1, EDG3 = 1, EDG4 = 1 )
CURVE( SELE, ID = 61 )
CURVE( SELE, ID = 39 )
CURVE( SELE, ID = 59 )
CURVE( SELE, ID = 2 )
MFACE( WIRE, EDG1 = 1, EDG2 = 1, EDG3 = 1, EDG4 = 1 )
CURVE( SELE, ID = 59 )
```

```
CURVE( SELE, ID = 35 )
CURVE( SELE, ID = 65 )
CURVE( SELE, ID = 12 )
MFACE( WIRE, EDG1 = 1, EDG2 = 1, EDG3 = 1, EDG4 = 1 )
CURVE( SELE, ID = 65 )
CURVE( SELE, ID = 36 )
CURVE( SELE, ID = 58 )
CURVE( SELE, ID = 13 )
MFACE( WIRE, EDG1 = 1, EDG2 = 1, EDG3 = 1, EDG4 = 1 )
CURVE( SELE, ID = 58 )
CURVE( SELE, ID = 37 )
CURVE( SELE, ID = 66 )
CURVE( SELE, ID = 15 )
MFACE( WIRE, EDG1 = 1, EDG2 = 1, EDG3 = 1, EDG4 = 1 )
CURVE( SELE, ID = 66 )
CURVE( SELE, ID = 38 )
CURVE( SELE, ID = 60 )
CURVE( SELE, ID = 14 )
MFACE( WIRE, EDG1 = 1, EDG2 = 1, EDG3 = 1, EDG4 = 1 )
CURVE( SELE, ID = 60 )
CURVE( SELE, ID = 47 )
CURVE( SELE, ID = 63 )
CURVE( SELE, ID = 3 )
MFACE( WIRE, EDG1 = 1, EDG2 = 1, EDG3 = 1, EDG4 = 1 )
CURVE( SELE, ID = 51 )
CURVE( SELE, ID = 25 )
CURVE( SELE, ID = 52 )
CURVE( SELE, ID = 5 )
MFACE( WIRE, EDG1 = 1, EDG2 = 1, EDG3 = 1, EDG4 = 1 )
CURVE( SELE, ID = 55 )
CURVE( SELE, ID = 26 )
CURVE( SELE, ID = 52 )
CURVE( SELE, ID = 9 )
MFACE( WIRE, EDG1 = 1, EDG2 = 1, EDG3 = 1, EDG4 = 1 )
CURVE( SELE, ID = 48 )
CURVE( SELE, ID = 28 )
CURVE( SELE, ID = 57 )
CURVE( SELE, ID = 11 )
MFACE( WIRE, EDG1 = 1, EDG2 = 1, EDG3 = 1, EDG4 = 1 )
CURVE( SELE, ID = 56 )
CURVE( SELE, ID = 30 )
CURVE( SELE, ID = 54 )
CURVE( SELE, ID = 10 )
MFACE( WIRE, EDG1 = 1, EDG2 = 1, EDG3 = 1, EDG4 = 1 )
CURVE( SELE, ID = 61 )
CURVE( SELE, ID = 40 )
CURVE( SELE, ID = 62 )
CURVE( SELE, ID = 5 )
MFACE( WIRE, EDG1 = 1, EDG2 = 1, EDG3 = 1, EDG4 = 1 )
CURVE( SELE, ID = 65 )
CURVE( SELE, ID = 41 )
```

```
CURVE( SELE, ID = 62 )
CURVE( SELE, ID = 9 )
MFACE( WIRE, EDG1 = 1, EDG2 = 1, EDG3 = 1, EDG4 = 1 )
CURVE( SELE, ID = 58 )
CURVE( SELE, ID = 43 )
CURVE( SELE, ID = 11 )
CURVE( SELE, ID = 67 )
MFACE( WIRE, EDG1 = 1, EDG2 = 1, EDG3 = 1, EDG4 = 1 )
CURVE( SELE, ID = 58 )
CURVE( SELE, ID = 43 )
CURVE( SELE, ID = 67 )
CURVE( SELE, ID = 11 )
MFACE( WIRE, EDG1 = 1, EDG2 = 1, EDG3 = 1, EDG4 = 1 )
CURVE( SELE, ID = 66 )
CURVE( SELE, ID = 45 )
CURVE( SELE, ID = 64 )
CURVE( SELE, ID = 10 )
MFACE( WIRE, EDG1 = 1, EDG2 = 1, EDG3 = 1, EDG4 = 1 )
CURVE( SELE, ID = 53 )
CURVE( SELE, ID = 31 )
CURVE( SELE, ID = 54 )
CURVE( SELE, ID = 6 )
MFACE( WIRE, EDG1 = 1, EDG2 = 1, EDG3 = 1, EDG4 = 1 )
CURVE( SELE, ID = 63 )
CURVE( SELE, ID = 46 )
CURVE( SELE, ID = 64 )
CURVE( SELE, ID = 6 )
MFACE( WIRE, EDG1 = 1, EDG2 = 1, EDG3 = 1, EDG4 = 1 )
CURVE( SELE, ID = 52 )
CURVE( SELE, ID = 27 )
CURVE( SELE, ID = 57 )
CURVE( SELE, ID = 16 )
MFACE( WIRE, EDG1 = 1, EDG2 = 1, EDG3 = 1, EDG4 = 1 )
CURVE( SELE, ID = 57 )
CURVE( SELE, ID = 29 )
CURVE( SELE, ID = 54 )
CURVE( SELE, ID = 17 )
MFACE( WIRE, EDG1 = 1, EDG2 = 1, EDG3 = 1, EDG4 = 1 )
CURVE( SELE, ID = 62 )
CURVE( SELE, ID = 42 )
CURVE( SELE, ID = 67 )
CURVE( SELE, ID = 16 )
MFACE( WIRE, EDG1 = 1, EDG2 = 1, EDG3 = 1, EDG4 = 1 )
CURVE( SELE, ID = 67 )
CURVE( SELE, ID = 44 )
CURVE( SELE, ID = 64 )
CURVE( SELE, ID = 17 )
MFACE( WIRE, EDG1 = 1, EDG2 = 1, EDG3 = 1, EDG4 = 1 )
POINT( ADD, COOR, X = 0.00465, Y = 0.00465, Z = 0.007 )
POINT( ADD, COOR, X = 0.00465, Y = 0.00465, Z = 0.0035 )
POINT( ADD, COOR, X = 0.00465, Y = 0.00465, Z = 0 )
```

```
POINT( SELE, ID = 15 )
POINT( SELE, ID = 31 )
CURVE( ADD, LINE )
POINT( SELE, ID = 31 )
POINT( SELE, ID = 25 )
CURVE( ADD, LINE )
POINT( SELE, ID = 20 )
POINT( SELE, ID = 32 )
CURVE( ADD, LINE )
POINT( SELE, ID = 32 )
POINT( SELE, ID = 30 )
CURVE( ADD, LINE )
POINT( SELE, ID = 17 )
POINT( SELE, ID = 33 )
CURVE( ADD, LINE )
POINT( SELE, ID = 33 )
POINT( SELE, ID = 27 )
CURVE( ADD, LINE )
POINT( SELE, ID = 31 )
POINT( SELE, ID = 32 )
CURVE( ADD, LINE )
POINT( SELE, ID = 32 )
POINT( SELE, ID = 33 )
CURVE( ADD, LINE )
CURVE( SELE, ID = 68 )
CURVE( SELE, ID = 69 )
CURVE( SELE, ID = 70 )
CURVE( SELE, ID = 71 )
CURVE( SELE, ID = 72 )
CURVE( SELE, ID = 73 )
CURVE( SELE, ID = 74 )
CURVE( SELE, ID = 75 )
MEDGE( ADD, SUCC, INTE = 9, RATI = 0, 2RAT = 0, PCEN = 0 )
CURVE( SELE, ID = 52 )
CURVE( SELE, ID = 68 )
CURVE( SELE, ID = 69 )
CURVE( SELE, ID = 62 )
MFACE( WIRE, EDG1 = 1, EDG2 = 1, EDG3 = 1, EDG4 = 1 )
CURVE( SELE, ID = 48 )
UTILITY( UNSE, LAST )
CURVE( SELE, ID = 57 )
CURVE( SELE, ID = 67 )
CURVE( SELE, ID = 71 )
CURVE( SELE, ID = 70 )
MFACE( WIRE, EDG1 = 1, EDG2 = 1, EDG3 = 1, EDG4 = 1 )
CURVE( SELE, ID = 54 )
CURVE( SELE, ID = 64 )
CURVE( SELE, ID = 73 )
CURVE( SELE, ID = 72 )
MFACE( WIRE, EDG1 = 1, EDG2 = 1, EDG3 = 1, EDG4 = 1 )
CURVE( SELE, ID = 68 )
```

```
CURVE( SELE, ID = 27 )
CURVE( SELE, ID = 70 )
CURVE( SELE, ID = 74 )
MFACE( WIRE, EDG1 = 1, EDG2 = 1, EDG3 = 1, EDG4 = 1 )
CURVE( SELE, ID = 70 )
CURVE( SELE, ID = 29 )
CURVE( SELE, ID = 72 )
CURVE( SELE, ID = 75 )
MFACE( WIRE, EDG1 = 1, EDG2 = 1, EDG3 = 1, EDG4 = 1 )
CURVE( SELE, ID = 69 )
CURVE( SELE, ID = 74 )
CURVE( SELE, ID = 71 )
CURVE( SELE, ID = 42 )
MFACE( WIRE, EDG1 = 1, EDG2 = 1, EDG3 = 1, EDG4 = 1 )
CURVE( SELE, ID = 71 )
CURVE( SELE, ID = 44 )
CURVE( SELE, ID = 73 )
CURVE( SELE, ID = 75 )
MFACE( WIRE, EDG1 = 1, EDG2 = 1, EDG3 = 1, EDG4 = 1 )
MFACE( SELE, ID = 5 )
MFACE( SELE, ID = 1 )
MFACE( SELE, ID = 13 )
MFACE( SELE, ID = 14 )
MFACE( SELE, ID = 26 )
MFACE( SELE, ID = 25 )
MSHELL( ADD, VISI, NOSH )
MFACE( SELE, ID = 6 )
MFACE( SELE, ID = 2 )
MFACE( SELE, ID = 26 )
MFACE( SELE, ID = 15 )
MFACE( SELE, ID = 27 )
MFACE( SELE, ID = 35 )
MSHELL( ADD, VISI, NOSH )
MFACE( SELE, ID = 7 )
MFACE( SELE, ID = 3 )
MFACE( SELE, ID = 16 )
MFACE( SELE, ID = 28 )
MFACE( SELE, ID = 36 )
MFACE( SELE, ID = 27 )
MSHELL( ADD, VISI, NOSH )
MFACE( SELE, ID = 8 )
MFACE( SELE, ID = 4 )
MFACE( SELE, ID = 17 )
MFACE( SELE, ID = 18 )
MFACE( SELE, ID = 33 )
MFACE( SELE, ID = 28 )
MSHELL( ADD, VISI, NOSH )
MFACE( SELE, ID = 9 )
MFACE( SELE, ID = 1 )
MFACE( SELE, ID = 19 )
MFACE( SELE, ID = 20 )
```

```
MFACE( SELE, ID = 30 )
MFACE( SELE, ID = 29 )
MSHELL( ADD, VISI, NOSH )
MFACE( SELE, ID = 10 )
MFACE( SELE, ID = 2 )
MFACE( SELE, ID = 30 )
MFACE( SELE, ID = 21 )
MFACE( SELE, ID = 31 )
MFACE( SELE, ID = 37 )
MSHELL( ADD, VISI, NOSH )
MFACE( SELE, ID = 11 )
MFACE( SELE, ID = 3 )
MFACE( SELE, ID = 31 )
MFACE( SELE, ID = 22 )
MFACE( SELE, ID = 32 )
MFACE( SELE, ID = 38 )
MSHELL( ADD, VISI, NOSH )
MFACE( SELE, ID = 12 )
MFACE( SELE, ID = 4 )
MFACE( SELE, ID = 23 )
MFACE( SELE, ID = 24 )
MFACE( SELE, ID = 34 )
MFACE( SELE, ID = 32 )
MSHELL( ADD, VISI, NOSH )
MFACE( SELE, ID = 39 )
MFACE( SELE, ID = 40 )
MFACE( SELE, ID = 35 )
MFACE( SELE, ID = 37 )
MFACE( SELE, ID = 44 )
MFACE( SELE, ID = 42 )
MSHELL( ADD, VISI, NOSH )
MFACE( SELE, ID = 40 )
MFACE( SELE, ID = 41 )
MFACE( SELE, ID = 38 )
MFACE( SELE, ID = 36 )
MFACE( SELE, ID = 43 )
MFACE( SELE, ID = 45 )
MSHELL( ADD, VISI, NOSH )
MSHELL( SELE, ID = 1 )
MSOLID( ADD, MAP )
MSHELL( SELE, ID = 2 )
MSOLID( ADD, MAP )
MSHELL( SELE, ID = 3 )
MSOLID( ADD, MAP )
MSHELL( SELE, ID = 4 )
MSOLID( ADD, MAP )
MSHELL( SELE, ID = 5 )
MSOLID( ADD, MAP )
MSHELL( SELE, ID = 6 )
MSOLID( ADD, MAP )
MSHELL( SELE, ID = 7 )
```

```
MSOLID( ADD, MAP )
MSHELL( SELE, ID = 8 )
MSOLID( ADD, MAP )
MSHELL( SELE, ID = 9 )
MSOLID( ADD, MAP )
MSHELL( SELE, ID = 10 )
MSOLID( ADD, MAP )
MSOLID( SELE, ID = 1 )
ELEMENT( SETD, BRIC, NODE = 8 )
MSOLID( MESH, MAP, ENTI = "gel", ALG1 )
MSOLID( SELE, ID = 2 )
MSOLID( MESH, MAP, ENTI = "gel", ALG1 )
MSOLID( SELE, ID = 3 )
MSOLID( MESH, MAP, ENTI = "gel", ALG1 )
MSOLID( SELE, ID = 4 )
MSOLID( MESH, MAP, ENTI = "gel", ALG1 )
MSOLID( SELE, ID = 5 )
MSOLID( MESH, MAP, ENTI = "gel", ALG1 )
MSOLID( SELE, ID = 6 )
MSOLID( MESH, MAP, ENTI = "gel", ALG1 )
MSOLID( SELE, ID = 7 )
MSOLID( MESH, MAP, ENTI = "gel", ALG1 )
MSOLID( SELE, ID = 8 )
MSOLID( MESH, MAP, ENTI = "gel", ALG1 )
MSOLID( SELE, ID = 9 )
MSOLID( MESH, MAP, ENTI = "gel", ALG1 )
MSOLID( SELE, ID = 10 )
MSOLID( MESH, MAP, ENTI = "gel", ALG1 )
END(  )
FI-BC(  )
WINDOW(CHANGE= 1, MATRIX )
    -.707107    -.408248     .577350     .000000
     .707107    -.408248     .577350     .000000
     .000000     .816497     .577350     .000000
     .000000     .000000     .000000    1.000000
     -.00666      .00666     -.00403      .00595     -.00024      .00965
WINDOW( CHAN = 1, MATR )
-0.707107, -0.408248, 0.57735,     0
0.707107, -0.408248, 0.57735,     0
    0, 0.816497, 0.57735,     0
    0,     0,     0,     1
-0.00666, 0.00666, -0.00403, 0.00595, -0.00024, 0.00965
BGADD( SELE, FACE, INCL, ID, WIND = 1 )
BGADD( SELE, FACE, INCL, ID, WIND = 1 )
   20
   37
BGADD( SELE, FACE, INCL, ID, WIND = 1 )
   45
BGADD( ADD, FACE, ENTI = "inflow", INCL )
BGADD( SELE, FACE, INCL, ID, WIND = 1 )
    4
```

```
   24
   39
BGADD( ADD, FACE, ENTI = "outflow", INCL )
BGADD( SELE, FACE, INCL, ID, WIND = 1 )
    2
BGADD( SELE, FACE, INCL, ID, WIND = 1 )
    7
BGADD( SELE, FACE, INCL, ID, WIND = 1 )
   13
BGADD( SELE, FACE, INCL, ID, WIND = 1 )
   18
BGADD( ADD, FACE, ENTI = "fiber1", INCL )
BGADD( SELE, FACE, INCL, ID, WIND = 1 )
   23
BGADD( SELE, FACE, INCL, ID, WIND = 1 )
   27
BGADD( SELE, FACE, INCL, ID, WIND = 1 )
   32
BGADD( SELE, FACE, INCL, ID, WIND = 1 )
   36
BGADD( ADD, FACE, ENTI = "fiber2", INCL )
BGADD( SELE, FACE, INCL, ID, WIND = 1 )
    1
BGADD( ADD, FACE, ENTI = "symmetry1", INCL )
BGADD( SELE, FACE, INCL, ID, WIND = 1 )
   22
BGADD( ADD, FACE, ENTI = "symmetry2", INCL )
BGADD( SELE, FACE, INCL, ID, WIND = 1 )
   17
BGADD( ADD, FACE, ENTI = "symmetry3", INCL )
BGADD( SELE, FACE, INCL, ID, WIND = 1 )
   35
BGADD( ADD, FACE, ENTI = "symmetry4", INCL )
BGADD( SELE, FACE, INCL, ID, WIND = 1 )
    3
BGADD( SELE, FACE, INCL, ID, WIND = 1 )
    8
BGADD( SELE, FACE, INCL, ID, WIND = 1 )
   14
BGADD( SELE, FACE, INCL, ID, WIND = 1 )
   19
BGADD( SELE, FACE, INCL, ID, WIND = 1 )
   40
BGADD( SELE, FACE, INCL, ID, WIND = 1 )
   43
BGADD( ADD, FACE, ENTI = "symmetry5", INCL )
BGADD( SELE, FACE, INCL, ID, WIND = 1 )
   26
BGADD( SELE, FACE, INCL, ID, WIND = 1 )
   30
BGADD( SELE, FACE, INCL, ID, WIND = 1 )
```

```
   34
BGADD( SELE, FACE, INCL, ID, WIND = 1 )
   38
BGADD( SELE, FACE, INCL, ID, WIND = 1 )
   41
BGADD( SELE, FACE, INCL, ID, WIND = 1 )
   44
BGADD( ADD, FACE, ENTI = "symmetry6", INCL )
BCSENTITY( BCNO )
BCSENTITY( SELE, ID, WIND = 1 )
    6
    8
BCSENTITY( SELE, ID, WIND = 1 )
   11
BCNODE( UY, GSEL, ZERO )
UTILITY( UNSE, ALL )
BCSENTITY( BCNO )
BCSENTITY( SELE, ID, WIND = 1 )
    7
BCSENTITY( SELE, ID, WIND = 1 )
    9
BCSENTITY( SELE, ID, WIND = 1 )
   10
BCNODE( UX, GSEL, ZERO )
UTILITY( UNSE, ALL )
BCSENTITY( BCNO )
BCSENTITY( SELE, ID, WIND = 1 )
    4
BCSENTITY( SELE, ID, WIND = 1 )
    5
BCNODE( UN3, GSEL, ZERO )
UTILITY( UNSE, ALL )
BCSENTITY( BCFL )
BCSENTITY( SELE, ID, WIND = 1 )
    2
BCFLUX( Z, GSEL, CONS = 133322.3684 )
END(  )
FIPREP(  )
EXECUTION( ADD, NEWJ )
PRESSURE( ADD, MIXE = 1e-23, DISC )
PROBLEM( ADD, 3-D, INCO, STEA, LAMI, NONL, NEWT, MOME, ISOT, FIXE, SING )
SOLUTION( ADD, SEGR = 500, PREC = 21, ACCF = 0, PPRO )
ENTITY( ADD, NAME = "gel", PORO )
ENTITY( ADD, NAME = "inflow", PLOT )
ENTITY( ADD, NAME = "outflow", PLOT )
ENTITY( ADD, NAME = "symmetry1", PLOT )
ENTITY( ADD, NAME = "symmetry2", PLOT )
ENTITY( ADD, NAME = "symmetry3", PLOT )
ENTITY( ADD, NAME = "symmetry4", PLOT )
ENTITY( ADD, NAME = "symmetry5", PLOT )
ENTITY( ADD, NAME = "symmetry6", PLOT )
```

```
ENTITY( ADD, NAME = "fiber1", SLIP )
ENTITY( ADD, NAME = "fiber2", SLIP )
DENSITY( ADD, SET = 1, CONS = 1 )
PERMEABILITY( ADD, SET = 1, ACOE, CONS = 100, X = 2.1697e-13, Y = 2.1697e-13,
Z = 2.1697e-13 )
VISCOSITY( ADD, SET = 1, CONS = 8.904e-05 )
END(  )
CREATE( FISO )
RUN( FISOLV, IDEN = "mesh", FORE, FISOLVME = 2000000, COMP )
FIPOST(  )
FLOWRATE( ENTI = "inflow" )
END(  )
```

APPENDIX B

FORTRAN Code: Laminar Boundary Layer Model for Concentration Polarization in Stirred Ultrafiltration Cells

The following Appendix contains the FORTRAN code used to solve the boundary value problem given by Eqs. 3-26 through 3-29 using the numerical method outlined in Section 3.2.6. The code was compiled using FORTRAN77 on an Athena workstation.

```
------------------------------------------------------------------------------------------------------------
**************************************************************************
* This program uses a modified Crank-Nicolson method to solve for the  *
* concentration of a solute in a stirred UF cell in the presence of    *
* Bodewadt flow.  For more information on this problem, see memo from  *
* WMD on this topic (7/31/97).  The form of the equation is:           *
*                                                                      *
*     (Y-1)(fp*Z+gamma*Z^2)*(df/dY)-(fp*Z^2+delta*Z^3+alpha)*(df/dZ)   *
*     = d2f/dZ2                                                        *
*                                                                      *
*      where:  f  = psi                                                *
*              Y  = non-dim. radial coord. = 1 - r/R                   *
*              Z  = non-dim. axial coord. (see definition in thesis)   *
*              fp = F'(0) = -0.941971                                  *
*              gamma, delta = higher order velocity terms (see below)  *
*              alpha = non-dim. filtration term                        *
*                                                                      *
*      other notation:                                                 *
*              Sc = Schmidt number                                     *
*              beta = F'(0)                                            *
*              fpp = F''(0) = 1.10                                     *
*              vavg = average filtration velocity                      *
*              omega = stirring rate                                   *
*              nu = kinematic viscosity                                *
*              mtcavg = average mass transfer coefficient              *
*              diff = diffusivity                                      *
*              Lp = hydraulic permeability                             *
*              Cinf = bulk solute concentration                        *
```

```
*              sigma = filtration reflection coefficient                *
*              R = gas constant                                         *
*              T = temp. (K)                                            *
*              charge = molecule charge (for Vilker et al. expression)  *
*              A2, A3, ms = see Vilker et al. expression                *
*              MWbsa = molecular weight of albumin (Vilker et al.)      *
*              factor = iteration factor (given as f in text)           *
*              Cavg = average concentration at membrane surface         *
*              Pavg = pressure (not osmotic) average at membrane        *
*              Darcy = Darcy permeability                               *
*              thick = thickness of membrane                            *
*              mixcup = mixing cup average of filtrate conc.            *
*              Cfavg = measured filtrate concentration                  *
*              theta = sieving coefficient (true)                       *
*************************************************************************
      PROGRAM polarize

      INTEGER zmax, fdim, ydim, count
      DOUBLE PRECISION ystep, zstep, Z, Y, beta, delta
      DOUBLE PRECISION gamma, Sc, fpp, fp
      DOUBLE PRECISION vavg, omega, nu, epsilon, mtcavg, mtcavgn
      DOUBLE PRECISION change, errtol, diff, mtcsum, Lp, Cinf
      DOUBLE PRECISION sigma, R, T, charge, A2, A3, MWbsa, ms
      DOUBLE PRECISION slope, vavgold, Cavg, Pavg, xcoord, ycoord
      DOUBLE PRECISION factor
      DOUBLE PRECISION Darcy, thick, mixcupold, mixcup, Cfavg
      DOUBLE PRECISION theta, Nfavg

c     Note:  Code is commented out for runs where solute has been
c            assumed to be dilute enough so that osmotic pressure
c            does not affect results.  Uncomment lines as necessary!

c     Set iteration factor

c      PARAMETER (factor = 0.5)

c     Set parameters

c     Note:  Code is written for Ficoll (7.0 nm).  Change numbers
c            as needed (diff, Sc)

      PARAMETER (Sc = 15728.3333*6.0/3.571)
      PARAMETER (fp = -0.941971)
      PARAMETER (fpp = 1.10)
      PARAMETER (beta = fp)

c     If including higher order velocity terms:

      PARAMETER (delta = 1.0/3.0*fpp*Sc**(-1.0/3.0))
      PARAMETER (gamma = 0.5*fpp*Sc**(-1.0/3.0))
```

```
c     If neglecting higher order velocity terms:

c      PARAMETER (delta = 0.0)
c      PARAMETER (gamma = 0.0)

      PARAMETER (omega = 23.034*0.36)
      PARAMETER (nu = 0.009437)
      PARAMETER (errtol = 0.000000000000001)
      PARAMETER (diff = 0.0000003571)
      PARAMETER (R = 62.36)
      PARAMETER (T = 298.0)
      PARAMETER (A2 = -0.008252433)
      PARAMETER (A3 = 0.000106579)
      PARAMETER (charge = -18.144528)
      PARAMETER (MWbsa = 68000.0)
      PARAMETER (ms = 0.1)

      PARAMETER (zmax = 10)
      PARAMETER (zstep = 0.1)
      PARAMETER (ystep = 0.01)
      PARAMETER (fdim = (zmax/zstep) + 1)
      PARAMETER (ydim = (1.0/ystep) + 1)

c     If have Lp, enter Lp, if have Darcy, enter
c     Darcy and calculate Lp from Darcy (below)

c      PARAMETER (Lp = 6.17592e-9)
      PARAMETER (Darcy = 4.64615e-14)
      PARAMETER (thick = 0.007)

c     For comparing to Smith and Colton:
c      Lp = 0.0

      PARAMETER (theta = 0.135)
c      PARAMETER (sigma = 1.0 - theta)

c     An initial guess

      PARAMETER (Cinf = 2.17290595)

c     Arrays

      DOUBLE PRECISION f(fdim), ft(fdim), fn(fdim), LHS1(fdim,3)
      DOUBLE PRECISION LHS2(fdim,3), ff(fdim,ydim), l(fdim), d(fdim)
      DOUBLE PRECISION u(fdim), RHS1(fdim), RHS2(fdim)
      DOUBLE PRECISION vf(ydim), alpha(ydim), V(ydim),dfdZ(ydim)
      DOUBLE PRECISION dfdzeta(ydim), dfdzee(ydim), mtc(ydim)
      DOUBLE PRECISION Cm(ydim), DPstat(ydim), DPi(ydim)
      DOUBLE PRECISION nalpha(ydim)
      DOUBLE PRECISION Cf(ydim)
```

```
c     Calculate Lp from Darcy permeability (my mesh factor)

      Lp = 0.510*Darcy/(0.009437*thick)

c     Setup initial filtration information

      DO i=1,ydim
         Cm(i) = 2.75116364
         Cf(i) = 0.35370021

c     To use Vilker expression:

c         DPi(i) = R*T*(2.0*((charge*Cm(i)/(2.0*MWbsa))**2 +
c     &             ms**2)**(0.5) - 2.0*ms) + R*T/MWbsa*
c     &             (Cm(i) + A2*Cm(i)**2 + A3*Cm(i)**3) -
c     &             (R*T*(2.0*((charge*Cf(i)/(2.0*MWbsa))**2 +
c     &             ms**2)**(0.5) - 2.0*ms) + R*T/MWbsa*
c     &             (Cf(i) + A2*Cf(i)**2 + A3*Cf(i)**3))

c     Static pressure (neglect or keep radial variation)
c     Note need for number for cell radius (1.05 for 10 ml cell)

c         DPstat(i) = 137499.7352
         DPstat(i) = 140550.6998 + (omega**2*1.05**2/2.0)*
     &               (((1.05*(1.0 - (i-1)*ystep))/(1.05))**2 -
     &               0.5)

c     Filtration rate (with or without osmotic pressure)

c         vf(i) = Lp*(DPstat(i) - sigma*DPi(i)*
c     &           1.01325e5/760.0*10.0)
         vf(i) = Lp*(DPstat(i))

      ENDDO

c     Calculate vavg using Simpson's Rule

      vavg = 0.0

      DO i=1,ydim
         IF (i .EQ. 1) THEN
            vavg = vavg + vf(i)*(1.0 - (i-1)*ystep)
         ELSEIF (i .EQ. ydim) THEN
            vavg = vavg + vf(i)*(1.0 - (i-1)*ystep)
         ELSEIF (MOD(i,2) .EQ. 0) THEN
            vavg = vavg + 4.0*vf(i)*(1.0 - (i-1)*ystep)
         ELSE
            vavg = vavg + 2.0*vf(i)*(1.0 - (i-1)*ystep)
         ENDIF
      ENDDO
```

```
      vavg = 2.0/3.0*ystep*vavg

c      vavg = vf(1)

      epsilon = vavg/(omega*nu)**(0.5)

      DO i=1,ydim
         V(i) = vf(i)/vavg
         alpha(i) = epsilon*Sc**(2.0/3.0)*V(i)

c     For comparison with Smith and Colton:
c         alpha(i) = 0.0

      ENDDO

      count = 0

c     Iterate on the mixing cup average or vavg

c      vavgold = 0.00001
      mixcupold = 5.0

c     Calculate first mixing cup average

      mixcup = Cf(1)

c     BEGIN OVERALL ITERATION

c 100  change = (vavg - vavgold)/vavgold
 100  change = (mixcup - mixcupold)/mixcupold

      WRITE(*,*) count

      IF (change .LT. 0.0) THEN
         change = change*(-1.0)
      ENDIF

      IF (change .LT. errtol) THEN
         GOTO 500
      ENDIF

      count = count + 1

c     Initialize ff (matrix to store final conc. field)

      DO i=1,fdim
         DO j=1,ydim
            ff(i,j) = 0.0
         ENDDO
      ENDDO
```

```
c     Write BC for cell wall (Y = 0) into f and ff matrix

      DO i=1, fdim
         f(i) = 1.0
         ff(i,1) = f(i)
      ENDDO

      Y = 0.0


c     **********BEGIN ITERATION**********

      DO k = 2, ydim

         Y = (k - 1.0)*ystep

      Z = 0.0

c     Initialize vectors

         DO i=1, fdim
            ft(i) = 0.0
            fn(i) = 0.0
            l(i) = 0.0
            d(i) = 0.0
            u(i) = 0.0
            RHS1(i) = 0.0
            RHS2(i) = 0.0
         ENDDO

c     Initialize LHS1 and LHS2

         DO i=1,fdim
            DO j=1,3
               LHS1(i,j) = 0.0
               LHS2(i,j) = 0.0
            ENDDO
         ENDDO

c     Form LHS1

         DO i=1,fdim
            Z = (i - 1.0)*zstep
            IF (i .EQ. 1) THEN
               DO j=1,3
                  IF (j .EQ. 1) THEN
                     LHS1(i,j) = 0.0
                  ELSE
                     IF (j .EQ. 2) THEN
                        LHS1(i,j) = (alpha(k)*(1.0 - theta)
     &                                 - (1.0/zstep))
```

```
c     For comparing with Smith and Colton (constant conc. at surface):
c                        LHS1(i,j) = 1.0

                      ELSE
                         LHS1(i,j) = 1.0/zstep

c     For comparing with Smith and Colton (constant conc. at surface):
c                        LHS1(i,j) = 0.0

                      ENDIF
                   ENDIF
                ENDDO
             ELSE
                IF (i .LT. fdim) THEN
                   DO j=1,3
                      IF (j .EQ. 2) THEN
                         LHS1(i,j) = -2.0/zstep**2 - 2.0*(1.0-
     &                                    (Y-0.5*ystep))*
     &                                    (-1.0*beta*Z-gamma*Z**2)/ystep
                      ELSE
                         LHS1(i,j) = 1.0/((zstep)**2)
                      ENDIF
                   ENDDO
                ELSE
                   DO j=1,3

c     For constant conc. at large Z:
c                     IF (j.EQ. 2) THEN
c                        LHS1(i,j) = 1.0
c                     ENDIF
c     For zero gradient at large Z:
                   IF (j .EQ. 1) THEN
                      LHS1(i,j) = -1.0
                   ELSE
                      IF (j .EQ. 2) THEN
                         LHS1(i,j) = 1.0
                      ELSE
                         LHS1(i,j) = 0.0
                      ENDIF
                   ENDIF
                   ENDDO
                ENDIF
             ENDIF
          ENDDO

c     Write pieces of LHS1 into the 3 vectors for Thomas algorithm

          DO i=1,fdim
             l(i) = LHS1(i,1)
             d(i) = LHS1(i,2)
```

```
            u(i) = LHS1(i,3)
         ENDDO

c     Form RHS1

         Z = 0.0
         DO i=1,fdim
            Z = (i - 1.0)*zstep
            IF (i .EQ. 1) THEN
               RHS1(i) = 0.0

c     For comparing with Smith and Colton (constant conc. at surface):
c              RHS1(i) = Cm(i)/Cinf

            ELSEIF (i .LT. fdim) THEN
               RHS1(i) = -(alpha(k)+beta*Z**2+delta*Z**3)*
     &                    (f(i+1)-f(i-1))/
     &                    (2.0*zstep)-2.0*(1.0 -
     &                    (Y-0.5*ystep))*
     &                    (-1.0*beta*Z-gamma*Z**2)*f(i)/ystep
            ELSE

c     For constant concentration at large Z:
c              RHS1(i) = 1.0
c     For zero gradient at large Z:
               RHS1(i) = 0.0
            ENDIF
         ENDDO


c     Thomas Algorithm

         DO i=2,fdim
            d(i) = d(i) - (l(i)/d(i-1))*u(i-1)
         ENDDO

         DO i=2,fdim
            RHS1(i) = RHS1(i)-(l(i)/d(i-1))*RHS1(i-1)
         ENDDO

         ft(fdim)=RHS1(fdim)/d(fdim)

         DO i=fdim-1,1, -1
            ft(i) = (RHS1(i) - u(i)*ft(i+1))/d(i)
         ENDDO

c     Begin second half step

         Z = 0.0

c     Form LHS2
```

```
      DO i=1,fdim
         Z = (i - 1.0)*zstep
         IF (i .EQ. 1) THEN
            DO j=1,3
               IF (j .EQ. 1) THEN
                  LHS2(i,j) = 0.0
               ELSE
                  IF (j .EQ. 2) THEN
                     LHS2(i,j) = (alpha(k)*(1.0 - theta)
     &                              - (1.0/zstep))

c     For comparing with Smith and Colton (constant conc. at surface):
c                       LHS2(i,j) = 1.0

                  ELSE
                     LHS2(i,j) = 1.0/zstep

c     For comparing with Smith and Colton (constant conc. at surface):
c                       LHS2(i,j) = 0.0

                  ENDIF
               ENDIF
            ENDDO
         ELSE
            IF (i .LT. fdim) THEN
               DO j=1,3
                  IF (j .EQ. 2) THEN
                     LHS2(i,j) = -1.0/(zstep)**2 - (1.0-Y)*
     &                              (-1.0*beta*Z-gamma*Z**2)/ystep
                  ELSE
                     LHS2(i,j) = 1.0/(2.0*(zstep)**2)
                  ENDIF
               ENDDO
            ELSE
               DO j=1,3

c     For constant conc. at large Z:
c                     IF (j.EQ. 2) THEN
c                        LHS2(i,j) = 1.0
c                     ENDIF
c     For zero gradient at large Z:
                  IF (j .EQ. 1) THEN
                     LHS2(i,j) = -1.0
                  ELSE
                     IF (j .EQ. 2) THEN
                        LHS2(i,j) = 1.0
                     ELSE
                        LHS2(i,j) = 0.0
                     ENDIF
                  ENDIF
```

```
                  ENDDO
               ENDIF
            ENDIF
         ENDDO

c     Write pieces of LHS2 into the 3 vectors for Thomas algorithm

         DO i=1,fdim
            l(i) = LHS2(i,1)
            d(i) = LHS2(i,2)
            u(i) = LHS2(i,3)
         ENDDO

c     Form RHS2

         Z = 0.0
         DO i=1,fdim
            Z = (i - 1.0)*zstep
            IF (i .EQ. 1) THEN
               RHS2(i) = 0.0

c     For comparing with Smith and Colton (constant conc. at surface):
c              RHS2(i) = Cm(i)/Cinf

            ELSEIF (i .LT. fdim) THEN
               RHS2(i) = -0.5*((f(i+1)-2.0*f(i)+f(i-1))/(zstep**2))
     $                   -(alpha(k)+beta*Z**2+delta*Z**3)*
     $                   ((ft(i+1) - ft(i-1))/(2.0*zstep))
     $                   -(1.0-Y)*(-1.0*beta*Z-gamma*Z**2)*f(i)/ystep
            ELSE

c     For constant conc. at large Z:
c              RHS2(i) = 1.0
c     For zero gradient at large Z:
               RHS2(i) = 0.0
            ENDIF
         ENDDO

c     Thomas Algorithm

         DO i=2,fdim
            d(i) = d(i) - l(i)/d(i-1)*u(i-1)
         ENDDO

         DO i=2,fdim
            RHS2(i) = RHS2(i)-(l(i)/d(i-1))*RHS2(i-1)
         ENDDO

         fn(fdim)=RHS2(fdim)/d(fdim)

         DO i=fdim-1,1, -1
```

```
            fn(i) = (RHS2(i) - u(i)*fn(i+1))/d(i)
         ENDDO

c     Write fn into the ff matrix

         DO i=1,fdim
           ff(i,k) = fn(i)
         ENDDO

c     Rewrite f

         DO i=1,fdim
            f(i) = fn(i)
         ENDDO

      ENDDO

c     Calculate average mass transfer coefficient

c     Finish region near center, first capping concentration
c     at equilibrium value

      DO i=ydim-2,ydim
         ff(1,i) = ff(1,ydim-3)
         ff(2,i) = ff(2,ydim-3)
      ENDDO

      DO i=1,ydim
         dfdZ(i) = 0.0
         dfdzeta(i) = 0.0
         dfdzee(i) = 0.0
         mtc(i) = 0.0
      ENDDO

      DO i=1,ydim
         dfdZ(i) = (ff(2,i) - ff(1,i))/zstep
         dfdzeta(i) = dfdZ(i)*Sc**(1.0/3.0)
         dfdzee(i) = dfdzeta(i)*(omega/nu)**(0.5)
         mtc(i) = -1.0*diff*(1.0/(ff(1,i) - 1.0))*dfdzee(i)
      ENDDO

      mtcsum = 0.0

      DO i=2,ydim-1
         mtcsum = mtcsum + mtc(i)
      ENDDO

      mtcavg = mtcavgn

      mtcavgn = 0.0
```

```
      DO i=2,ydim-1
         IF (i .EQ. 2) THEN
            mtcavgn = mtcavgn + mtc(i)*(1.0 - (i-1)*ystep)
         ELSEIF (i .EQ. ydim-1) THEN
            mtcavgn = mtcavgn + mtc(i)*(1.0 - (i-1)*ystep)
         ELSEIF (MOD(i,2) .EQ. 1) THEN
            mtcavgn = mtcavgn + mtc(i)*4.0*(1.0 - (i-1)*ystep)
         ELSE
            mtcavgn = mtcavgn + mtc(i)*2.0*(1.0 - (i-1)*ystep)
         ENDIF
      ENDDO

      mtcavgn = 2.0/3.0*ystep*mtcavgn

c     Calculate new velocities

c     Write vavg into vavgold

c      vavgold = vavg


c     Finish

      DO i=1,ydim
         Cm(i) = ff(1,i)*Cinf

c     If using osmotic pressure, uncomment lines below:

c         DPi(i) = R*T*(2.0*((charge*Cm(i)/(2.0*MWbsa))**2 +
c     &             ms**2)**(0.5) - 2.0*ms) + R*T/MWbsa*
c     &             (Cm(i) + A2*Cm(i)**2 + A3*Cm(i)**3)
c         vf(i) = Lp*(DPstat(i) - sigma*DPi(i)*
c     &           1.01325e5/760.0*10.0)

      ENDDO

c     calculate vavg using Simpson's Rule

c      vavg = 0.0

c      DO i=1,ydim
c         IF (i .EQ. 1) THEN
c            vavg = vavg + vf(i)*(1.0 - (i-1)*ystep)
c         ELSEIF (i .EQ. ydim) THEN
c            vavg = vavg + vf(i)*(1.0 - (i-1)*ystep)
c         ELSEIF (MOD(i,2) .EQ. 0) THEN
c            vavg = vavg + 4.0*vf(i)*(1.0 - (i-1)*ystep)
c         ELSE
c            vavg = vavg + 2.0*vf(i)*(1.0 - (i-1)*ystep)
c         ENDIF
c      ENDDO
```

```
c       vavg = 2.0/3.0*ystep*vavg

c       epsilon = vavg/(omega*nu)**(0.5)

c       DO i=1,ydim
c          nalpha(i) = 0.0
c       ENDDO

c       DO i=1,ydim
c          V(i) = vf(i)/vavg
c          nalpha(i) = epsilon*Sc**(2.0/3.0)*V(i)
c       ENDDO

c       DO i=1,ydim
c          IF (nalpha(i) .LT. alpha(i)) THEN
c             alpha(i) = alpha(i) - factor*(alpha(i)
c      &                  - nalpha(i))
c          ELSE
c             alpha(i) = alpha(i) + factor*(nalpha(i)
c      &                  - alpha(i))
c          ENDIF
c       ENDDO

c      Calculate Cf(r) and mixing cup average

       DO i=1,ydim
          Cf(i) = theta*Cm(i)
       ENDDO

c      Use Nfavg for variable filtration rate.  If rate
c      does not vary with radial position, mixing cup is
c      jut equal to area average.

       Cfavg = 0.0
       Nfavg = 0.0

       DO i=1,ydim
          IF (i .EQ. 2) THEN
             Nfavg = Nfavg + vf(i)*Cf(i)*(1.0 - (i-1)*ystep)
          ELSEIF (i .EQ. ydim-1) THEN
             Nfavg = Nfavg + vf(i)*Cf(i)*(1.0 - (i-1)*ystep)
          ELSEIF (MOD(i,2) .EQ. 1) THEN
             Nfavg = Nfavg + vf(i)*Cf(i)*4.0*(1.0 - (i-1)*ystep)
          ELSE
             Nfavg = Nfavg + vf(i)*Cf(i)*2.0*(1.0 - (i-1)*ystep)
          ENDIF
       ENDDO

c       DO i=1,ydim
c          IF (i .EQ. 2) THEN
```

```
c            Cfavg = Cfavg + Cf(i)*(1.0 - (i-1)*ystep)
c         ELSEIF (i .EQ. ydim-1) THEN
c            Cfavg = Cfavg + Cf(i)*(1.0 - (i-1)*ystep)
c         ELSEIF (MOD(i,2) .EQ. 1) THEN
c            Cfavg = Cfavg + Cf(i)*4.0*(1.0 - (i-1)*ystep)
c         ELSE
c            Cfavg = Cfavg + Cf(i)*2.0*(1.0 - (i-1)*ystep)
c         ENDIF
c      ENDDO

      Nfavg = 2.0/3.0*ystep*Nfavg
c      Cfavg = 2.0/3.0*ystep*Cfavg

      Cfavg = Nfavg/vavg

      mixcupold = mixcup

      mixcup = Cfavg

      GOTO 100

 500  DO i=1,ydim
         WRITE(*,*) Cm(i),'   ',Cf(i),'   ',Cf(i)/Cm(i)
      ENDDO

      DO i=1,ydim
         IF (i .EQ. 1) THEN
            Cavg = Cavg + Cm(i)*(1.0 - (i-1)*ystep)
         ELSEIF (i .EQ. ydim) THEN
            Cavg = Cavg + Cm(i)*(1.0 - (i-1)*ystep)
         ELSEIF (MOD(i,2) .EQ. 0) THEN
            Cavg = Cavg + 4.0*Cm(i)*(1.0 - (i-1)*ystep)
         ELSE
            Cavg = Cavg + 2.0*Cm(i)*(1.0 - (i-1)*ystep)
         ENDIF
      ENDDO

      Cavg = 2.0/3.0*ystep*Cavg

c     Correct final mtcavg for the fact that part of the
c     area was not used in determining the average.  This
c     correction will vary with step size in the radial
c     direction!

      mtcavgn = mtcavgn/0.98

      WRITE(*,*)'final mtcavg = ',mtcavgn
      WRITE(*,*)'final vavg = ',vavg
      WRITE(*,*)'final Cavg = ',Cavg
      WRITE(*,*)'final Cfavg = ',Cfavg
```

```
      OPEN (UNIT = 10, FILE = 'f.out', FORM = 'formatted',
     &          STATUS = 'unknown')

      OPEN (UNIT = 20, FILE = 'v.out', FORM = 'formatted',
     &          STATUS = 'unknown')

 50       FORMAT (1X, 5001E25.10)

          DO i=1,ydim
             WRITE (10,50)(ff(j,i),j=1,fdim)
          ENDDO

      DO i=1,ydim
         WRITE(20,*) vf(i)
      ENDDO

      END
```

BIBLIOGRAPHY

Anderson, J. L., "Configurational Effect of the Reflection Coefficient for Rigid Solutes in Capillary Pores," *J. Theor. Biol.*, **90**, 405-426 (1981).

Anderson, J. L., and Malone, D. M., "Mechanism of Osmotic Flow in Porous Membranes," *Biophys. J.*, **14**, 957-982 (1974).

Battacharjee, S., Kim, A. S., and Elimelech, M., "Concentration Polarization of Interacting Solute Particles in Cross-Flow Membrane Filtration," *J. Colloid Interface Sci.*, **212**, 81-99 (1999).

Blatt, W. F., Dravid, A., Michaels, A. S., and Nelsen, L., "Solute Polarization and Cake Formation in Membrane Ultrafiltration," in Flinn, J. E. (Ed.), Membrane Science and Technology, Plenum Press, New York (1970).

Brenner, B. M., and Rector, F. C. Jr. (Eds.), The Kidney, 2nd Ed., W. B. Saunders Co., Philadelphia (1981).

Bungay, P. M., and Brenner, H., "The Motion of a Closely-Fitting Sphere in a Fluid-Filled Tube," *Int. J. Multiph. Flow*, **1**, 25-56 (1973).

Colton, C. K., and Smith, K. A., "Mass Transfer to a Rotating Fluid: Part II. Transport from the Base of an Agitated Cylindrical Tank," *AIChE J.*, **18**, 958-967 (1972).

De Belder, A. N., and Granath, K., "Preparation and Properties of Fluorescein-Labelled Dextrans," *Carbohydrate Res.*, **30**, 375-378 (1973).

Deen, W. M., "Hindered Transport of Large Molecules in Liquid-Filled Pores," *AIChE J.*, **33**, 1409-1425 (1987).

Deen, W. M., Analysis of Transport Phenomena, Oxford University Press, New York (1998).

Denisov, G. A., "Theory of Concentration Polarization in Cross-Flow Ultrafiltration: Gel-Layer Model and Osmotic-Pressure Model," *J. Membrane Sci.*, **91**, 173-187 (1994).

Djabourov, M., Clark, A. H., Rowlands, D. W., and Ross-Murphy, S. B., "Small Angle X-Ray Scattering Characterization of Agarose Sols and Gels," *Macromolecules*, **22**, 180-188 (1989).

Drummond, J. E., and Tahir, M. I., "Laminar Viscous Flow through Regular Arrays of Parallel and Solid Cylinders," *Int. J. Multiph. Flow*, **10**, 515-540 (1984).

Clague, D. S., and Phillips, R. J., "Hindered Diffusion of Spherical Macromolecules through Dilute Fibrous Media," *Phys. Fluids*, **8**, 1720-1731 (1996).

Clague, D. S., and Phillips, R. J., "A Numerical Calculation of the Hydraulic Permeability of Three-Dimensional Disordered Fibrous Media," *Phys. Fluids*, **9**, 1562-1572 (1997).

Curry, F. E., "Mechanics and Thermodynamics of Transcapillary Exchange," in Handbook of Physiology, Section 2, Vol. IV, R. M. Berne (Ed.), American Physiological Society, Bethesda, 309-374 (1984).

Curry, F. E., and Michel, C. C., "A Fiber Matrix Model of Capillary Permeability," *Microvas. Res.*, **20**, 96-99 (1980).

Gibbs, S. J., Lightfoot, E. N., and Root, T. W., "Protein Diffusion in Porous Gel-Filtration Chromatography Media Studied by Pulsed Field Gradient NMR-Spectroscopy," *J. Phys. Chem.*, **96**, 7458-7462 (1992).

Gill, W. N., Wiley, D. E., Fell, C. J. D., and Fane, A. G., "Effect of Viscosity on Concentration Polarization in Ultrafiltration," *AIChE J.*, **34**, 1563-1567 (1988).

Jackson, G. W., and James, D. F., "The Hydrodynamic Resistance of Hyaluronic Acid and Its Contribution to Tissue Permeability," *Biorheology*, **19**, 317-330 (1982).

Jackson, G. W., and James, D. F., "The Permeability of Fibrous Porous Media," *Can. J. Chem. Eng.*, **64**, 364-374 (1986).

Johansson, L., and Löfroth, J. E., "Diffusion and Interaction in Gels and Solutions. 4. Hard Sphere Brownian Dynamics Simulations," *J. Chem. Phys.*, **98**, 7471-7479 (1993).

Johnson, E. M., Partitioning and Diffusion of Macromolecules in Charged Gels, Ph.D. thesis, Massachusetts Institute of Technology, 1995.

Johnson, E. M., Berk, D. A., Jain, R. K., and Deen, W. M., "Diffusion and Partitioning of Proteins in Charged Agarose Gels," *Biophys. J.*, **68**, 1561-1568 (1995).

Johnson, E. M., Berk, D. A., Jain, R. K., and Deen, W. M., "Hindered Diffusion in Gels: Test of the Effective Medium Model," *Biophys. J.*, **70**, 1017-1026 (1996).

Johnson, E. M., and Deen, W. M., "Hydraulic Permeability of Agarose Gels," *AIChE J.*, **42**, 1220-1224 (1996).

Johnston, S. T., and Deen, W. M., "Hindered Convection of Proteins in Agarose Gels," *J. Membr. Sci.*, **153**, 271-279 (1999).

Kapur, V., Charkoudian, J., and Anderson, J. L., "Transport of Proteins through Gel-Filled Porous Membranes," *J. Membr. Sci.*, **131**, 143-153 (1997).

Kosar, T. F., and Phillips, R. J., "Measurement of Protein Diffusion in Dextran Solutions by Holographic Interferometry," *AIChE J.*, **41**, 701-711 (1995).

Kozinski, A. A., and Lightfoot, E. N., "Ultrafiltration of Proteins in Stagnation Flow," *AIChE J.*, **17**, 81-85 (1971).

Mackie, W., Sellen, D. B., and Sutcliffe, J., "Spectral Broadening of Light Scattered from Polysaccharide Gels," *Polymer*, **19**, 9-16 (1978).

Madireddi, K., Babcock, R. B., Levine, B., Kim, J. H., and Stenstrom, M. K., "An Unsteady-State Model to Predict Concentration Polarization in Commercial Spiral Wound Membranes," *J. Membrane Sci.*, **157**, 13-34 (1999).

Michaels, A. S., "New Separation Technique for the CPI," *Chem. Eng. Prog.*, **64**, 31-43 (1968).
Ogston, A. G., "The Spaces in a Uniform Random Suspension of Fibers," *Trans. Faraday Soc.*, **54**, 1754-1757 (1958).

Ogston, A. G., Preston, B. N., and Wells, J. D., "On the Transport of Compact Particles through Solutions of Chain Polymers," *Proc. Royal Soc. Lond. A.*, **333**, 297-316 (1973).

Opong, W. S., and Zydney, A. L., "Diffusive and Convective Protein Transport through Asymmetric Membranes," *AIChE J.*, **37**, 1497-1510 (1991).

Phillips, R. J., Deen, W. M., and Brady, J. F., "Hindered Transport of Spherical Macromolecules in Fibrous Membranes and Gels," *AIChE J.*, **35**, 1761-1769 (1989).

Phillips, R. J., Deen, W. M., and Brady, J. F., "Hindered Transport in Fibrous Membranes and Gels: Effect of Solute Size and Fiber Configuration," *J. Colloid Interface Sci.*, **139**, 363-373 (1990).

Potschka, M., "Universal Calibration of Gel Permeation Chromatography and Determination of Molecular Shape in Solution," *Anal. Biochem.*, **162**, 47-64 (1987).

Robinson, G. B., and Walton, H. A., "Ultrafiltration through Basement Membranes," in Basement Membranes in Health and Disease, R. G. Price and B. G. Hudson (Eds.), Academic Press, New York, 147-161 (1987).

Rogers, M. H., and Lance, G. N., "The Rotationally Symmetric Flow of a Viscous Fluid in the Presence of an Infinite Rotating Disk," *J. Fluid Mech.*, **7**, 617-631 (1960).

Saksena, S., and Zydney, A. L., "Influence of Protein-Protein Interactions on Bulk Mass Transport During Ultrafiltration," *J. Membrane Sci.*, **125**, 93-108 (1997).

Schlichting, H., Boundary Layer Theory, 7th Edition, McGraw-Hill, New York (1979).

Shen, J. J. S., and Probstein, R. F., "On the Prediction of Limiting Flux in Laminar Ultrafiltration of Macromolecular Solutions," *Ind. Eng. Chem. Fundam.*, **16**, 459-465 (1977).

Sherwood, T. K., Brian, P. L. T., Fisher, R. E., and Dresner, L., "Salt Concentration at Phase Boundaries in Desalination by Reverse Osmosis," *Ind. Eng. Chem. Fund.*, **4**, 113-118 (1965).

Smith, K. A., and Colton, C. K., "Mass Transfer to a Rotating Fluid: Part I. Transport from a Stationary Disk to a Fluid in Bödewadt Flow," *AIChE J.*, **18**, 949-958 (1972).

Solomentsev, Y. E., and Anderson, J. L., "Rotation of a Sphere in Brinkman Fluids," *Phys. Fluids*, **8**, 1119-1121.

Spielman, L., and Goren, S. L., "Model for Predicting Pressure Drop and Filtration Efficiency in Fibrous Media," *Envir. Sci. and Tech.*, **2**, 279-287 (1968).

Zydney, A. L., "Stagnant Film Model for Concentration Polarization in Membrane Systems," *J. Membrane Sci.*, **130**, 275-281 (1997).